UNIVERSITEIT VAN PRETORIA
UNIVERSITY OF PRETORIA
YUNIBESITHI YA PRETORIA

A DUAL-BAND DUAL-POLARIZED ANTENNA FOR WLAN APPLICATIONS

by

Johanna Mathilde Steyn

Submitted in partial fulfilment of the requirements for the degree

Master of Engineering
(Electronic Engineering)

in the

Faculty of Engineering, Built Environment and Information Technology

UNIVERSITY OF PRETORIA

July 2009

SUMMARY

A DUAL-BAND DUAL-POLARIZED ANTENNA FOR WLAN APPLICATIONS

Author: Johanna Mathilde Steyn
Promoters: Prof. J.W. Odendaal and Prof. J. Joubert
Department: Electrical, Electronic & Computer Engineering
University: University of Pretoria
Degree: Masters (Electronic Engineering)

Keywords: WLAN, dual-band, dual-polarized, dual-band dual-polarized, single-dielectric-layer substrate, wide bandwidths, high gain, end-fire radiation pattern, compact structure, IEEE 802.11b and IEEE 802.11a WLAN standards

The recent growth in the ambit of modern wireless communication and in particular WLAN (Wireless Local Area Network) systems has created a niche for novel designs that have the capacity to send and/or receive arbitrary orthogonal polarizations. The designs should also be able to support dual-band functionality, while maintaining a compact structure. The first aim of this dissertation was thus to develop a dual-band single radiating element that can cover the 2.4 GHz (2.4 – 2.484 GHz) band and the 5.2 GHz (5.15 – 5.85 GHz) band for the IEEE 802.11b and IEEE 802.11a WLAN standards respectively. Dual-frequency elements such as stacked-, notched- and dichroic patches have been considered, but due to the size and the high cross-polarization levels associated with these designs, the design process was propelled towards various dipole and monopole configurations. The attributes of various designs were compared, where the double Rhombus antenna pregnant with dual-band and dual-polarization potential was used as basis in the development of the DBDP (Dual-Band Dual-Polarized) antenna design. The single-element design exhibited wide bandwidths, good end-fire radiation patterns and relatively high gain over the 2.4/5.2 GHz bands. A two-element configuration was also designed and tested, to firstly increase the gain of the configuration and secondly to facilitate the transformation of the dipole design into a dual-polarized configuration.

The second aim of this dissertation was to develop a dual-polarized array, while making use of only two ports, each pertaining to a specific polarization and to implement the design on a single-dielectric-layer substrate. Most dual-polarized structures such as circular, square and annular microstrip antenna designs only support one band, where multi-dielectric-layer structures are the norm. The disadvantages associated with multi-layered designs, such as fabrication difficulties, high costs, high back lobes and the size of the arrays, further supported the notion of developing an alternative configuration. The second contribution was thus the orthogonal interleaving of the two-element array configurations, to address the paucity of single-dielectric-layer dual-band dual-polarized designs that can be implemented with only two ports. This design was first developed and simulated with the aid of the commercial software package CST Microwave Studio® and the results were later corroborated with the measured data obtained from the Compact Antenna Range at the University of Pretoria.

OPSOMMING

'N DUBBEL-BAND DUBBEL-GEPOLARISEERDE ANTENNA VIR DLAN TOEPASSINGS

Outeur: Johanna Mathilde Steyn
Promotors: Prof. J.W. Odendaal en Prof. J. Joubert
Departement: Elektries, Elektronies & Rekenaaringenieurswese
Universiteit: Universiteit van Pretoria
Graad: Meesters (Elektroniese Ingenieurswese)

Sleutelwoorde: DLAN, dubbel-band, dubbel-polarisasie, dubbel-band dubbel-gepolariseerd, enkel-diëlektriese-laag substraat, wye bandwydte, hoë wins, direktiewe stralingspatrone, kompakte struktuur, IEEE 802.11b en IEEE 802.11a WLAN standaarde

Die onlangse groei in die area van moderne draadlose kommunikasie en met spesifieke verwysing na DLAN (Draadlose Lokale Area Netwerk) stelsels, het 'n nis vir nuwe ontwerpe geskep. Daar word van hierdie nuwe ontwerpe die kapasiteit verlang om verskeie ortogonale polarisasies te stuur en/of te ontvang in samewerking met dubbel-band eienskappe, terwyl 'n kompakte struktuur nogsteeds aandag moet geniet. Die eerste doel met hierdie verhandeling was dus die ontwikkeling van 'n dubbel-band enkel stralingselement wat instaat is om die 2.4 GHz (2.4 – 2.484 GHz) band en die 5.2 GHz (5.15 – 5.85 GHz) band wat as die IEEE 802.11b en die IEEE 802.11a DLAN standaarde respektiewelik bekend staan, te bedek. Dubbel-frekwensie elemente soos onder andere die gepakte-, merkkepie- en dichromatiese strook antenne was as moontlike oplossings ondersoek, maar die grootte en hoë kruispolarisasie wat gewoonlik met hierdie ontwerpe gepaard gaan, het die ontwerpsproses in die rigting van verskeie dipool en monopool konfigurasies gestoot. Die aantreklike eienskappe van die verskeie ontwerpe was met mekaar vergelyk, waar die dubbel Rhombus antenna, verwagtend met dubbel-band dubbel-polarisasie potensiaal, as basis vir die ontwikkeling van die DBDP (Dubbel-Band Dubbel-Polarisasie) antenna ontwerp gebruik is. Die enkelelementontwerp het wye bandwydtes, goeie direktiewe stralingspatrone en relatiewe hoë wins oor die 2.4/5.2 GHz bande geopenbaar. Die twee-element konfigurasies was ook ontwerp en getoets om eerstens die

wins van die konfigurasie te verhoog en tweedens om die transformasie na ‘n dubbel-gepolariseerde konfigurasie te fassiliteer.

Die tweede doel van hierdie verhandeling was om ‘n dubbel-gepolariseerde elementopstelling met net twee poorte te ontwikkel, waar elkeen verantwoordelik is vir ‘n spesifieke polarisasie, en te implementeer op ‘n enkel-diëlektriese-laag substraat. Die meeste dubble-polarisasiestrukture, soos onder andere die sirkulêre-, vierkantige- en ringvormige antenne ontwerpe, kan net een frekwensieband onderhou en word gewoonlik met behulp van meervoudige-diëlektriese-laagstrukture geimplementeer. Die negatiewe eienskappe soos onder andere die vervaardigingsmoeilikhede, hoë kostes, hoë teruglobbe en die grootte van die meervoudige-elementopstellings wat aan hierdie meervoudige-diëlektriese-laagontwerpe behoort, het verder die denkbeeld van ‘n alternatiewe konfigurasie bekragtig. Die tweede hoofbydrae was dus die ortogonale insleuteling van die twee-element meervoudige-elementopstelling konfigurasies om die geringheid van enkel-diëlektriese-laag dubbel-band dubbel-polarisasie ontwerpe, wat net met twee poorte geïmplementeer kan word, te adresseer. Hierdie ontwerp was eers met behulp van die kommersiële sagtewarepakket CST Microwave Studio® ontwikkel en gesimuleer, waarna die resultate bevestig was deur meetings by die Kompakte Antenna Meetbaan van die Universiteit van Pretoria.

ACKNOWLEDGEMENTS

The total presence of God in everything and the divine nothingness that succumb our existence are the sole creative environment, which without I would not have been able to explore and resonate the ambit of electromagnetism in this dissertation.

I would like to express my sincere gratitude towards Professors Wimpie Odendaal and Johan Joubert for their time, support and endless pool of knowledge, which they shared with me.

I would like to thank Lukas Naude, the technical assistant at the Compact Range, for his time and willingness to help in the process of obtaining the measured data presented in this dissertation. I would also like to thank Marie Pretorius for the etching of the numerous antenna configurations.

My family, without which nothing would have made sense. Dad, Mom and Magritt, thank you for your love, compassion, support and also being there when I needed you the most. You mean everything to me. Here is to you!

To my parents, Ben and Neeltje and to my sister Magritt.

"To see the love of God in
everything and in everybody."
- Invalid, blind and paralyzed citizen of Columbus found in *The Way* (E.S. Jones)

"The most beautiful thing we can experience is the mysterious. It is the source of all true art and all science. He to whom this emotion is a stranger, who can no longer pause to wonder and stand rapt in awe, is as good as dead: his eyes are closed."
- Albert Einstein

LIST OF ABBREVIATIONS

Co-Pol	Co-polarization
CPS	Coplanar Stripline
D	Directivity
DBDP	Dual-Band Dual-Polarized
DFDP	Dual-Frequency Dual-Polarized
F-to-B	Front-to-Back
G	Gain
GPS	Global Positioning System
HP	Horizontal Polarization
MIMO	Multiple-Input Multiple-Output
OFDM	Orthogonal Frequency Division Muliplexing
PCB	Printed Circuit Board
RF	Radio Frequency
SAR	Synthetic Aperture Radar
VP	Vertical Polarization
VSWR	Voltage Standing Wave Ration
WLAN	Wireless Local Area Network
X-Pol	Cross-polarization

TABLE OF CONTENTS

CHAPTER 1

INTRODUCTION

"Anyone who has never made a mistake has never tried anything new."

- Albert Einstein

The recent growth in the ambit of modern wireless communication has increased the demand for multi-band antennas that can satisfy the requirements pertaining to WLANs (Wireless Local Area Networks). The development of dual-band antennas that can cover the 2.4 GHz (2.4 – 2.484 GHz) band and the 5.2 GHz (5.15 – 5.85 GHz) band for the IEEE 802.11b and IEEE 802.11a WLAN standards respectively, are thus highly desirable. A second requirement for WLAN applications is polarization diversity, which can be achieved by making use of dual-polarized arrays. This allows communication systems to be able to send and receive signals with more than one polarization [1]. The need for data rates higher than 54 Mbps and thus higher bandwidth efficiency [2] for WLAN systems have increased MIMO (Multiple-Input-Multiple-Output) related research [3]. MIMO systems not only use multipath propagation in a constructive way, but increase the robustness and capacity of the whole system. Polarization diversity or dual-polarized configurations can assist in realizing bandwidth efficient schemes such as the MIMO-OFDM (Multiple-Input-Multiple-Output – Orthogonal Frequency Division Multiplexing) scheme, by increasing the system capacity without adding additional antennas at the receiver and transmitter. Various adaptive modulation and demodulation methods have been proposed, in conjunction with the OFDM scheme [2], to provide a potentially more efficient solution.

It is relatively easy to realize a dual-polarized structure by making use of two ports in conjunction with a circular, square or annular microstrip antenna [4], but it is more challenging to design a structure that has the capacity to support dual-band and dual-polarized operations. A lot of research has been done to develop suitable antenna elements with the capacity to support orthogonal polarizations with dual frequency bands. Most of the dual-band dual-polarized (DBDP) designs make use of multiple-dielectric-layered

configurations [4] or are realized by means of multiple antenna arrays, where each array is responsible for a certain frequency band or specific polarization. The disadvantages associated with the multi-dielectric-layered structures are fabrication difficulties, high costs and high back lobes [5]. The larger arrays also consume a lot of realty space. A variety of designs have also been developed for SAR (Synthetic Aperture Radar) applications [6] in the C-band (4-8 GHz) and the X-band (8-12 GHz) and for cellular systems at lower frequency bands such as the 900/1800 MHz bands [7], [8]. The designs associated with SAR applications have not yet been modified to specifically target WLAN applications. The development of appropriate structures that comply with all the specifications for dual-band dual-polarized arrays, while aiming for single-dielectric-layered elements to reduce fabrication costs, are thus the next challenge for the successful implementation of WLAN communication systems.

Dual-frequency elements such as stacked-, notched- and dichroic patches have also been considered to be modified to facilitate dual-polarized operation. The size of the elements, the high cross-polarization levels associated with dichroic- and stacked patches and the complex routing of feeding networks needed to implement some of the antenna patch designs [4], disqualified these options in general to be used in dual-polarized arrays. Other printed dipoles and slot antennas, which occupy less space, have also been investigated and the feasibility of these options was ascertained in [6].

A variety of very attractive printed planar antennas have been developed for dual-band operations, but the feasibility of the designs being integrated into dual-polarized array configurations have not yet been ascertained. The favourable characteristics such as easy adaptability to different frequency bands, light weight, small dimensions and low manufacturing costs [9] entertained for dual-frequency band applications, is corroborated with the numerous monopole [10] – [18] and dipole [19], [20] antenna designs.

Another attractive printed planar design that has the potential capacity to support dual-frequency band operations, is the double Rhombus antenna presented in [9]. The Rhombus shaped dipoles with varying lengths, stable radiation patterns and relatively high gains have also not yet been considered for dual-polarized array configurations.

1.1 OBJECTIVES

The main objective is to provide an alternative configuration to the multi-dielectric-layered configurations that are usually associated with dual-polarized arrays with multi-frequency band capabilities. The main goal is thus to develop a compact structure, while reducing the cost of the prevalent designs and providing a design that is easier to fabricate. In order to achieve this objective, a thorough study of current designs is needed to make erudite decisions in terms of configuration, dimensions and substrate.

The first goal is thus to compare the various attributes pertaining to current dual-band and dual-polarized designs and to conduct a literature study on existing DBDP designs in order to facilitate the process of developing an alternative design. It is thus discernible that the next step will be to ascertain the feasibility of a single and most attractive dual-band element in order to develop a dual-polarized configuration. The aspiration with this endeavour is thus to develop a novel as well as an optimized design, which will be done with the aid of commercial software package CST Microwave Studio®. A parameter study of the various dimensions will also be conducted to maximize the capacity of the single-element, as well as the pinnacle of the dissertation, the nouveau DBDP design.

1.2 CONTRIBUTIONS OF THIS DISSERTATION

The main contribution to the field of applied electromagnetic principles is the development of an alternative dual-polarized dual-band (DPDB) antenna array with efficient bandwidth to cover the IEEE 802.11 WLAN standard frequency bands of 2.4 GHz (2.4 – 2.484 GHz), 5.2 GHz (5.15 – 5.350 GHz) and 5.8 GHz (5.725 – 5.825 GHz), adequate gains and stable end-fire radiation patterns, while maintaining low manufacturing costs, small dimensions and reduced number of antenna elements in the array configuration. The new design was developed for a relatively inexpensive substrate, thereby reducing the costs of the design.

One of the key elements in obtaining a discernible advantage over current designs is to develop a configuration that make use of only two ports, each pertaining to a specific polarization, in order to reduce equipment and installation costs [21]. Unlike the design presented in [22] where a DPDB array consists of sub-arrays, where each dual-polarized four-element Vivaldi sub-array is only responsible for one frequency band and is

implemented by means of multiple ports, the aspiration was to design a miniaturized antenna array with combined functionality. The latter design [22] was developed as a 20-element array with each element filling an area of 80 mm x 80 mm (L x W). The design presented in [21] alternatively did indeed realize a DBDP antenna for wireless communication with only two ports, but made use of a multi-dielectric-substrate configuration in conjunction with a shielding conducting box, which resulted in design with a size equal to 650 mm x 250 mm x 41.76 mm (L x W x H). The new DBDP presented in this dissertation only imbue a space of 148 mm x 148 mm x 101.3 mm (L x W x H), which reverberate the objective to design a compact structure as postulated in the section above.

The presented design is also more compact in terms of the height compared to the multi-dielectric-layered DBDP design seen in [7], with the dimensions equal to 131 mm x 129 mm x 120 mm (L x W x H). The wide bandwidth, as well as the relatively high gain achieved with the proposed design, also surpassed the characteristics of the DBDP microstrip design presented in [23]. The latter design exhibited bandwidths of 7.8% and 1.9% over the 1.275/5.3 GHz bands respectively, where the four-element DBDP array developed in this dissertation exhibited bandwidths in the order of 32.5% and 37.1% over the 2.4/5.2 GHz bands respectively. The design in [23] did evidently not meet the requirement in terms of the bandwidth pertaining to the C-band as specified by the WLAN standards. A multi-dielectric-layered structure was also employed in [23] and although the structure was slightly smaller, the gain of the new design was discernibly higher than the design presented in [23]. The maximum gain achieved with the newly developed four-element DBDP design was 8.8 dBi at 5.7 GHz, where the highest gain achieved in [23] was 2.7 dBi over the C-band. The average gains of 5.2 dBi and 5.6 dBi pertaining to the various polarizations were also an improvement compared to the compact design seen in [24], with the gains ranging from 4.2 dBi to 1.6 dBi.

The design in [25], which was also developed for SAR applications, exhibited even narrower bandwidths and was designed as a configuration consisting of four 4 x 4 element sub-arrays in conjunction with 2 x 3 dual-polarized slot arrays. The low directivity radiation patterns seen in [26] combined with the high cross-polarization in the boresight direction over the 2.4 GHz band was also contested by the new design and although the overall structure in [26] was more compact, the F-to-B (Front-to-Back) ratios of between

12.6 dB to 19 dB exhibited by the new design exceeded the results as presented in [26]. The new design presented in this dissertation also exhibited normalized cross-polarization levels lower than -30 dB in the boresight direction at 2.44 GHz, compared to the cross-polarization level of -6 dB exhibited by the design in [26]. The structure described in [27] imbued an area of 217 mm^2 with a height of 1.6 mm, made use of a via and although the area is substantially smaller, the gains of between 3.6 dBi to 3.9 dBi and 3 dBi to 4.2 dBi over the 2.4/5.2 GHz bands respectively are much lower weighed against the maximum gains of 5.4 dBi and 8.8 dBi of the new design. The design in [27] also suffered from high cross-polarization levels, with less than 10 dB down compared to the co-polarization levels. Another characteristic that was also prevalent with the new design was the stable radiation patterns compared to the slightly distorted radiation patterns at 5.2/5.8 GHz in [27].

As postulated in the objectives, the main goal was to design and optimize a dual-band single element in terms of bandwidth and gain and therefore, facilitate the development of a dual-polarized configuration by using the new single-element as building block. These directives were achieved by using the ground work done in [9] and designing a double dipole structure on a Rogers substrate RO4003C with a dielectric constant of 3.38, a height of 0.813 mm and a loss tangent (tan δ) of 0.0027. The single element was incorporated into a two-element array in order to increase the gain of the antenna and to ascertain the effect that identical or mirrored elements have on the overall performance of the array. The next provocative was to develop an appropriate feeding network to facilitate the transformation into a four-element DBDP array with only two ports. Dual polarization was achieved by orthogonally combining the two, two-element arrays. Each polarization was fed by a single port. A four-element compact array was thus developed with wide bandwidths, average gains of 5.1 dBi and 6.2 dBi over the 2.4/5.2 GHz bands respectively, high F-to-B ratios ranging from 12.6 dB to 19 dB and low cross-polarization levels close to -30 dB at boresight.

1.3 ORGANISATION OF THIS DISSERTATION

In Chapter 2 existing designs for dual-band, dual-polarized and dual-polarized dual-band antennas are first summarized and corroborated by the origins of some of the dual-band printed configurations, from the classic quasi-Yagi antenna to the modified bow-tie and Lotus antenna designs. The transformation from a single to a dual-polarized array configuration is also discussed to provide an adequate line of argument towards the final design and proposed solution.

Chapter 3 is focussed on the theory and the design of the single element, the two-element array, as well as the four-element dual-band dual-polarized array. The design procedure is discussed to provide clarity for each step taken towards the pinnacle of this dissertation.

The simulated and measured results are provided in Chapter 4. Two different single element designs were simulated and tested to find the best candidate for the two- and four-element arrays. The two-element as well as the four-element dual-polarized array were also simulated and tested to validate the feasibility of this design.

Chapter 5 gives an overview of the contributions made through the dissertation and highlights the achieved results in light of the specified objectives for this dissertation. The possibility of future work is also included.

CHAPTER 2

BACKGROUND: DUAL-BAND, DUAL-POLARIZED AND DUAL-BAND DUAL-POLARIZED CONFIGURATIONS

"All our knowledge has its origins in our perceptions."
"Learning never exhausts the mind."
- Leonardo da Vinci

The use of dipole, monopole and slot antenna designs in dual-band dual-polarized (DBDP) arrays have been ascertained for SAR (Synthetic Aperture Radar) and cellular system applications, but has not received a lot of attention for WLAN applications. Most of the dual-polarized designs only cover one of the WLAN frequency bands. Chapter 2 presents an overview of dual-band antenna designs and dual-polarized configurations, as well as dual-band dual-polarized configurations, with their advantages and disadvantages highlighted to facilitate the comparison process, to justify the design decisions made in this dissertation. Specific focus is also given to the Rhombus and bow-tie antenna designs presented in [9] and [1], since the two- and four-element array designs presented in this dissertation are based on these original designs.

2.1 DUAL-BAND CONFIGURATIONS

The two main methods of achieving dual-band operation are by using dual-frequency resonating elements or by making use of an interleaved network of single-frequency radiators [6]. A lot of research has thus been aimed at the development of dual-band monopole designs, with advantages such as small dimensions and the possibility to increase the relatively narrow impedance bandwidths of traditional monopole designs. The first part of section 2.1 is dedicated to monopole designs ascertained for dual-band operation over the two WLAN bands. A lot of research effort has gone into the improvement of dipole antennas in terms of bandwidth, stable radiation patterns, wide 3 dB

beam width and low cross-polarization levels. The second part of section 2.1 therefore explores the most frequently employed dipole antennas and in particular the double Rhombus antenna, due to the potential integration of the element in dual-polarized arrays.

As mentioned above, traditional monopole designs exhibit relatively narrow bandwidths. A variety of methods have been ascertained to improve the bandwidth, which include the use of meander lines [10] – [13], CPW (Coplanar Waveguide) feeding networks [14] – [16] and parasitic elements [17], [18]. The ring monopole [10], L-shaped monopole [11], G-shaped monopole [12] and inverted-F shaped monopole [13] are only some of the general printed monopole structures used in conjunction with meander radiating strips of varying lengths, to facilitate the operation in the two primary bands. These configurations are usually chosen due to their simple structures, although their gains are not so high when compared to slot antennas.

The ring monopole antenna presented in [10] was transformed into a more compact structure by making use of double rectangular meander lines and horizontal and vertical branched strips. This antenna exhibited wide impedance bandwidths of 12% and 39.3% for the two WLAN bands respectively and gains of 2.8 dBi and 4.9 dBi in the 2.4 and 5.0 GHz bands respectively. The G-shaped monopole antenna design [12] that incorporated a shorting pin between the ground and the radiating element also exhibited competitive bandwidths of 15.2% in the 2.4 GHz band and 19.4% in the 5.2 GHz band, with the second band slightly narrower than the ring monopole antenna. The peak gains were 2 dBi and 4 dBi, due to the omni-directional radiation patterns.

As mentioned above, CPW feedlines are also one of the methods employed to increase the bandwidths of monopole designs and one of the main attractions is the simple structure that consists of only a single metallic layer [14]. The design reported in [15] combined CPW and meander technology by replacing the normal stripline pertaining to a traditional CPW feeding network with a stripline that were built up by a number of meandering slits. The enhanced bandwidths exhibited by this design were 23.3% and 29.5% respectively for the two frequency bands and the peak gains were 2.4 dBi and 4.2 dBi. The cross-shaped slot CPW-fed antenna [16] incorporated slot-loaded technology to decrease the size of the antenna and achieved peak gains in the order of 3.8 dBi and 5.7 dBi, which were somewhat higher than the antenna design in [15]. The bandwidths associated with this design were

20% and 37% in the 2.4/5 GHz bands respectively, where the bandwidth covering the 5 GHz band surpassed the 29.5% bandwidth reported in [15].

Most of the designs that employ parasitic patches to obtain wider bandwidths use either a stacked geometry or a coplanar geometry that increases the width of the antenna structure. This can be avoided by making use of a half U-slot and patch antenna in conjunction with L-slits [17]. The L-slits effectively divides the planar structure into three resonating patches. The antenna boasts of a compact geometry with bandwidths of 5% and 25.2% for the two bands respectively. The peak gains achieved in the two bands were 1.3 dBi and 5.1 dBi respectively. An inverted U-shaped parasitic radiator in conjunction with an L-shaped microstrip line [18] delivered a slightly wider bandwidth for the lower band and a competitive bandwidth for the higher band compared to the antenna design in [17]. The bandwidths achieved in the 2.4/5 GHz bands were equal to 8.8% and 23.4% respectively. The radiation patterns over the two frequency bands differed in terms of the location of the peak gain or the width of the 3 dB beam width. The delivered peak gains of 0.8 dBi and 1.7 dBi were lower compared to the gains exhibited by the half U-slot and patch antenna with L-slits.

The folded half-wave dipole design [19] and the modified quasi-Yagi design [20] both deliver directional radiation patterns with the peak gains between 3.7 – 5 dBi and 5 – 5.3 dBi respectively. The geometry pertaining to the folded half-wave dipole antenna has the advantage of being self-balancing, thus eliminating the need for a balun. The modified quasi-Yagi design on the other hand was presented with a broadband hook-shaped balun to balance the structure. Both designs make use of three dipoles with the folded half-wave dipole consisting of two series fed smaller dipoles covering the upper band and the larger dipole the lower band. This configuration exhibited an impedance bandwidth of 7% in the 2.4 GHz band and 26.6% in the 5 GHz band with the peak gains equal to 3.7 dBi and 5 dBi respectively. As mentioned above, the modified quasi-Yagi design also employed three dipoles with the longest dipole acting as the reflector, the midlength dipole as the director and the shortest dipole as the resonator. A wide bandwidth of 37.1% was achieved over the first band and a narrow bandwidth of 13.6% over the second band. Directional radiation patterns were generated with peak gains of 5 dBi and 5.3 dBi respectively for the 2.4/5 GHz bands.

The double dipole design presented in [28] delivered a usable bandwidth of 84% and consisted of two parallel dipoles. The length associated with each dipole differed to create two resonances. The bandwidth was achieved mainly by the shape of the antenna, which acted as a matching circuit for the microstrip feedline. The return loss levels between the two main resonances were controlled by varying the distance between die first dipole and the truncated ground, as well as the distance between the two dipoles. The bandwidth was increased further by modifying the shape of the dipoles and by increasing the height of the substrate [1]. The Rhombus shaped dipoles introduced varying paths for the current, which ensured that densely spaced multi-resonances were achieved. This increased the bandwidth to 103%. The height of the antenna was also lower than the normal bow-tie antenna. The double Rhombus antenna design presented in [9] is a novel microstrip-fed antenna with very favourable characteristics and has the potential to be used in a dual-polarized array with the varying dipole lengths and to facilitate the dual frequency specifications associated with WLAN applications. The key advantages thus associated with this design include an ultra-wide bandwidth, stable radiation patterns, as well as low cross-polarization levels in conjunction with small dimensions.

The radiation patterns of the monopole designs are generally omni-directional in the one plane and monopole-like in the other planes, with the exception of the microstrip-fed coplanar antenna [27] that exhibit nearly omni-directional patterns in both the primary planes. The dipole designs in [19] and [20] deliver good directional patterns with high gains and are thus aimed at applications where end-fire radiation patterns are a prerequisite. The key characteristics pertaining to a successful WLAN antenna design are thus the size of the antenna, the bandwidth, the gain, as well as stable radiation patterns over the two primary WLAN bands.

2.2 DUAL-POLARIZED CONFIGURATIONS

The dual-polarized antenna design ambit is well represented and populated by a variety of interleaved patch antenna designs. The wide band stacked patch antenna design presented in [29] operated over the 2.4 GHz WLAN band, as well as the UMTS (1.92 – 2.17 GHz) and the UMTS II (2.5 – 2.69 GHz) bands. Dual-polarization was achieved by stacking two patches, two foam layers, a slot plane and ground plane in conjunction with two ports. The two ports respectively corresponded to the -45º/+45º polarization and the isolation over the

2.4 GHz band was 16 dB and higher. The maximum cross-polarization was equal to -25 dB and the gains varied between 7.5 dB and 9 dB. The patch microstrip antenna design presented in [30] was also a -45º/+45º dual-polarized design that exhibited isolation higher than 16 dB as with the previous mentioned design. The bandwidth pertaining to the frequency band that ranged from 5.3 GHz to 5.55 GHz was 4.3%, assuming a VSWR of 2:1. The aim with the patch design seen in [31] was to reduce the overall area of the dual-polarized antenna by means of peripheral slits. The authors succeed in doing so by reducing the structure by 48%, but had to accept the narrow bandwidth associated with the design. The bandwidth over the 1.81 GHz band was equal to 0.5%. The design also exhibited cross-polarization levels lower than -30 dB and a maximum gain of 7.1 dBi. The dual-polarized Fourpoint antenna presented in [32] was an improvement on the Foursquare antenna with an 30% increase in bandwidth, from 37% to 67% over the 2.0 GHz band. The antenna consisted out of four modified square-point structures and was characterized by cross-polarization levels below -30 dB and gains between 8 dBi and 9 dBi. The overall dimensions of the design were 61 mm x 61 mm x 27.4 mm (L x W x H).

An omni-directional slot antenna [33] was optimized for the 5.2 GHz band, with an area of 217 mm x 217 mm and an impedance bandwidth of 10.6%. The gains of the two polarizations were 2.6 dB and 3.5 dB, with the isolation between the two ports below -59 dB. The design unfortunately suffered from high cross-polarization levels in the one plane, but this propensity was not perpetuated in the other plane with levels as low as -60 dB. The low-profile design presented in [34] also made use of a square slot in conjunction with a patch of 36 mm x 36 mm and were designed to cover the 5.2 GHz band, as well as the 5.8 GHz band. The bandwidths and the peak gains associated with the 5.2/5.8 GHz bands respectively were 7.3% and 3.3%, and 3 dBi and 4 dBi. The results of both designs were discernibly similar, where the major difference was seen between the filled areas of each design.

Various dipole configurations have also been investigated for possible transformation into dual-polarized configurations. The folded metal dipole configuration presented in [35] exhibited a bandwidth of 15% over the frequency band 824 – 960 MHz. The gain ranged from 9.4 dB up to 10.4 dB and the cross-polarization levels were below 25 dB relative to boresight. The four-element dual-polarized configuration was housed in a box to improve the isolation between the two ports. A double-sided dipole design [36] was also employed

for dual-polarization and consisted out of an upper and lower array in conjunction with two foam layers and a ground plane. Bandwidths in the order of 10% were achieved with the cross-polarization levels between -17 dB and -23 dB. The design also exhibited high gains.

The modified bow-tie design in [1] also exhibited very favourable characteristics and is more thoroughly discussed in section 2.4.3. The printed dipole design exhibited a wide bandwidth of 91% that covered both the C- and X-bands. The highest coupling levels were around -19 dB. The design also exhibited low cross-polarization levels in the boresight direction and F-to-B (Front-to-Back) ratios equal and above 12 dB. The dual-polarized array presented in [1] was only simulated and not confirmed by means of measured results. The simulated model also made use of four ports.

2.3 DUAL-BAND DUAL-POLARIZED CONFIGURATIONS

The development of dual-polarized configurations for the two standard WLAN frequency bands was conceived as a provocative in order to increase the data rates for future generation WLAN systems, without adding additional antennas [3]. As mentioned in Chapter 1, polarization diversity plays a seminal role in the realization of MIMO-OFDM (Multiple-Input-Multiple-Output - Orthogonal Frequency Division Multiplexing) systems in conjunction with various modulation and demodulation techniques. The future development of more effective WLAN systems thus entails the development of miniaturized antenna arrays with combined functionality, such as the capacity to send and receive both horizontally and vertically polarized signals.

A variety of designs with multi-dielectric-layered structures have been developed to address the need for DBDP designs. The design presented in [4] exhibited 6% and 10% bandwidths over the 1.25/9.5 GHz bands respectively, with the coupling levels between 18 dB and 20 dB. The cross-polarization levels were also between 16 dB and 20 dB below the main beam. An area of 92.5 mm x 92.5 mm x 8.47 mm (L x W x H) was occupied by the configuration, with the height an impending advantage for applications that require a low-profile structure. Another multi-layered configuration discussed in Chapter 1, presented in [7] also exhibited bandwidths in the order of 10% over the 900/1800 MHz bands, but with a slightly larger configuration that imbued an area of 131 mm x 129 mm x 120 mm. This configuration was designed to generate broadside radiation patterns. The microstrip

antenna in [21] developed for wireless communications, operating over the 920/1795 MHz bands, was characterized by low cross-polarization levels near -25 dB in the boresight direction and bandwidths equal to 14.3 % over the 920 MHz band and 14.7% over the 1795 MHz band. The only slight disadvantage of the design was the size, which was equal to 650 mm x 250 mm x 41.76 mm (L x W x H). Another DBDP microstrip antenna design presented in [25], that operated over the L- and the C-bands made use of complex feeding networks in conjunction with multiple sub-arrays and larger arrays. The bandwidths associated with this design were also very narrow. The design was also specifically developed for SAR applications as was the design seen in [23], with bandwidths equal to 100 MHz over the 1.275/5.3 GHz bands. The bandwidths belonging to the 5.3 GHz band did not adhere to the minimum bandwidth pertaining to the IEEE 802.11a WLAN standard of 14.4%. The approximate maximum gains exhibited by the latter design were 7 dB and 2.7 dB over the L- and C-band respectively.

The DBDP rectangular patch design excited by an inclined coupling slot presented in [26] adhered to both the WLAN standards with the bandwidths over the 2.4/5.2 GHz bands equal to 5% and 23% respectively. The design was also characterized by high cross-polarizations with the levels 6 dB and 20 dB down relative to the boresight at 2.43/5.2 GHz respectively. The dual-frequency microstrip antenna that was assembled with two parasitic patches imbued an area equal to 75 mm x 75 mm x 0.8 mm (L x W x H), with the height a discernible advantage. Another advantage pertaining to the design was the relative high gain of 7 dBi, although the high back-radiation levels, which were caused by the resonant slot, resulted in F-to-B ratios in the order of 7 dB. The microstrip antenna presented in [24] also boasted of a compact structure of 100 mm x 100 mm x 1.6 mm (L x W x H), with the height an apparent advantage. Good F-to-B ratios were observed over the lower band (2 GHz), but were not perpetuated at the second band (2.78 GHz) and were in the vicinity of 4 dB. The gains pertaining to ports 1 and 2 were 4.2 dBi and 1.6 dBi respectively, with a prominent disparity between the lower and upper frequency bands pertaining to ports 1 and 2. Narrow bandwidths were also prevalent to the design. The non-directive radiation patterns in the H-plane and the slightly distorted radiation patterns at 5.2 GHz and 5.8 GHz in conjunction with the high cross-polarization levels overshadowed the relatively wide bandwidths of 14% and 22% over the two WLAN bands respectively and the gains that ranged from 3.6 dBi to 4.2 dBi pertaining to the design in [27].

The majority of the DBDP designs examined above made use of a multi-layered architecture with gains in the vicinity of 4 dBi and bandwidths that ranged from 5% to 23%. As seen above, each design exhibited beneficial traits and contributed to the body of knowledge regarding DBDP antenna design. The limitations of the designs can be the aim of future research.

2.4 DOUBLE DIPOLE DESIGN

The ground work done on the double Rhombus antenna in [9] was used as building blocks in this dissertation to develop and design a DBDP configuration. It was thus thought to be prudent to first discuss the background leading to the design that ultimately facilitated the development of a new design that adhered to new specifications and applications. Section 2.4.2 is dedicated to the two-element array designs that were used in the four-element configurations. The method used to transform the dipole design in [1] into a four-element dual-polarized array is discussed in Section 2.4.3.

2.4.1 Background pertaining to the double Rhombus design

The quasi-Yagi, printed Lotus, as well as bow-tie antennas are some of the most frequently employed antennas in phased arrays. It is reported in [1] that the quasi-Yagi antenna is capable of delivering a bandwidth equal to 48%. The bow-tie antenna was an improvement on the regular quasi-Yagi antenna in terms of bandwidth and size, where the bow-tie antenna exhibited bandwidths up to 60% [37]. This transition was facilitated by replacing the dipole and the director associated with the traditional design of the quasi-Yagi antenna with a bow-tie. This also had the effect of reducing the overall antenna size by 20%.

The printed Lotus antenna presented in [38] also exhibited 2:1 VSWR of 60% with low return loss levels. A vast number of microstrip antennas are fed with the aid of a coplanar stripline (CPS), as in the case of the novel slot and printed Lotus antenna, due to the favourable characteristics associated with this type of transmission line. This balanced uniplanar transmission line exhibits characteristics which include a compact size and low discontinuity parasitics [39], and although this structure falls outside the ambit of this study, the theory provides insight into alternative designs. A balun is used in conjunction with the printed Lotus antenna to facilitate the microstrip-to-coplanar transition. The word

balun is composed from the words BALunced and UNbalanced, which refers to its main function to transform an unbalanced source impedance to a balanced load impedance, such as a dipole antenna or a two wire line [40]. The balun structure used in this application was first introduced in the quasi-Yagi antenna design, which is based on the Yagi-Uda antenna presented in 1928 [41]. The microstrip-to-coplanar balun used to feed the quasi-Yagi antenna introduce a 180° phase shift at the centre frequency, as well as a half wavelength delay on the one side of the microstrip line [38]. This is done to suppress the even mode over the impedance bandwidth and to provide the coplanar stripline with an odd mode. By choosing to place the truncated ground close to the balun, the even mode impedance becomes large enough to guarantee the suppression of the even mode in the stripline [42]. The odd mode is responsible for the occurrence of an equal potential in terms of magnitude on each branch of the coplanar-stripline, which is also 180° out of phase. It is thus evident that this specific balun configuration delivers a sufficiently good impedance match between the unbalanced input and the balanced output, with a small odd mode impedance. Although this is a promising alternative to the printing of the dipoles on both sides of the substrate, the balun is designed to operate at the centre frequency. The half-wave delay thus has a limiting effect on the bandwidth and is also responsible for the deterioration of the radiation patterns at high frequencies. The Lotus antenna in conjunction with the above described balun is thus not capable of supporting dual frequency band operations with the current configuration. Further adjustments are thus rudimentary to any additional development of this antenna in an array environment. The bow-tie antenna design was modified even further in [1] to provide a single element that can support operation in two frequency bands. The claimed simulated impedance bandwidth of 91% was corroborated by the practical results presented in [1].

2.4.2 Two-element array

Two identical two-element array designs with different feeding networks were developed in this dissertation. This was firstly done to increase the gain of the configuration and secondly, to make use of the method shown in [1] to transform a dipole design into a dual-polarized configuration. In the paper related to the modified bow-tie design [1], two different two-element configurations were developed to determine the optimum design in terms of bandwidth and gain. This was done to facilitate the development of the four-element dual-polarized design also presented in this paper. The prototypes used to

corroborate the simulated results were fed with two separate ports. The grating lobes were reduced by increasing the distance between the two elements. The first array was configured such that the two halves of the bow-tie dipoles on the top of the substrate were directed in the same direction, ensuring that the surface currents were in the same direction. The second array was designed with the bow-tie dipoles mirroring each other and a 180° phase shift were introduced to ensure that this configuration also had surface currents in the same direction. These two configurations can be seen in Fig. 2.1 (a) and (b). The second configuration proved to be the superior design in terms of beam width, cross-polarization levels, symmetry and usable bandwidth.

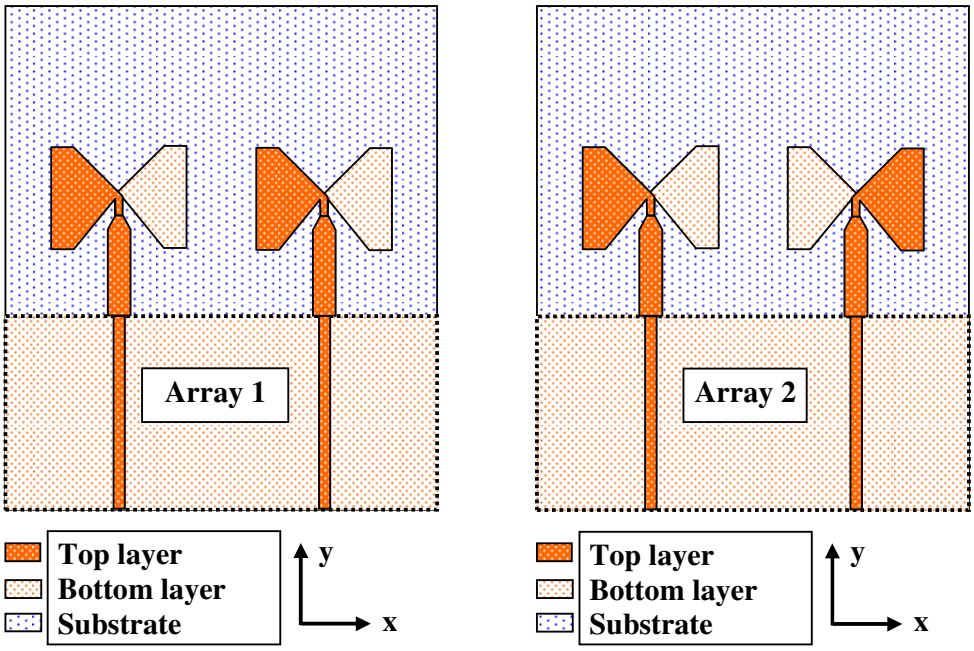

FIGURE 2.1: Two-element array configuration. (a) Array 1. (b) Array 2.

A two-element array was also tested and simulated in [9] to determine the performance of the novel Rhombus-shaped double dipole design in an array environment. The two elements were mirrored along the y-axis and a 180° phase shift was also introduced to reduce the effect of the substrate height on the radiation patterns by ensuring that the direction of the surface currents are in the same direction. The electric currents along the y-axis are thus in opposite directions with reference to each other and the electric fields between the two layers are also in opposite directions relative to the neighbouring element. This effectively reduces the cross-polarization level by canceling out the majority of cross-polarization fields. A slit in the ground plane was also introduced, which creates a

disturbance in the path of the waves traveling through the surface of the substrate, in order to reduce the coupling between neighbouring elements. The slit in the ground plane as well as the direction of the surface currents can be seen in Fig. 2.2. The elements can thus be more densely packed due to this modification. As expected the gain of the two-element array was also higher than the gain achieved with the single-element.

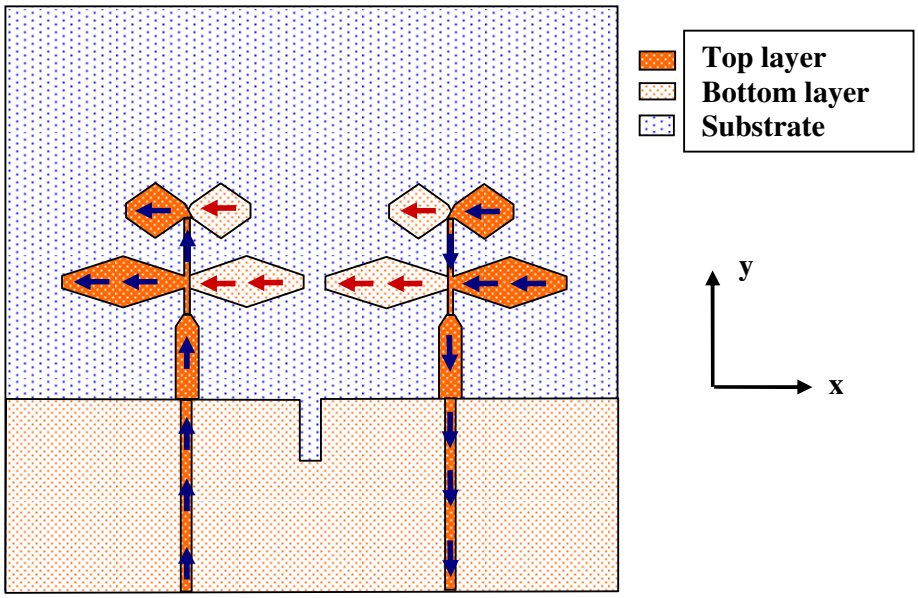

FIGURE 2.2: The two-element double Rhombus antenna array configuration with a slit in the ground plane.

2.4.3 Dual-polarized array configuration

As mentioned in Section 2.4.2, the notion of a dual-polarized array that can be realized with the aid of a bow-tie was also ascertained in [1]. The wide-band modified bow-tie antenna element exhibited a wide bandwidth of 91% that covered the C- and the X-band. Two different dual-polarized array configurations were simulated with four ports, where only two of the ports were excited. Each configuration incorporated four printed bow-tie antennas and was based on the two-element array configurations also presented in the paper. The first configuration consisted of an array of two sets of two identical bow-tie antennas, whereas the second configuration introduced a 180º phase shift by rotating one of the bow-tie elements in the two-element array. The second configuration again proved to be superior in terms of cross-polarization levels, beam widths and usable bandwidth,

whereas the return loss and coupling pertaining to each configuration were very similar. This configuration can be seen in Fig. 2.3. The four-element dual-polarized array results presented were only simulated and not verified by means of physical measurements.

The double Rhombus antenna [9] pregnant with potential, naturally lends towards the synergy between the proposed dual-polarized array configurations presented in [1] and the Rhombus antenna design.

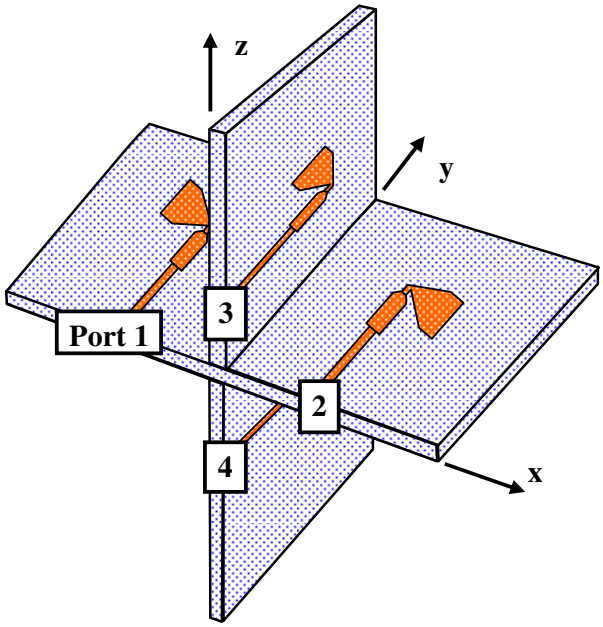

FIGURE 2.3: Four-element dual-polarized array.

CHAPTER 3

THEORY AND DESIGN OF A DUAL-BAND DUAL-POLARIZED WLAN ANTENNA

"To do is to be." – John Stuart Mill
"To be is to do." – Jean-Paul Sartre
"Do-be-do-be-do." – Frank Sinatra

The theory and the metamorphoses of the original double Rhombus antenna presented in [9], that led to the pinnacle of this dissertation, is laid out in Chapter 3. The first objectives were to design a single-element to operate over the two standard WLAN bands and to ascertain the effect that the different dimensions have on the width of the band, as well as the radiation patterns and therefore also the boresight gain. The optimization of the single antenna element was thus rudimentary to the development of an appropriate array for the dual-band dual-polarized configuration. The second part of Chapter 3 is dedicated to the two- and four-element array designs.

3.1 SINGLE DUAL-BAND ANTENNA DESIGN

3.1.1 Antenna geometry and parameters

As mentioned above, the first aspiration was to ascertain the effect of the various dimensions on the overall performance of the dual-band WLAN single-element design by conducting a parameter study. The antenna was designed to operate over the 2.4 GHz and 5.2 GHz bands on a Rogers RO4003C substrate with a dielectric constant of 3.38, a height of 0.813 mm and a loss tangent (tan δ) of 0.0027. The final optimized design proliferated out of a series of etched designs that were simulated and measured.

The initial "trial and error" single-element antenna design consisted of two parallel quasi-rhombus-shaped dipoles fed by a microstrip line with the lengths of the two dipoles being the key parameter responsible for the limits of the operating frequency bands. The

two halves of the dipoles were printed on either sides of the substrate to ensure that the structure was balanced and thus eliminated the need to implement a balun. The geometry as well as the antenna dimensional parameters can be seen in Figs. 3.1 and 3.2, respectively.

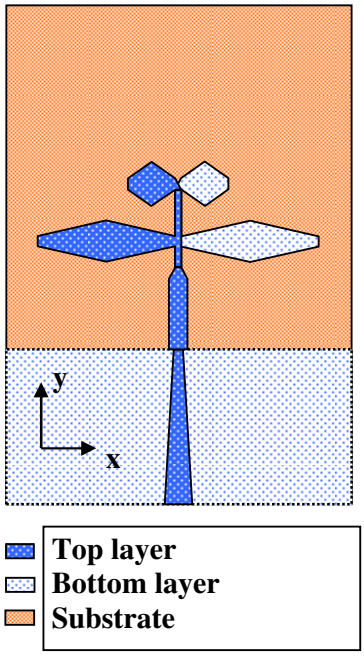

FIGURE 3.1: The upper level of the single-element.

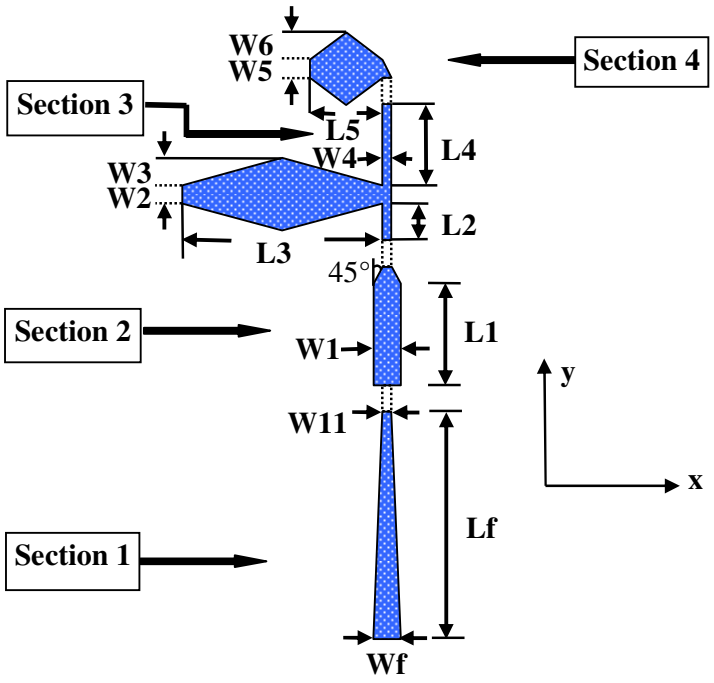

FIGURE 3.2: The upper layer of the antenna element showing the design parameters.

The truncated planar ground plane that acts as a reflector was printed on the lower layer of the substrate. The antenna was designed to be connected to a 50 Ω coaxial cable by means of a tapered microstrip line. This part of the geometry is indicated in Fig. 3.2 as Section 1. Section 2 is the matching stub that is used to compensate for the transition between the microstrip line, in conjunction with the truncated ground plane and the upper and lower halves of the two dipoles. The length L2 in conjunction with L3 controls the lower operating frequency band and connects the longer rhombus-shaped dipole to the matching stub. The dimension L2 was found to be detrimental to the bandwidth covering the 2.4 GHz band. L4 connects the two dipoles and plays a crucial role on the reflection coefficient levels between the two frequency bands. The length L5 is used to control the upper frequency band and is connected to the microstrip line with the width W4, via a mitered trapezoid section as indicated in Fig. 3.2.

The rhombus shape plays a key role in this design and has the advantage of reducing the size of the antenna compared to normal dipole and bow-tie antennas. The shape of the dipole facilitates multi-current paths which differ in length to ensure that the bandwidth is increased by achieving densely spaced multi-resonances [9].

The effective relative permittivity was first calculated to acquire a good starting point for the two dipole lengths needed to facilitate the operations in the two WLAN bands. Most textbooks provide equations to calculate the effective relative permittivity of a stripline, microstrip and a PCB (Printed Circuit Board). The effective relative permittivity is then used further in the rest of the equations to take into account that the above-mentioned mediums are inhomogeneous, where the electric fields exist not only in the dielectric but also in the air [43]. The inhomogeneous medium is thus replaced by a homogeneous medium with an effective relative permittivity. Eq. (3.1) is usually used to calculate the effective relative permittivity for a microstrip line. This was only used to obtain a rough estimate of the effective relative permittivity, since there is no ground present below the two parallel dipoles. The approximate effective relative permittivity was in turn used to calculate the half wavelengths at the two centre frequencies as starting points for the design.

$$\varepsilon_r' = \frac{\varepsilon_r + 1}{2} + \frac{\varepsilon_r + 1}{2} \frac{1}{\sqrt{1 + 10\frac{h}{w}}} \tag{3.1}$$

The symbols h and w represents the height of the substrate and the width of the strip respectively. The strip width was taken as 1.8 mm, which was the chosen width for W4. The effective relative permittivity was calculated to be equal to 2.697.

The lengths L3 and L5 pertaining to the long and short dipole respectively, which control the two main resonances, were determined with Eq. (3.2) and Eq. (3.3). The symbols f_{c1} and f_{c2} represent the two centre frequencies of the respective bands.

$$L3 = \frac{1}{2} \times \frac{3 \times 10^8}{f_{c1}\sqrt{\varepsilon_{eff}}} \tag{3.2}$$

$$L5 = \frac{1}{2} \times \frac{3 \times 10^8}{f_{c2}\sqrt{\varepsilon_{eff}}} \tag{3.3}$$

The widths W1 and Wf were determined with the aid of LineGauge, a software package that provides the user with a good estimate for the dimensions needed to obtain a 50 Ω microstrip line for the initial design.

The simulations were conducted with the aid of the commercial software package CST Microwave Studio® and the measurements were taken at the Compact Antenna Range of the University of Pretoria. In order to optimize the design in terms of bandwidth, a parameter study was conducted to determine the effect of each dimension on the reflection coefficient.

3.1.2. Parameter study

The microstrip feedline was the first dimension to be modified to ensure that the antenna can be matched to a 50 Ω coaxial cable. This was done by making use of a tapered microstrip line. The effect that the lengths L1, L2 and L4 have on the reflection coefficient was used to optimize the design even further. The design presented in [9] used a substrate with a very high permittivity, which resulted in an antenna with practical dimensions and

thus a compact structure. The dimension L1 given in [9] was approximately equal to one wavelength at the centre frequency of the band. The initial modified design that delivered promising results made use of a feedline with the length equal to half a wavelength to reduce the overall size of the antenna. The other two dimensions were also adjusted to compensate for the use of a substrate with a lower permittivity. The rest of the dimensions used in the initial design can be seen in Table 3.1, with the size of the overall structure equal to 69 x 71 mm^2. These dimensions were used as a starting block for the parameter study.

TABLE 3.1: Antenna dimensions.

L1	L2	L3	L4	L5	Lf	W1	W11	W2	W3	W4	W5	W6	Wf
4.7	1.0	24.7	5.7	7.2	38	1.9	1.8	5.4	3.6	1.8	3.6	1.8	1.8

The effect of each parameter was ascertained separately in order to understand the role that each dimension has on the performance of this design. The reflection coefficient was computed to facilitate the optimization of the element in terms of bandwidth. The "L" parameters were first scrutinized to improve the design.

The length L1 was adjusted from 4.7 mm to 19 mm, which is approximately quarter a wavelength at the lower band's centre frequency. Fig. 3.3 shows that the lower limit of the 5.2 GHz band shifted left and therefore increased the bandwidth, while increasing the level of the reflection coefficient in general over the band. The reflection coefficient level was also increased over the 2.4 GHz band, while the width of the lower band remained almost the same.

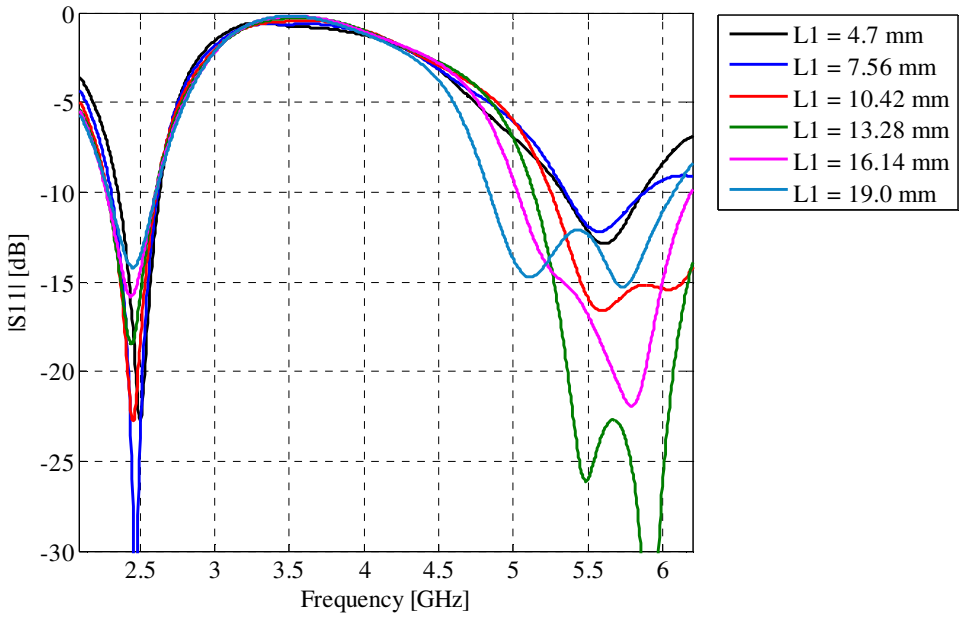

FIGURE 3.3: The effect of the dimension L1 on the reflection coefficient.

The dimension L2 plays a prominent role in the realization of the upper frequency band and was varied from 1 mm to 4.3 mm. This is shown in Fig. 3.4, where the increase of L2 also increased the bandwidth over the 5.2 GHz band by lowering the reflection coefficient level and shifting the band to the left. This ensured that the desired frequency range was covered. The bandwidth covering the 2.4 GHz band was also increased, where the upper limit was shifted to the right.

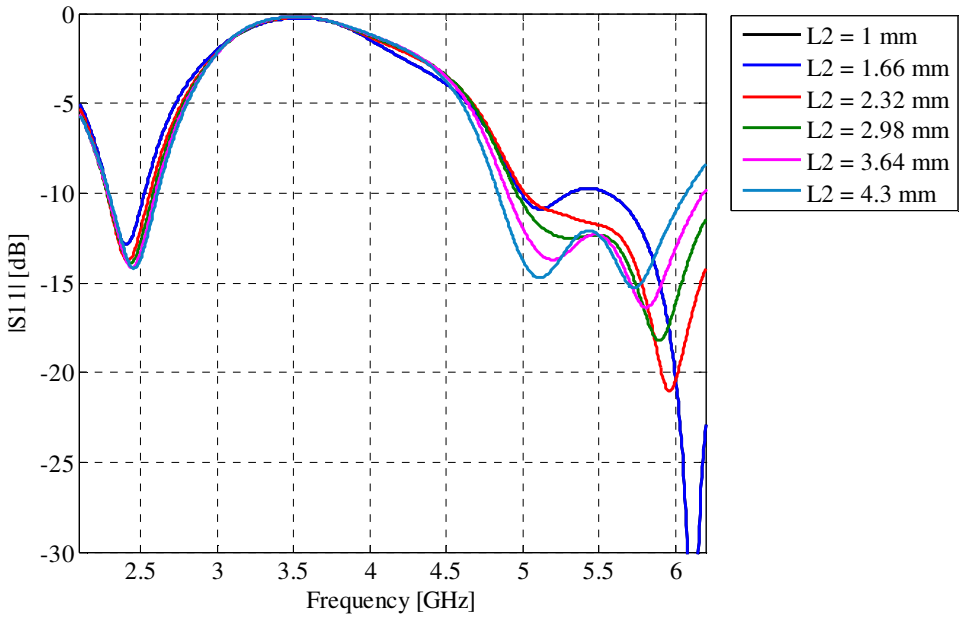

FIGURE 3.4: The effect of the dimension L2 on the reflection coefficient.

The parameter L4 was also adjusted and was varied from 3.7 mm to 7.7 mm. As shown in Fig. 3.5, the reflection coefficient level over the lower band increased with an increase in the length L4. This tendency can be seen over the 5.2 GHz band.

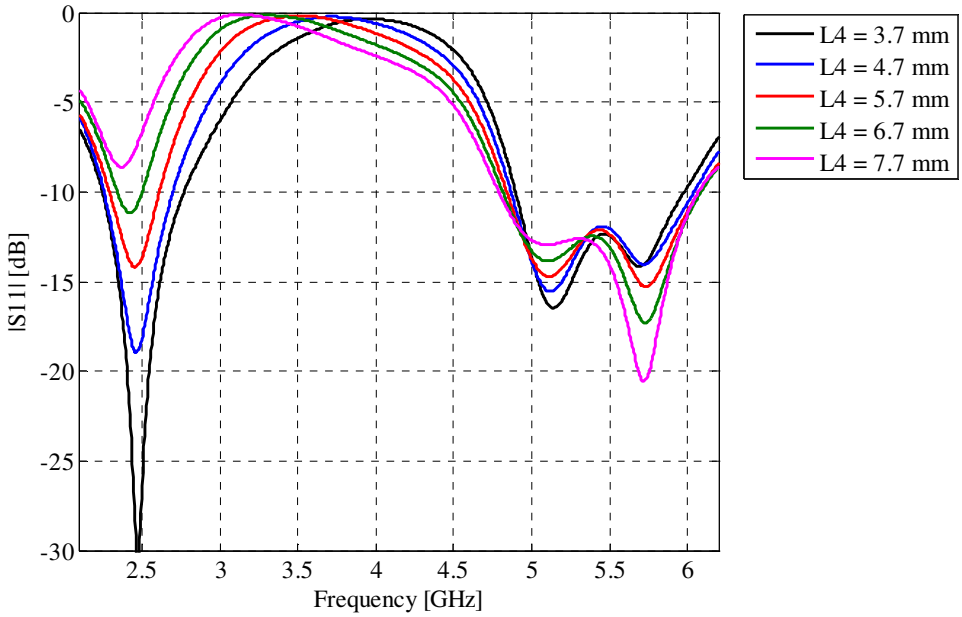

FIGURE 3.5: The effect of the dimension L4 on the reflection coefficient.

The lengths L3 and L5 were not only adjusted to ensure that the right frequency bands were obtained, but also to make sure that the standard WLAN bands were adequately covered. As shown in Fig. 3.6, the length of L3 only has an effect on the lower frequency band. The increase of L3 shifted the limits of the 2.4 GHz band to the left of the frequency spectrum, as expected.

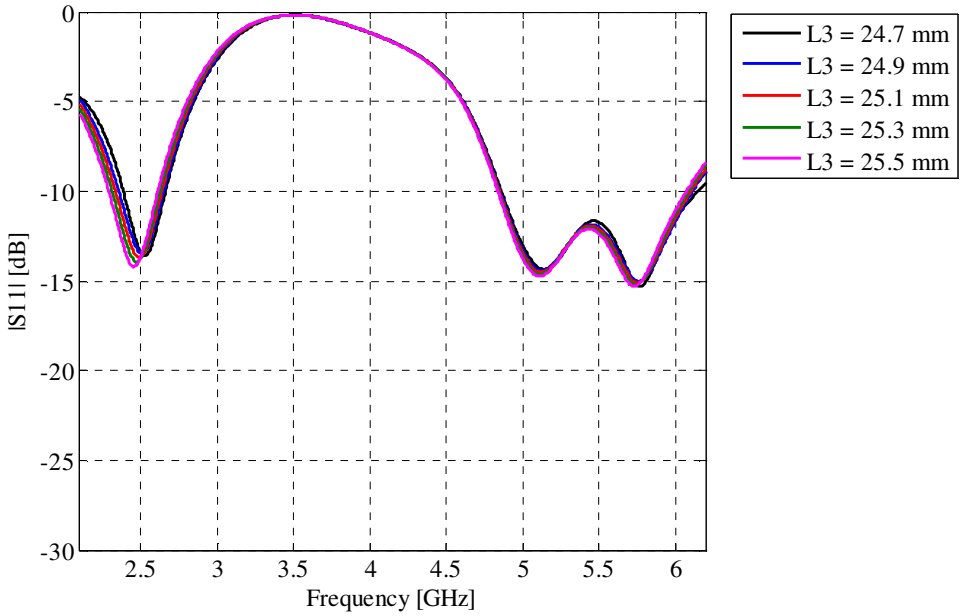

FIGURE 3.6: The effect of the dimension L3 on the reflection coefficient.

Fig. 3.7 gives a clear indication of the important role that the length L5 plays in the bandwidth of the upper frequency band. It can be seen that an increase in the length of L5 lowers the reflection coefficient level over the 5.2 GHz band, but has a reducing effect on the bandwidth of the 2.4 GHz band. The reduction over the lower band was relatively minor compared to the effect that the increase of L5 had on the upper band.

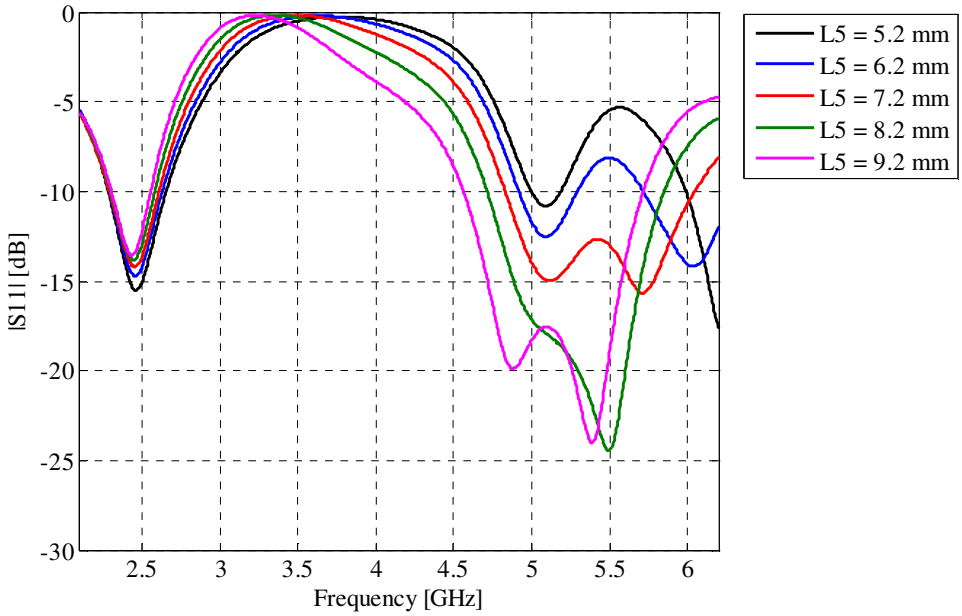

FIGURE 3.7: The effect of the dimension L5 on the reflection coefficient.

The effect that the "W" parameters have on the bandwidth was also ascertained. The widths associated with the symbols W1 and Wf were reduced to ensure that the microstrip feedline was able to be connected to the standard 50 Ω coaxial cable. The width W11 was reduced to create a tapered microstripline, which was more suited for this design. Fig. 3.8 shows that by reducing W11 lowers the reflection coefficient level over the 2.4 GHz band and also delivers the widest bandwidth over the 5.2 GHz band.

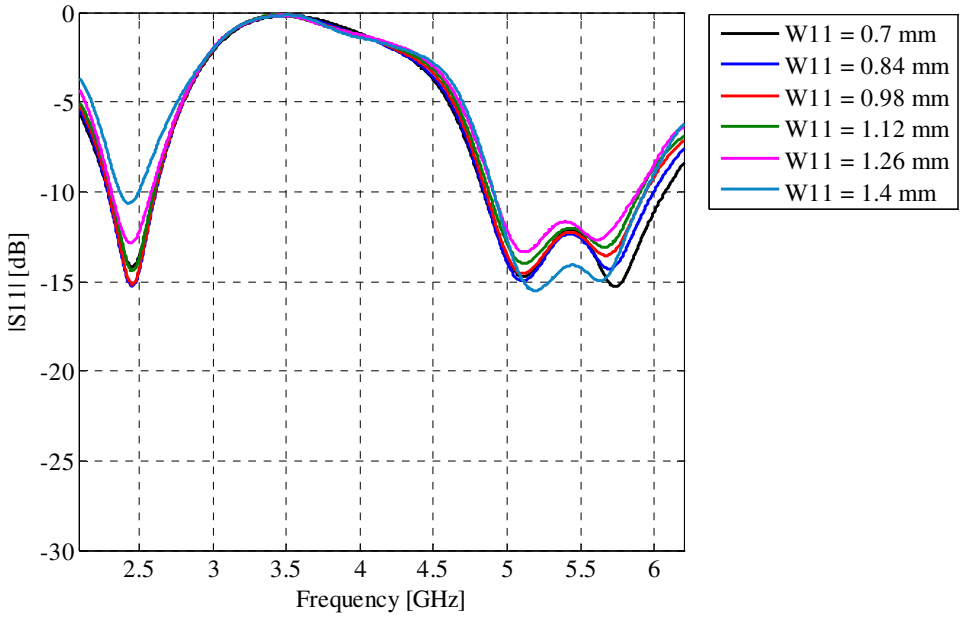

FIGURE 3.8: The effect of the dimension W11 on the reflection coefficient.

The width W1, the dimension pertaining to Section 2 was also adjusted to visually determine the effect that the width of the matching stub has on the overall performance of the antenna in terms of bandwidth. The reflection coefficient level increased over the 2.4 GHz band and decreased over the 5.2 GHz band by decreasing the width W1. A narrower matching stub was chosen for this design, to obtain an adequate bandwidth over the upper frequency band.

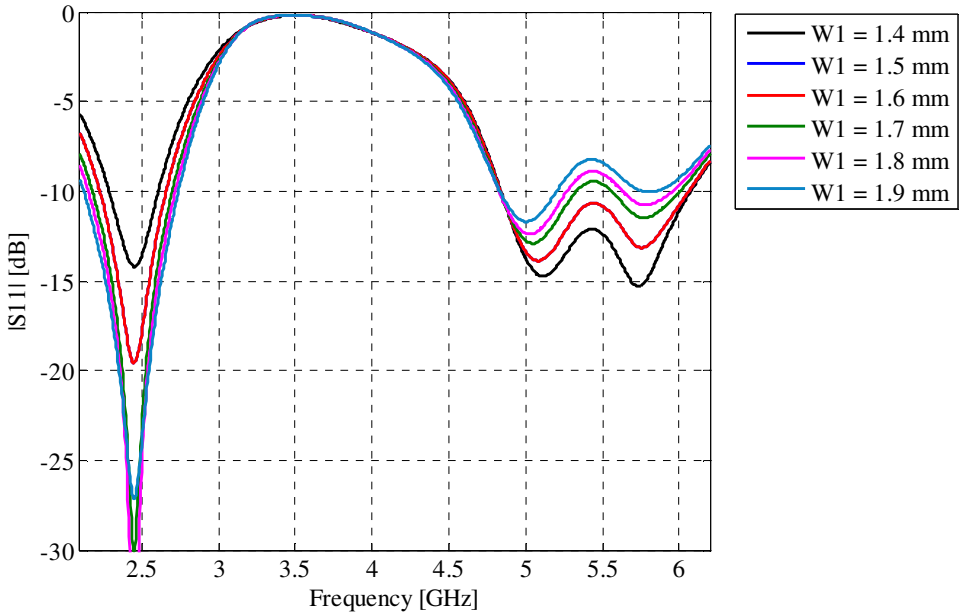

FIGURE 3.9: The effect of the dimension W1 on the reflection coefficient.

The width W2 was reduced from 5.4 mm to 4.2 mm, as well as the width W3, which was also reduced from 3.6 mm to 2.8 mm. The reduction of the width W2 delivered opposing results over the two frequency bands. The reflection coefficient level over the first band was lower due to the reduction of the width W2, while the reflection coefficient level increased over the second band. The narrower width was chosen to ensure that the required bandwidth over the first band was attained. As shown in Fig. 3.11, the reflection coefficient level increased with the reduction of the width W3 and decreased over the second band, especially around the frequency of 5.8 GHz.

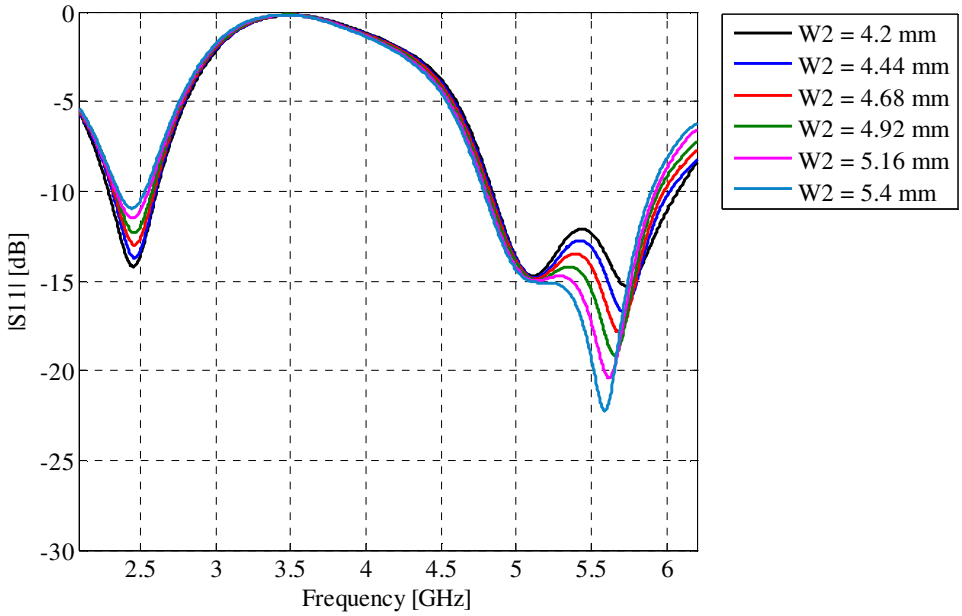

FIGURE 3.10: The effect of the dimension W2 on the reflection coefficient.

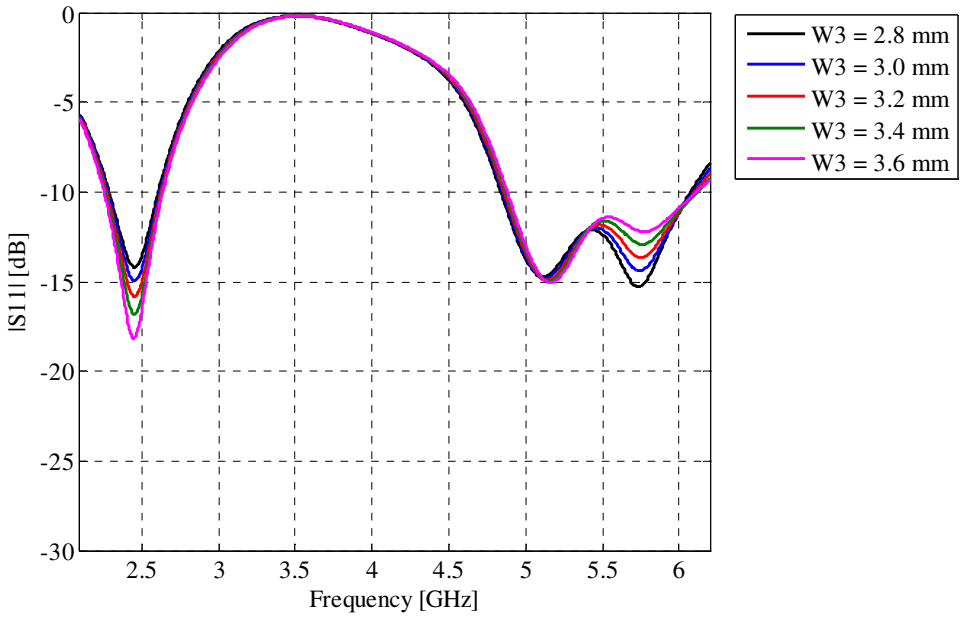

FIGURE 3.11: The effect of the dimension W3 on the reflection coefficient.

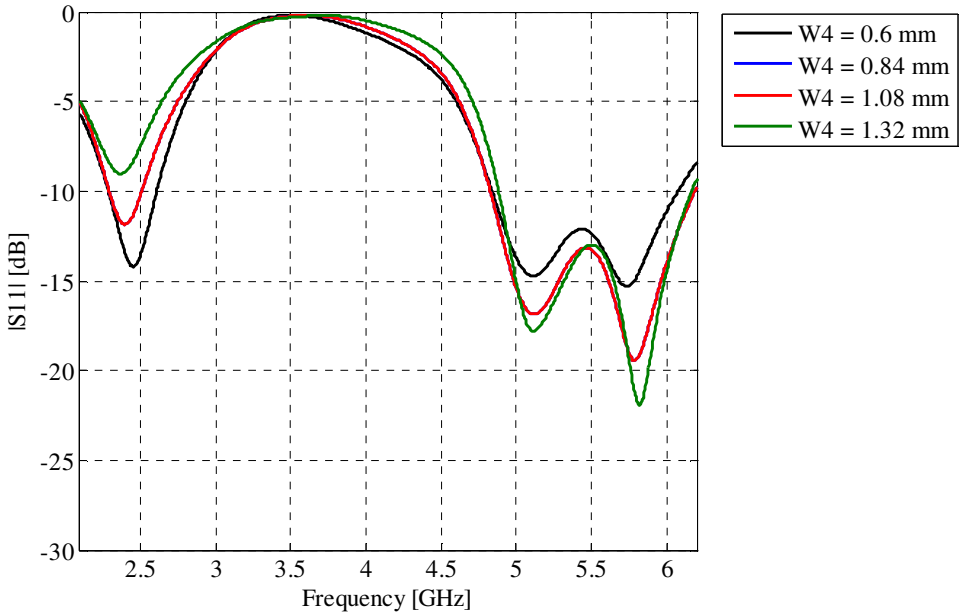

FIGURE 3.12: The effect of the dimension W4 on the reflection coefficient.

As seen from Fig. 3.12, by increasing the width of W4 the bandwidth of the 2.4 GHz band was totally annihilated, whereas the reflection coefficient level over the 5.2 GHz band was lower compared to the wider width. The width W5 has little effect on the second frequency band as seen in Fig. 3.13, but the increase in the width W5 has a negative effect on the reflection coefficient level over the first frequency band.

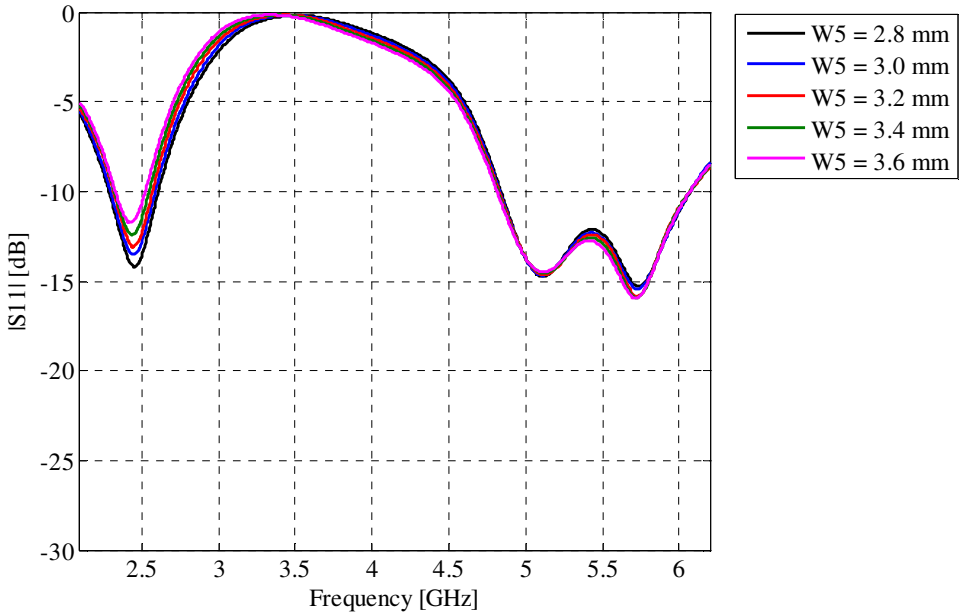

FIGURE 3.13: The effect of the dimension W5 on the reflection coefficient.

As shown in Fig. 3.14, the adjustment of width W6 has no visible effect on the performance of the antenna, in terms of the reflection coefficient level and also on the bandwidths over the 2.4 GHz and the 5.2 GHz bands.

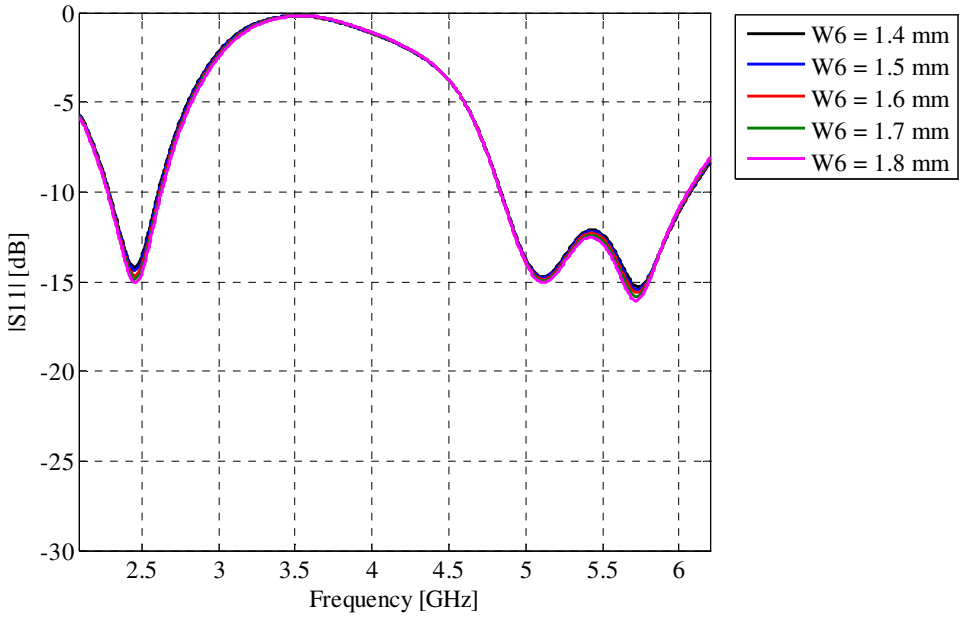

FIGURE 3.14: The effect of the dimension W6 on the reflection coefficient.

The results obtained from the parameter study was incorporated into a new design with the new dimensions given in Table 3.2, with the size of the overall structure equal to 90 x 96 mm^2. The design that proliferated out of the parameter study was used further in the development of the final single-element design, as well as for the two- and four-element arrays.

TABLE 3.2: Antenna dimensions.

L1	L2	L3	L4	L5	Lf	W1	W11	W2	W3	W4	W5	W6	Wf
19	4.3	25.5	5.7	7.1	39	1.4	0.7	4.2	2.8	0.6	2.8	1.4	1.4

3.1.3. The most influential parameters

The distance between the planar ground and the first dipole, defined by the combination of L1 and L2 played an extremely important role in terms of achieving the required bandwidths over both bands. The increase in distance led to wider bandwidths, with L1

having the most significant effect on the 5.2 GHz band. A trade-off was seen with the width of the matching stub (W1), where a centre value was chosen to optimize both bandwidths. The decrease in the width W4 improved the match between the antenna components. This effect was discernibly clear over the 2.4 GHz band. The length L4, which constitutes the distance between the lower and upper dipole, also had a major effect on the 2.4 GHz band's bandwidth. By placing the two dipoles closer to each other, the bandwidth increased. The main resonances were achieved by adjusting L3 and L5, to cover the specified bandwidths. The dimensions defining the widths of the dipoles (W2 – W6) had a minor influence on the bandwidths. All of the dimensions were chosen to firstly, increase the bandwidth, and secondly to minimize the substrate height. As mentioned in [9], the stability of the radiation patterns at the higher frequencies depends on the substrate height. The height should not be significantly larger compared to the free space wavelength at the higher frequencies. The substrate height was still within bounds, but can be reduced by making use of a higher permittivity substrate. The overall size of the antenna, as well as the substrate height, can be reduced by implementing the design on a substrate with a higher dielectric constant. The size of the element reduces by the square root of the dielectric constant. One of the major considerations during the design process was to develop a relatively inexpensive antenna and therefore, a middle way was taken to ensure that the design adheres to the economical demands of this dissertation. A high quality substrate was thus selected and the design was created to operate optimally with the specified characteristics of the chosen substrate.

3.1.4. Final design parameters

It was seen from the simulated H-plane field patterns at the higher frequencies that the boresight gain was not always the peak gain as expected. This was due to the influence of the longer dipole on the shorter dipole, where the length L4 connects the two parallel dipoles. The short length of the parameter L4 has a negative effect on the radiation patterns and in particular in terms of the location of the peak gain. The lengthening of L4 on the other hand has a negative effect on the bandwidth. The non-ideal spacing between the two dipoles was compensated for by adding a passive director to the design, which is usually associated with antennas such as the quasi-Yagi antenna. The boresight gain of the antenna was improved without reducing the bandwidth achieved with this adjustment. The passive director was applied to the single-element design. The shape of the short dipole, which was

responsible for the higher frequency band, also had to be changed into a rectangle, in order to achieve the desired effect in conjunction with the director. The upper band proved to be inherently wide and therefore, had the capacity to sacrifice some of the bandwidth achieved with the rhombus shape in order to implement this design. This design can be seen in Fig. 3.15, with the antenna dimensions given in Table 3.3.

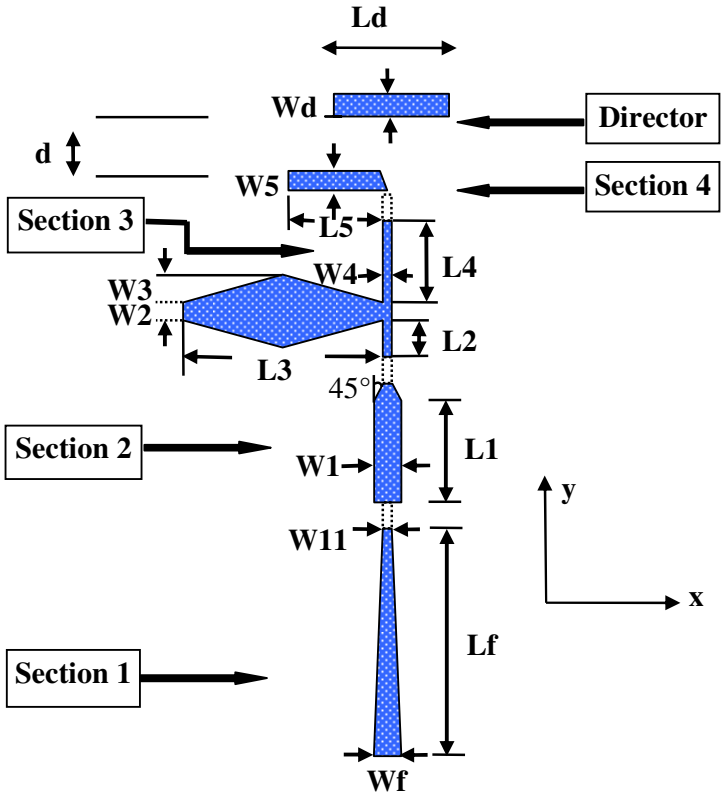

FIGURE 3.15: The upper layer of the single-element showing the design parameters.

TABLE 3.3: Antenna dimensions.

L1	L2	L3	L4	L5	Lf	Ld	W1	W11	W2	W3	W4	W5	Wf	Wd	d
19	4.3	25.0	3.0	9.5	39	17	1.4	0.7	4.2	2.5	0.6	2.5	1.4	1.0	3.5

This modification not only improved the gain of the antenna, but also the bandwidths associated with each frequency band. This can be seen in Fig. 3.16, where the inclusion of the passive director (red graph) lowered the reflection coefficient level and clearly shifted the left limit of the upper frequency band and thereby increasing the overall bandwidth.

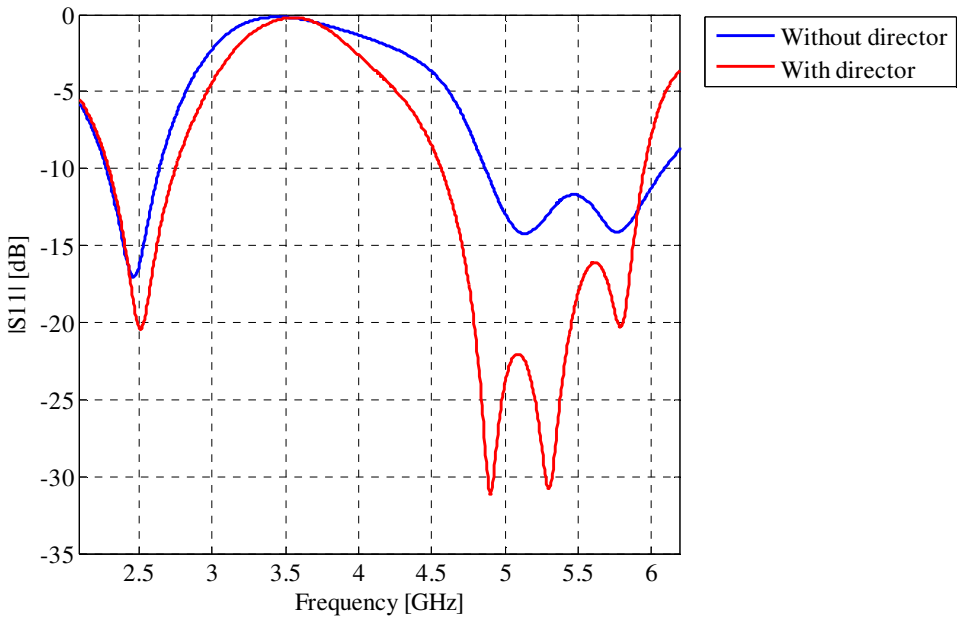

FIGURE 3.16: The effect of the director on the reflection coefficient.

The most prominent effect of the passive director was seen at the higher frequencies as indicated in Fig. 3.18, where the red graph represents the improved radiation patterns. The same tendency was seen at the lower frequencies as shown in Fig. 3.17, but not with the same degree of improvement as seen at 5.55 GHz. The main goal was to improve the radiation patterns at the higher frequencies and this modification allowed this objective to be realized. The different simulated gains achieved without and with the director can also be seen in Figs. 3.19 and 3.20, which corroborate the radiation patterns seen in Figs. 3.17 and 3.18. As seen with the latter mentioned graphs, the most discernible improvement was achieved over the 5.2 GHz band. The close proximity of the long Rhombus shaped dipoles to each other was responsible for the slightly less increase in gain over the 2.4 GHz band compared to the increase seen over the higher band. The main focus was to obtain the widest possible bandwidth while maintaining adequate gain, where the emphasis was on the bandwidth. Thus according to the value system the bandwidth was the main determining factor on which further design decisions were based. The bandwidth of the optimized design with the director improved from 13.7% to 17.9% over the first band and from 22.4% to 26.4% over the second band. This is shown in Fig. 3.16.

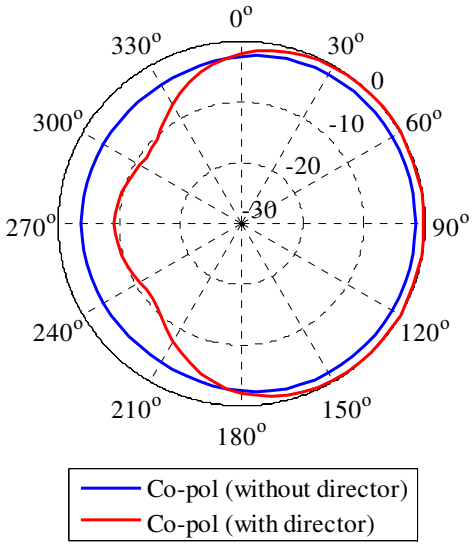

FIGURE 3.17: The simulated radiation pattern with and without the passive director at 2.44 GHz in the H-plane.

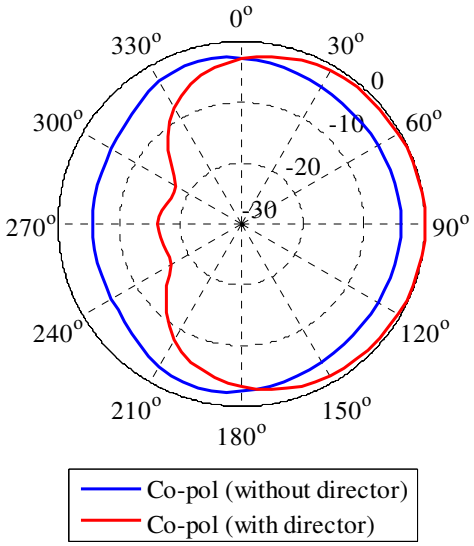

FIGURE 3.18: The simulated radiation pattern with and without the passive director at 5.55 GHz in the H-plane.

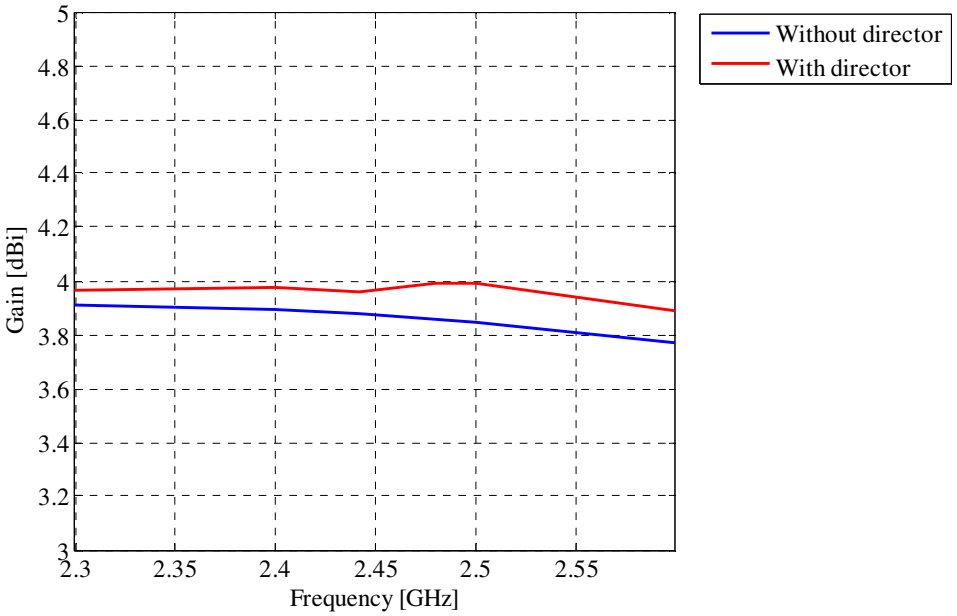

FIGURE 3.19: The simulated gain over the 2.4 GHz band.

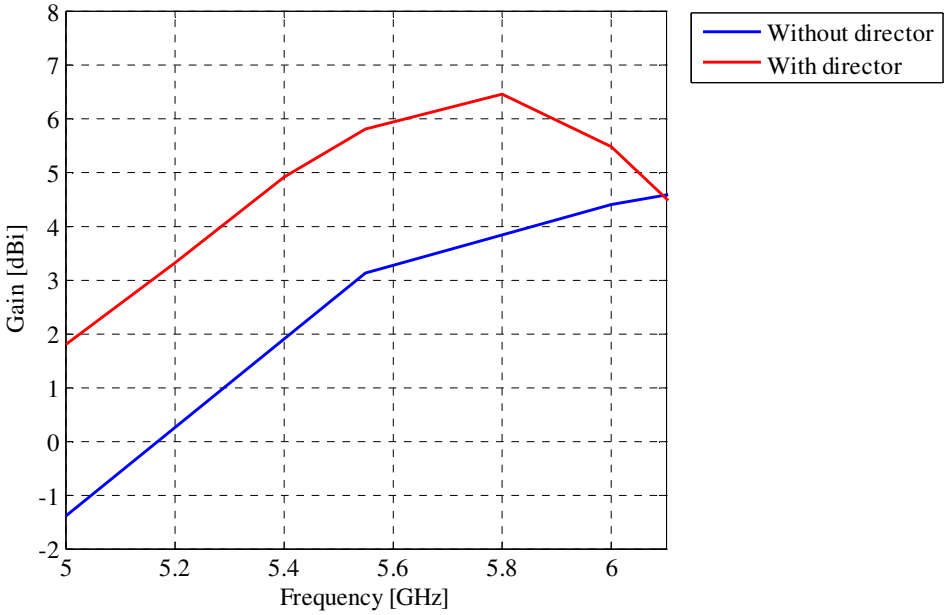

FIGURE 3.20: The simulated gain over the 5.2 GHz band.

The performance of the various designs was also compared in terms of their 3 dB beam widths, front-to-back ratios (F-to-B) and the maximum cross-polarization (X-pol.) levels within the main lobe. The far field radiation properties can be seen in Table 3.4.

TABLE 3.4: Far field radiation properties.

Antenna	f (GHz)	3dB beam width		F-to-B ration (dB)	X-pol. Levels (dB)	
		E-plane	H-plane		E-plane	H-plane
Without director	2.44	85.1º	195.4º	8.9	-30.0	-18.5
	5.55	43.6º	73.2º	9.4	-24.8	-11.5
With director	2.44	84.7º	194º	9.1	-30.4	-19.1
	5.55	58.3º	178.8º	15.1	-28.9	-14

3.1.5 Conclusion

The designs presented in the above section were compared, in order to select the best design in terms of bandwidth and gain, while taking into account the 3 dB beam width, F-to-B ratio and cross-polarization levels as secondary priorities. The design that incorporated the dimensions determined through the parameter study and the passive director proved to be superior in terms of bandwidth, 3 dB beam width and cross-polarization levels, with the F-to-B ratio 3 dB less compared to the initial "trial and error" design. The gain of the final optimized design, that incorporated a director to compensate for the lack of directivity, proved to be slightly less than the initial "trial and error" design with the narrower bandwidth. The gain over the second band surpassed the initial design from 5.5 GHz to 6 GHz.

The wide bandwidths of 17.9% and 26.4% over the 2.4 GHz and 5.2 GHz bands respectively of the final optimized design with the director, together with good radiation patterns, proved to be the best candidate for the two-element, as well as the four-element arrays. The average gain of 4 dBi over the first and second band was an improvement compared to the 3.9 dBi and 1.9 dBi of the optimized design without the director, over the respective bands with the major contribution made over the second band. The average gain of the initial "trial and error" design over the two bands were 4.8 dBi and 5.4 dBi and although the last design achieved lower averages, the bandwidth improvement from 7.5% to 19.6% and from 17.9% to 26.4% made up for the sacrifice of 0.8 dBi and 1.4 dBi over the 2.4 GHz and 5.2 GHz bands. All in all, the optimized design with the director exhibited characteristics suited for the next step in the design process, while addressing all the trade-offs seen with each design.

3.2. TWO- AND FOUR-ELEMENT ARRAY DESIGNS

3.2.1 Two-element array geometry and parameters

The two-element configurations were assembled by combining the two single-elements that incorporated a passive director and proliferated out of the results obtained through the parameter study, in order to ultimately design a four-element configuration that adheres to all the prerequisites stated in Chapter 1. As seen from Fig. 3.20, two identical elements were used in this configuration, unlike the suggested two-element design presented in [9], where the two elements were mirrored and thereby reducing the cross-polarization pertaining to the array. The main goal of this design was however to provide a configuration that can be fed by a single port. This can only be achieved by making use of a 180º phase shift at the second port to ensure that the surface currents are in the same direction. This will require a half wavelength delay that can only be tailored for one of the frequency bands, while the radiation patterns further away from the design frequency will deteriorate. The reduction in cross-polarization was thus not substantial enough to justify the effort in achieving the above described modifications.

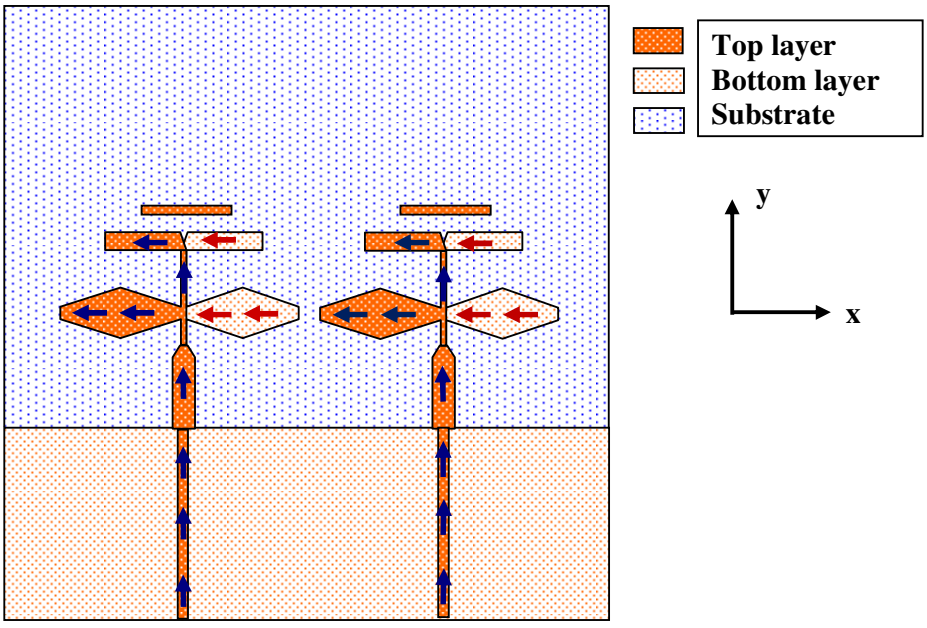

FIGURE 3.21: The two-element configuration with the respective surface currents.

The first step was to choose an appropriate distance between the two elements to minimize the coupling, which might cause anomalies within the specified frequency bands [9], but at the same time provide the most compact structure. The two-element design presented in Fig. 3.21 was thus simulated using CST Microwave Studio® and the distance between the centres of the two elements was chosen to be equal to 58 mm. This distance is equal to $0.44\lambda_0$ at 2.3 GHz, the lower limit of the first frequency band and equal to $1.13\lambda_0$ at 5.85 GHz, the upper frequency limit of the 5.2 GHz WLAN frequency band. Fig. 3.22 shows the coupling between the two elements, where the highest S21 was exhibited over the first frequency band and was equal to -12.8 dB, which was still within reasonable limits. The average coupling across both frequency bands proved to be as low as -29.2 dB.

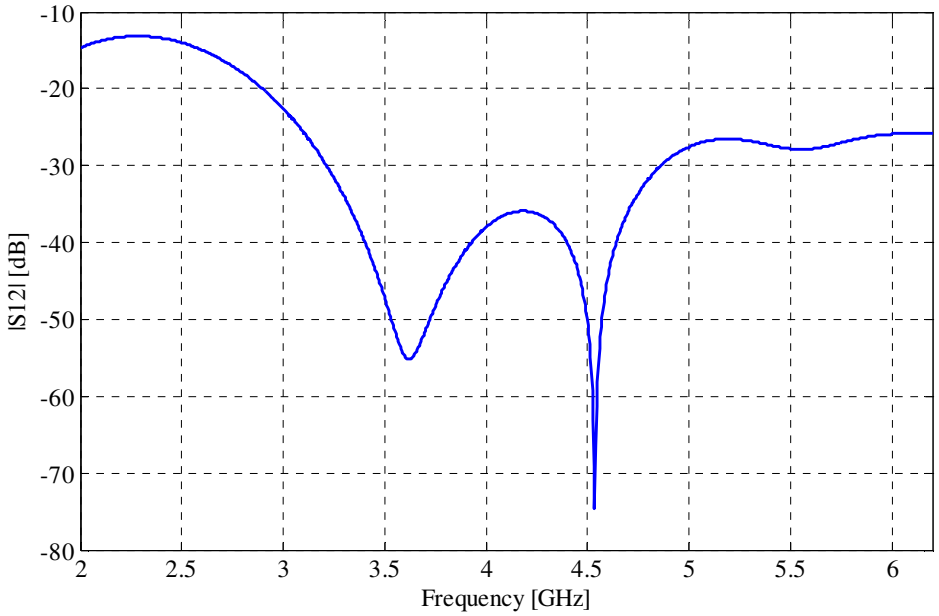

FIGURE 3.22: The simulated coupling between the elements.

The next objective was to design a balanced feed capable of combining two elements, while keeping in mind the final product, the four-element array. The first obstacle was the fact that the option of using a centre fed microstripline, which in the end combines the two 100 Ω feedlines of each element, was not feasible. This was due to the negative effect that the second substrate of the second two-element array together with the overlapping of the two primary 50 Ω feedlines would have on the overall performance of both two-element arrays. This complication was overcome by making use of an off-centre feed configuration, where an extra length of line was added to provide a balanced feed. A further adjustment

was necessary to avoid the overlapping and touching of the ground planes and the respective feeding lines. A square of 5 by 5 mm^2 was thus cut from the ground plane to prevail with this specific configuration. The cut was done in accordance with the height of the horizontal section of the feedline pertaining to the second two-element array configuration. A second modification was also necessary, in order to facilitate the realization of the pinnacle of this dissertation, the four-element array. The final array entails the combination of two similar arrays with minor differences, with the two substrates orthogonally inserted through each other. Slits from above and below, with the width equal to the substrate thickness, thus needed to be made to ensure that no feedline was cut in the process, as well as providing an adequate ground plane for each array. The 1st two-element configuration can be seen in Fig. 3.23, with the 2nd configuration presented in Fig. 3.24. The 2nd configuration had to be implemented with a lower feed, in order to ensure that there was no overlapping of the two feedlines. It was also essential to strive in achieving approximately the same results in terms of bandwidth, gain and other radiation pattern characteristics with both arrays, in order to provide both polarizations with the same antenna characteristics.

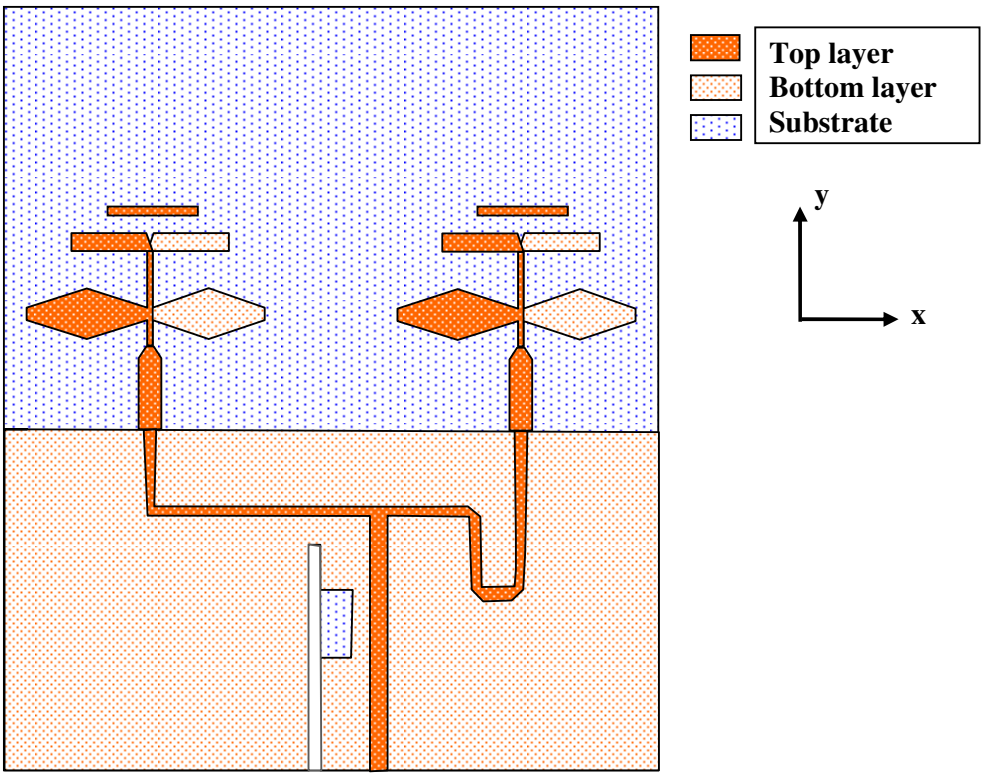

FIGURE 3.23: The 1st two-element configuration.

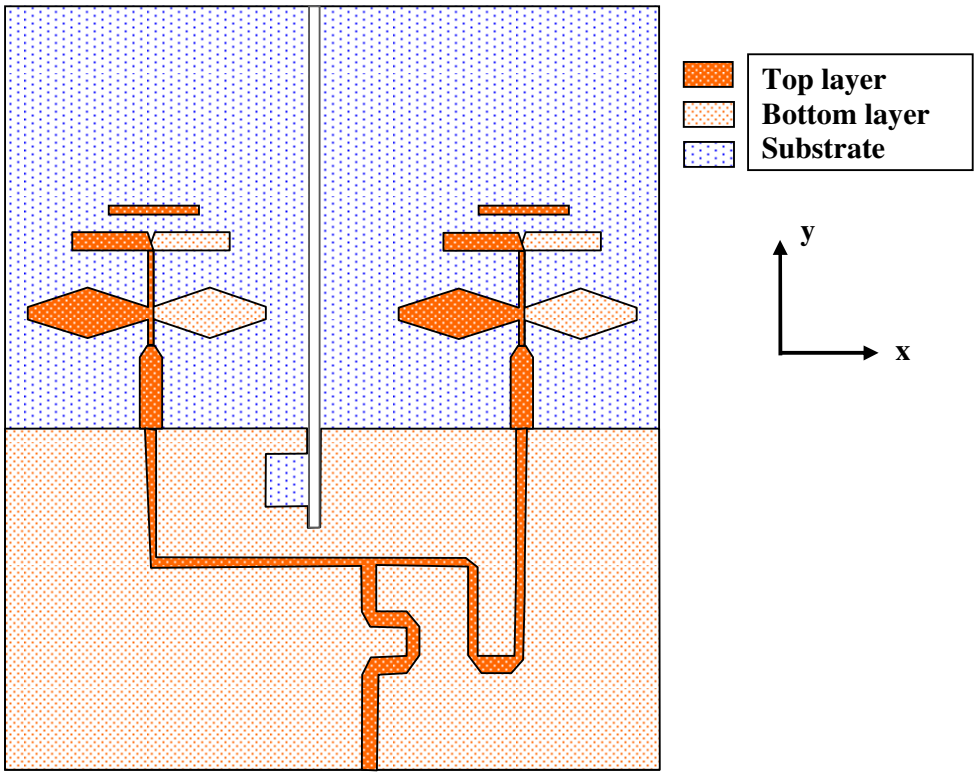

FIGURE 3.24: The 2nd two-element configuration.

The extra dimensions associated with the feeds of the above configurations can be seen in Fig. 3.25, with the dimensions summarized in Table 3.5 in mm. The width of both feedlines at the base of the Section 2, the matching stub as seen in Fig. 3.15, was equal to 0.7 mm, the width pertaining to W11 as seen in Table 3.3. The width of the horizontal section that combines the two elements was equal to 0.6 mm, with the vertical section of the feed equal to Wf. Sections Lt1 and Lt2 were also slightly tapered as seen in Figs. 3.23, 3.24 and 3.25. The lower cut through the first substrate was equal to 32 mm and the upper cut through the second substrate was equal to 69.3 mm.

Table 3.5: Feed dimensions.

Ls	Le	Lt1	Lt2	Lh	Lu1	Lu2	Lv1	Lv2	We	Wu
44.3	8.9	6.6	18.6	37.8	6.8	11.3	37.7	25.7	4.6	3.7

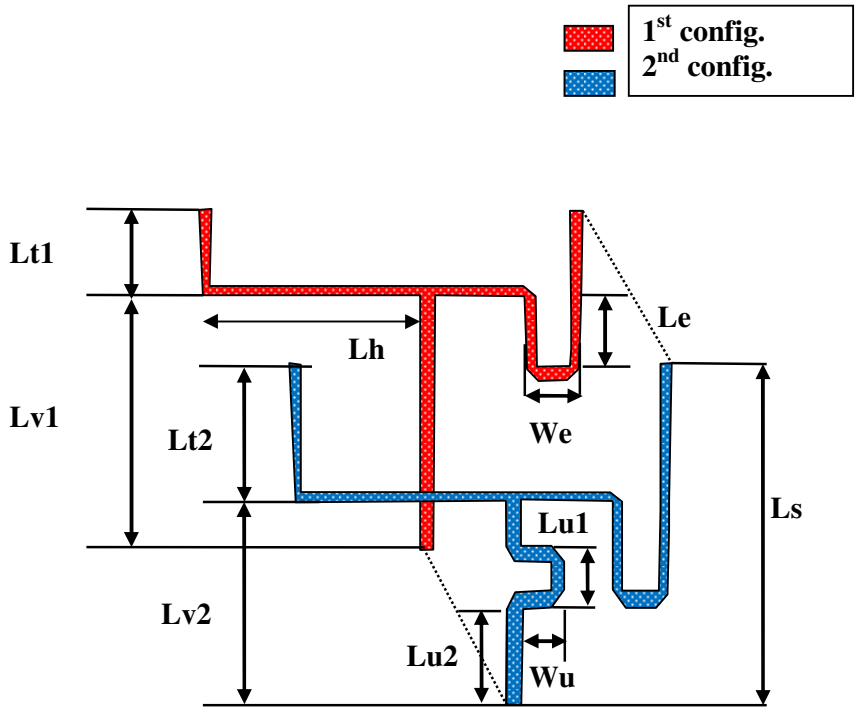

FIGURE 3.25: The geometry and parameters pertaining to each feed configuration.

3.2.2 Comparisons between the two configurations

The two different arrays were simulated separately with the respective slits in the substrates, as well as in the ground plane from below and above as seen in Figs. 3.23 and 3.24. The size of the various configurations still allowed very accurate simulations to be run with the meshing equal to 35 lines/λ. The calculated reflection coefficient of both configurations proved to be within the defined specifications and compared well to each other. This can be seen in Fig. 3.26. The 1st configuration was implemented with the longer straight off-centre microstripline feed and exhibited bandwidths equal to 23.8% (2.11 – 2.68 GHz) and 29.9% (4.46 – 6.03 GHz) over the 2.4/5.2 GHz bands respectively. The 2nd configuration was implemented with the horizontal section of the feed lower, which resulted in the use of a modified off-centre microstripline feed. The alteration visible in Fig. 3.24 ensured that the feedline remained the same length and with the same input impedance as used with the 1st configuration. The bandwidths achieved with the 2nd configuration proved to be slightly narrower with the first band covered from 2.29 GHz to 2.60 GHz (12.7%) and the second band covered from 4.58 GHz to 5.99 GHz (26.7%).

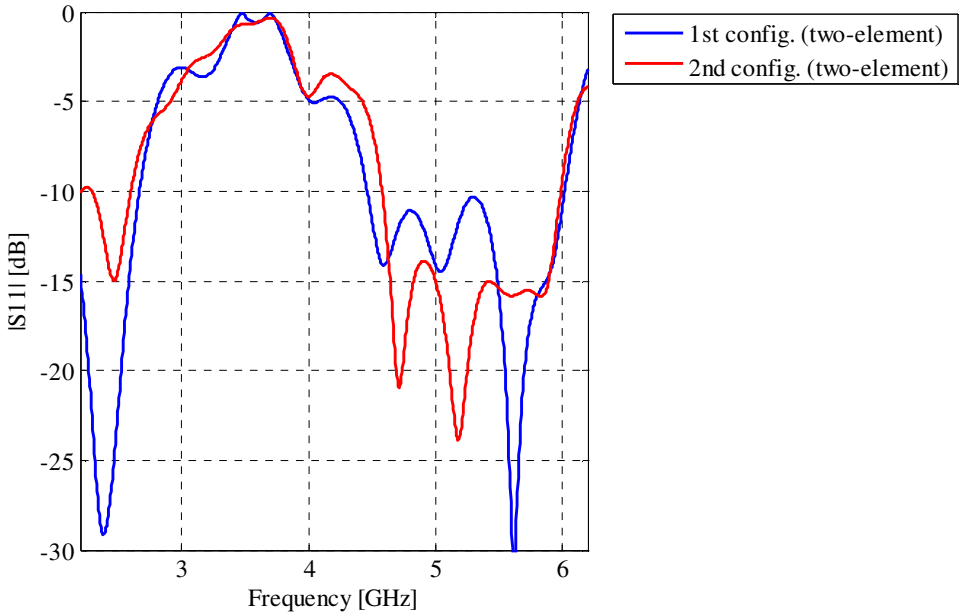

FIGURE 3.26: The simulated reflection coefficient for both configurations.

The boresight gain of the two different configurations also proved to be close to each other as seen from Figs. 3.27 and 3.28. The two-element configurations delivered average gains in the order of 5.2 dBi and 5.6 dBi over the first band and 7.6 dBi and 7.5 dBi over the second band. The improvement in terms of gain was discernibly visible between the results pertaining to the single-element and both the two-element arrays as seen in Figs. 3.27 and 3.28. The average gain of the single-element design was 4 dBi over both the 2.4/5.2 GHz bands. The increase in boresight gain over the first band was thus around 1.6 dBi and around 3.5 dBi over the second band.

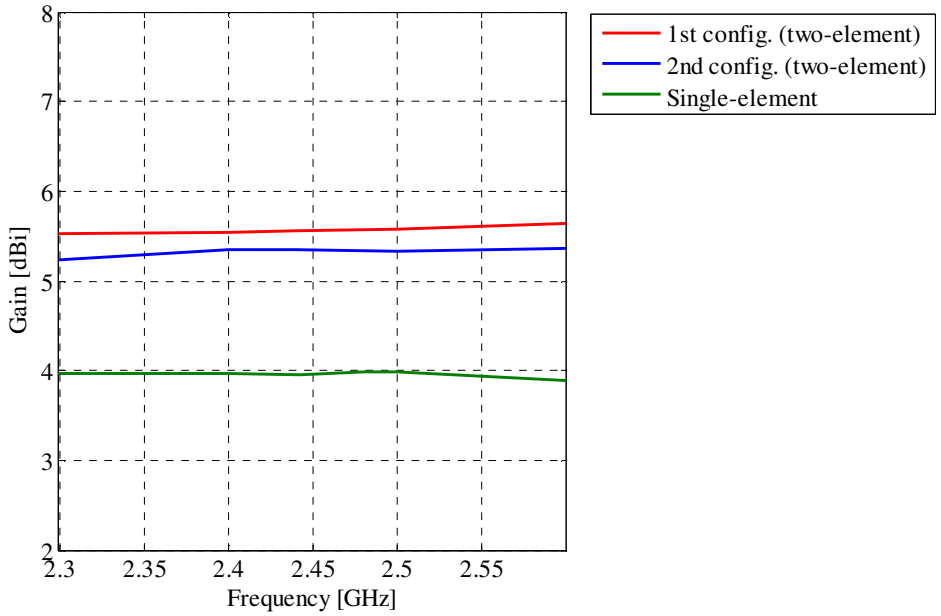

FIGURE 3.27: The simulated boresight gain of the two-element arrays and the single-element over the 2.4 GHz band.

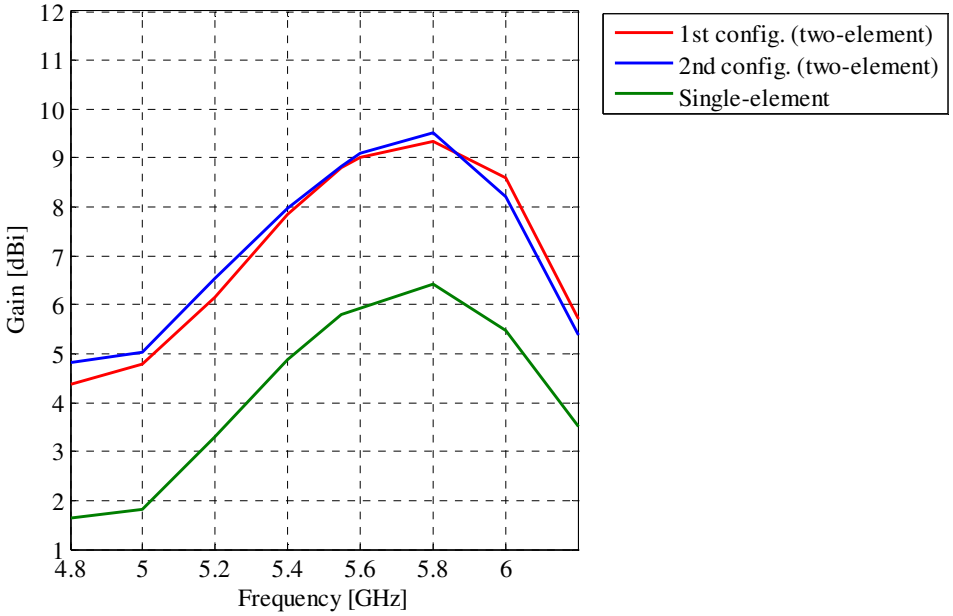

FIGURE 3.28: The simulated boresight gain of the two-element arrays and the single-element over the 5.2 GHz band.

The two different configurations were also compared in terms of their 3 dB beam widths, front-to-back ratios (F-to-B) and the maximum cross-polarization (X-pol.) levels

within the 3 dB beam width of the main lobe. The far field radiation properties were calculated at selective frequencies and can be seen in Table 3.6.

Table 3.6: Far field radiation properties of the two-element configurations.

Configuration	f (GHz)	3dB beam width		F-to-B ration (dB)	X-pol. Levels (dB)	
		E-plane	H-plane		E-plane	H-plane
1	2.44	50.6º	198.5º	8.9	-29.3	-16
	5.2	23.7º	234º	12.6	-26	-10
	5.55	24.5º	181.4º	17	-36.1	-16
	5.8	22.8º	163.5º	15.1	-30	-18.4
2	2.44	50º	205.5º	8.8	-29.3	-14.8
	5.2	25.3º	233.2º	13	-24.9	-11.1
	5.55	23.6º	178.6º	15.7	-27	-15.9
	5.8	22.9º	158.9º	14.1	-26.3	-17.6

The highest cross-polarization levels of the first design were -10 dB and -26 dB in the H-plane and the E-plane respectively, whereas the highest cross-polarization levels of the second design were -11.1 dB and -24.9 dB in the H-plane and the E-plane respectively. Similar side lobe levels were seen with the two two-element array designs, as with the single-element design. In the H-plane, the radiation patterns of both configurations were so broad that no real side lobes could be observed. The highest side lobe levels of the 1st and 2nd configuration, in the E-plane, were equal to -4.8 dB and -7.3 dB respectively, which was somewhat higher than the -9.6 dB seen from the simulated results of the single-element design. The F-to-B ratios ranged from 8.9 dB to 17 dB over the operating bands. Very good correlation was achieved between the various characteristics of each two-element array configuration.

3.2.3 Four-element array geometry and parameters

The four-element design was simulated and optimized, in order to achieve a dual-polarized array capable of operating over the two WLAN bands with adequate boresight gain. This was done, due to the growing importance of dual-polarized arrays for WLAN communication systems. As mentioned in Chapter 2, the capacity to send and receive horizontal and vertical polarizations is a very attractive feature for applications such as WLAN MIMO systems [1]. This section was dedicated to the design of a four-element array, with the above mentioned attributes. The two-element array configurations discussed

in the previous section was used in the four-element design. The assembly of the two designs can be seen in Fig. 3.29. The physical prototype can be seen in Figs. 3.30 – 3.34.

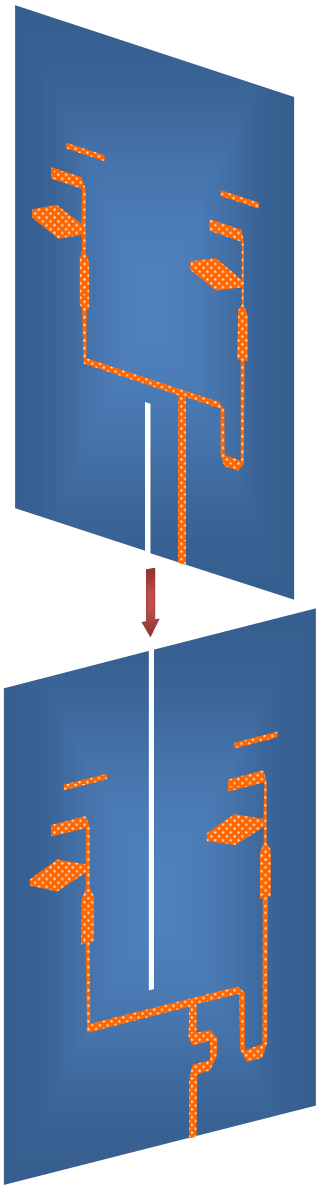

FIGURE 3.29: The assembly of the four-element configuration.

The 1st and 2nd configurations presented in the previous section were orthogonally interleaved as illustrated above, with the respective polarizations excited by separate ports. Port 1 was arbitrarily selected to represent the horizontal polarization, whereas Port 2 was excited to observe the characteristics of the vertical polarization. The 1st and 2nd configurations were thus excited by Port 1 and Port 2 respectively. The horizontal and

vertical polarized arrays were referred to as the H-Array and the V-Array respectively, from this section on.

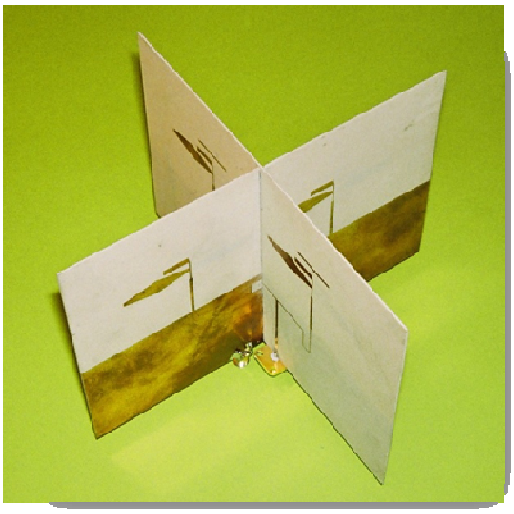

FIGURE 3.30: The top side view of the physical prototype.

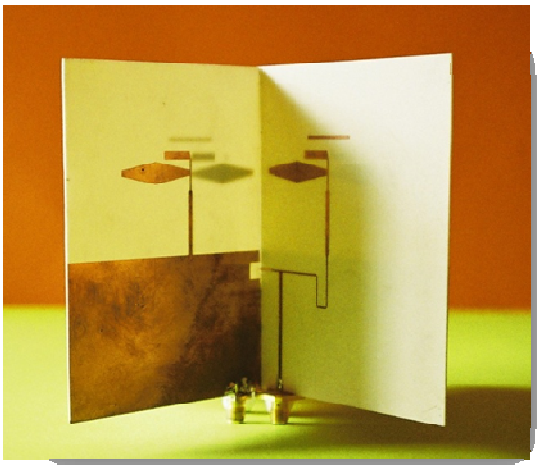

FIGURE 3.31: The one half of the back (left) and front (right) view pertaining to the horizontally and vertically polarized arrays respectively of the physical prototype.

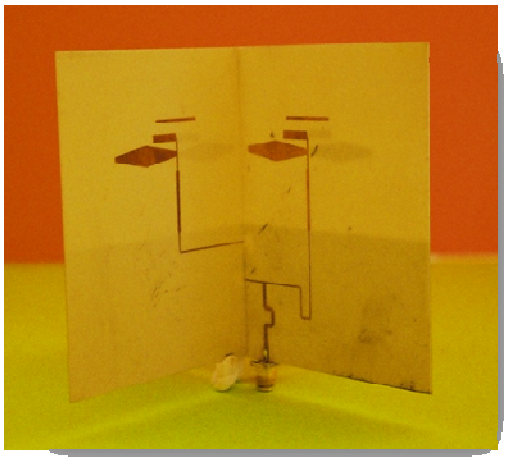

FIGURE 3.32: The one half of both the front views pertaining to the horizontally (left) and vertically (right) polarized arrays of the physical prototype.

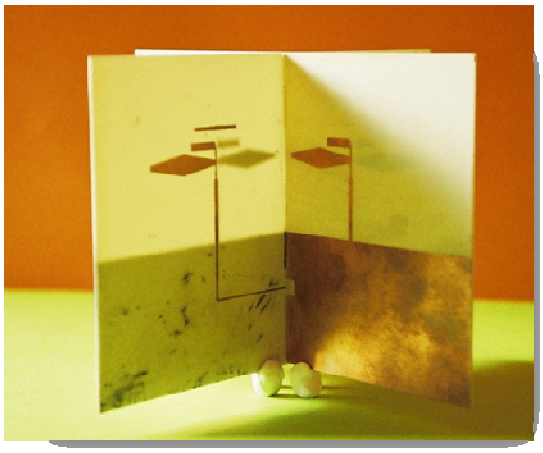

FIGURE 3.33: The one half of the front (left) and back (right) view pertaining to the vertically and horizontally polarized arrays respectively of the physical prototype.

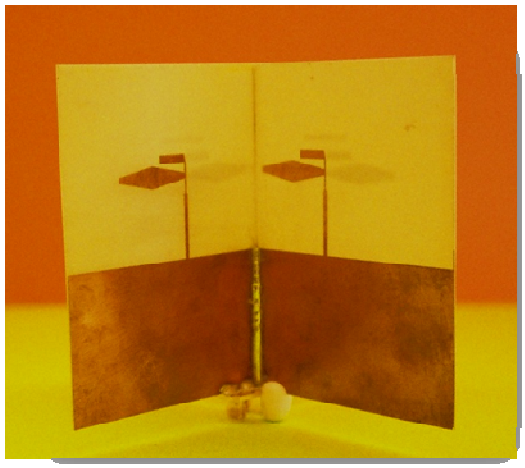

FIGURE 3.34: The one half of both the back views pertaining to the horizontally (left) and vertically (right) polarized arrays of the physical prototype.

The four-element configuration could only be calculated with the mesh set to 20 lines/λ, where the previous simulations were done with the mesh equal to 35 lines/λ, due to the size of the array. The discrepancies between the measured and simulated results, as seen in Chapter 4, may partially be due to the reduced accuracy, because of the coarser mesh used. The simulated coupling given in Fig. 3.35, shows that the highest coupling exhibited by this configuration was equal to -16.9 dB and lower than -20 dB over the majority of the respective frequency bands.

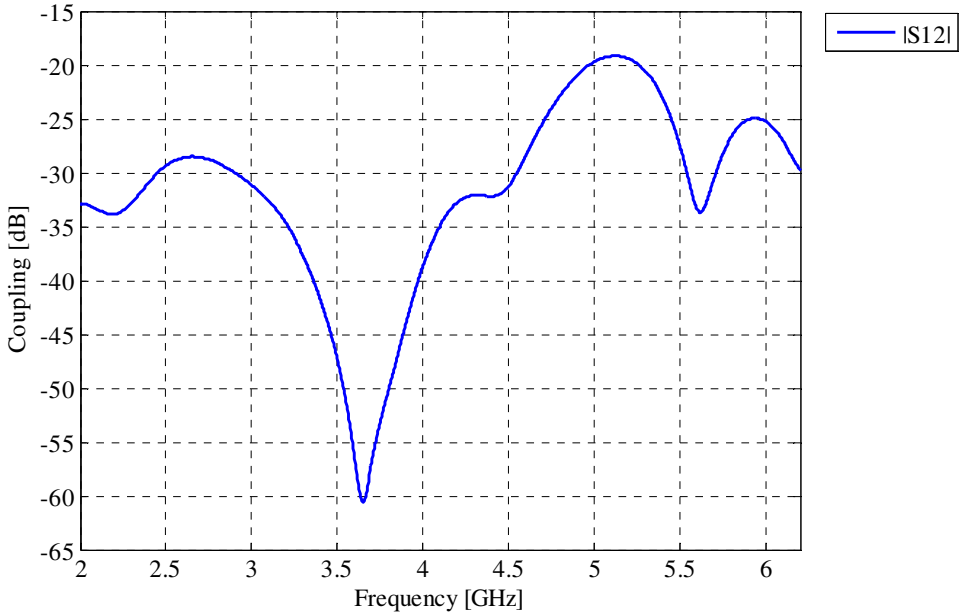

FIGURE 3.35: The simulated coupling between the two ports of the four-element array.

The simulated reflection coefficient can be seen in Fig. 3.36, where both frequency bands were adequately covered. The H-Array, also referred to as the two-element configuration fed by the straight microstripline, exhibited bandwidths of 24.3% (2.08 – 2.65 GHz) and 18.6% (4.96 – 5.98 GHz). The V-Array exhibited a slightly narrower bandwidth of 22.9% (2 – 2.52 GHz) over the first band and a wider bandwidth of 25.2% (4.59 – 5.91 GHz) over the second band. The H-Array also delivered a competitive bandwidth over the 5.2 GHz band, if the small section ranging from 4.43 GHz to 4.72 GHz were also incorporated in the calculations. The recalculated bandwidth of the above-mentioned band can potentially be equal to 29.8% (4.43 – 5.98 GHz).

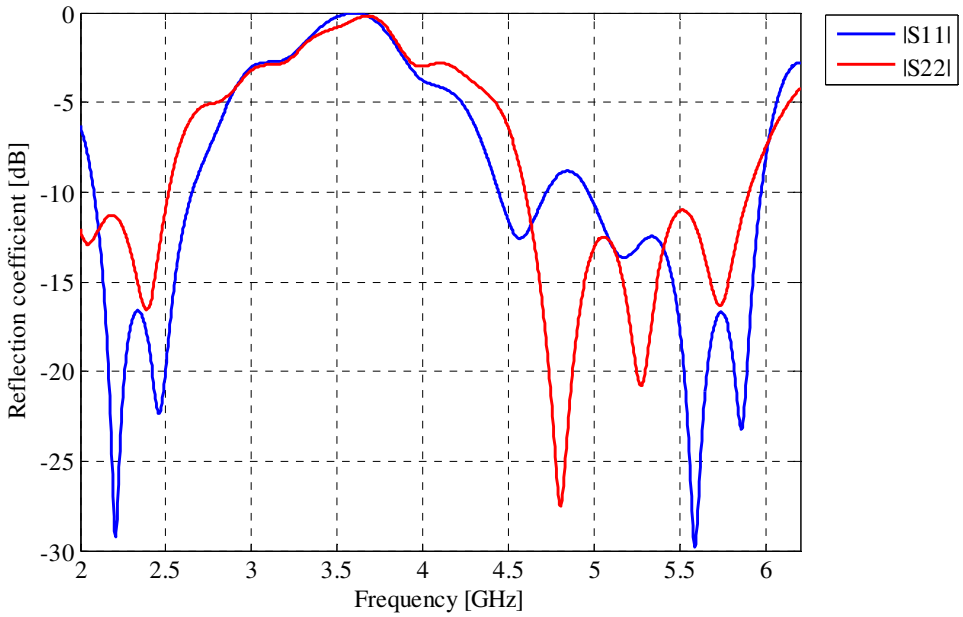

FIGURE 3.36: The simulated reflection coefficient of the four-element array.

The radiation characteristics of each array/configuration were determined by exciting the respective ports, where the simulated results were summarized in Table 3.7.

TABLE 3.7: Far field radiation properties of the four-element configurations.

Array	f (GHz)	3dB beam width		F-to-B ration (dB)	Gain (dB)	X-pol. Levels (dB)	
		E-plane	H-plane			E-plane	H-plane
H	2.44	49.3º	203.9º	11	5.3	-23.1	-15.1
	5.2	26.7º	236.1º	15.3	5.8	-18.5	-10.9
	5.55	24.2º	172.4º	17.4	8.9	-26.3	-20.2
	5.8	22.8º	161.4º	15.6	9.4	-25.7	-17.1
V	2.44	51.2º	205º	10.4	5.2	-30.9	-15.1

	5.2	27.4º	215.3º	14.2	6.6	-18	-10
	5.55	24.º	165.8º	16.6	9.2	-23	-18.6
	5.8	23.1º	159.3º	14.8	9.2	-25.9	-15.1

Good agreement was observed between the two arrays/configurations with only minor discrepancies as seen from Table 3.7. The average F-to-B ratio exhibited by the H-Array was equal to 11 dB and 16.1 dB, over the 2.4/5.2 GHz bands respectively, with the highest ratio at the centre frequency of the second frequency band. The same trend can be seen from the V-Array results, with the average F-to-B ratio over the 5.2 GHz band equal to 15.2 dB. The maximum cross-polarizations, within the 3 dB beam width of the main lobe, were -10.9 dB and -10 dB in the H-plane with the H- and V- Arrays respectively, while the maximum levels in the E-plane were -18.5 dB and -18 dB. Both arrays exhibited narrow beam widths in the E-plane and very wide beam widths in the H-plane. The side lobe levels in the E-plane ranged from -5.6 dB at 5.2 GHz to -10.1 dB at 2.44 GHz with the H-Array and from -7.5 dB at 5.2 GHz to -8.9 dB at 5.55 GHz with the V-Array. The 3 dB beam widths associated with the radiation patterns of both arrays in the H-plane were so broad that no real side lobes could be observed. As with the two-element designs, most of the main beams were focussed towards φ/θ equal to 90º.

3.2.4 Conclusion

The results delivered with the separate two-element arrays and the combined four-element array closely resembled each other, although the mesh density associated with the simulations had to be adjusted to compensate for the larger scale of the four-element array. In order to compare the results, the two-element arrays were also simulated with the mesh equal to 20 lines/λ. This was also done to see if the results deteriorated with the lower mesh density. The reflection coefficient level of each configuration, used to facilitate the comparison, can be seen in Figs. 3.37 and 3.38. The 1st two-element configuration delivered lower reflection coefficient levels with the increased mesh density (green graph) and thus a wider bandwidth. It was interesting to note that the array used in the four-element array with Port 1 excited, resembled the results of the simulations done with the separate two-element array. This was a good indication that the measured data might correlate with the results calculated with the aid of CST Microwave Studio®. The same trend was observed with the 2nd two-element array as indicated in Fig. 3.38, where the

results were not exacerbated by making use of a denser mesh. On the basis of these results the design was built and tested with the dimensions as specified in Tables 3.3 and 3.4.

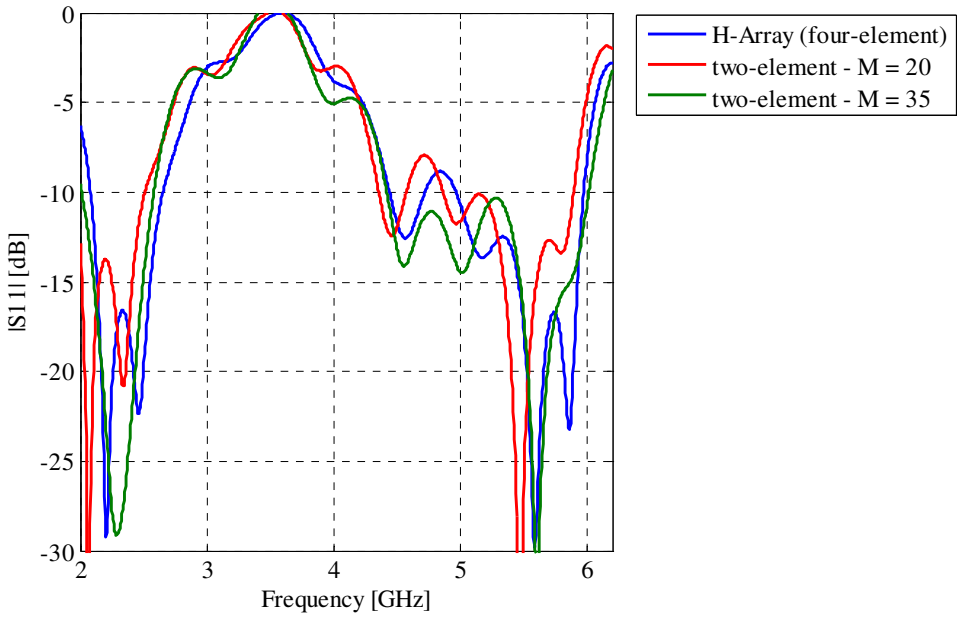

FIGURE 3.37: The simulated reflection coefficient of the H-Array and the 1st two-element configuration.

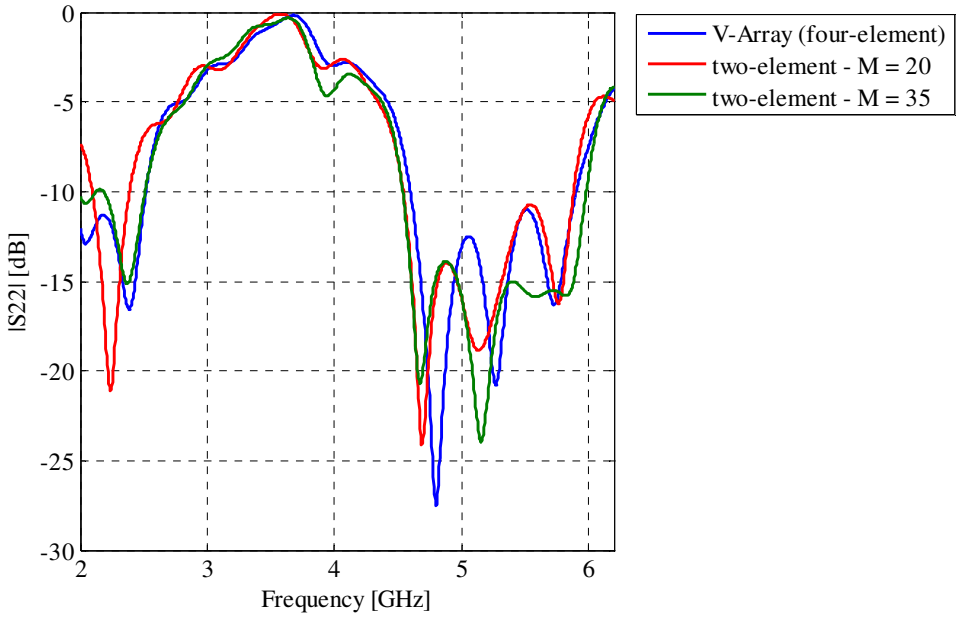

FIGURE 3.38: The simulated reflection coefficient of the V-Array and the 2nd two-element configuration.

CHAPTER 4

SIMULATED AND MEASURED RESULTS: SINGLE-, TWO- AND FOUR- ELEMENT CONFIGURATIONS

"This is this, this is also that."

- Chuang Tzu

"What you see is what you get, honey!"

- Geraldine (Flip Wilson)

4.1 SINGLE ANTENNA CONFIGURATION

The initial single-element, as well as the design that proliferated out of the parameter study in conjunction with the passive director were built and measured at the Compact Antenna Range of the University of Pretoria. The measured results of the initial "trial and error" design correlated well with the simulated results, which was a good indicator that the simulations were conducted with appropriate accuracy and thus correct meshing. The physical prototype of the final design with a passive director also performed as expected and predicted by the simulations. The first part of Section 4.1 is dedicated to the results obtained with the initial "trial and error" design, with the design parameters visually shown in Fig. 3.2. The measured and simulated results for the final design with the director, where the quasi-Yagi antenna was used as inspiration to improve the gain, are discussed in the second part of Section 4.1. The design parameters of the final design are shown in Fig. 3.15.

4.1.1 Initial "trial and error" single-element design

4.1.1.1 Reflection coefficient and gain

The initial "trial and error" antenna configuration was based on the design presented in [9], with the antenna dimensions given in Table 3.1. The antenna was designed to operate over the 2.4 GHz and 5.2 GHz WLAN bands on a Rogers RO4003C substrate with a dielectric constant of 3.38, which was much lower than the dielectric constant of 10.2, used with the double Rhombus design seen in [9]. The simulated reflection coefficient levels claimed in Chapter 3 were supported by the measured results. This can be seen in Fig. 4.1, where the measured bandwidth of the 2.4 GHz band showed only a small deviation of 1.7% from the simulated results, where the band associated with the measured and simulated results were 0.14 GHz (2.34 – 2.48 GHz) and 0.18 GHz (2.35 – 2.53 GHz) respectively. The second band also proved to be smaller than the simulated bandwidth of 19.7% (4.93 – 6 GHz), with the measured bandwidth being equal to 17% (4.93 – 5.84 GHz). The measured bandwidth of 5.8% and 17% over the 2.4/5.2 GHz bands respectively, still adhered to the minimum requirements of 3.4% and 14.4%. Surplus bandwidth was however needed to ensure that the later designs, where the design consisted of more than one element, still met the above specified requirements pertaining to the WLAN standards.

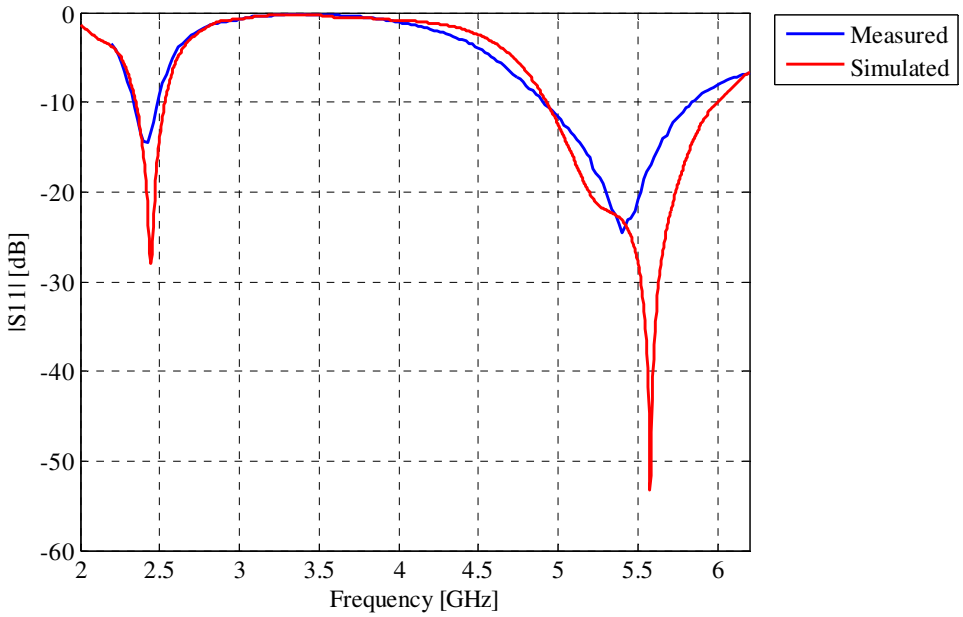

FIGURE 4.1: The measured and simulated reflection coefficient.

The measured gain proved to be slightly higher than the simulated results over the 2.4 GHz band, as seen in Fig. 4.2. For the 5.2 GHz band the measured results fell just short of the simulated results, from 5.24 GHz to 5.44 GHz, as seen in Fig. 4.3. The maximum measured boresight gain of 5.8 dBi was achieved over the 5.2 GHz at 5.7 GHz. An even higher gain of 6.7 dBi was recorded slightly outside the required bandwidth, at 4.97 GHz. It can also be seen from the measured results that the average gain, over the 2.4 GHz and the 5.2 GHz bands of 4.8 dBi and 5.4 dBi respectively, proved to be adequate and aligned with the results of the alternative designs, as discussed in Chapter 2. The peak measured gains of 5.2 dBi and 5.8 dBi over the respective bands surpassed the gains exhibited by the designs presented in [10], [12], and [15-20]. The simulated average gains of 4.7 dBi and 5.3 dBi over the 2.4 GHz/5.2 GHz bands respectively, compared well with the above mentioned measured gains.

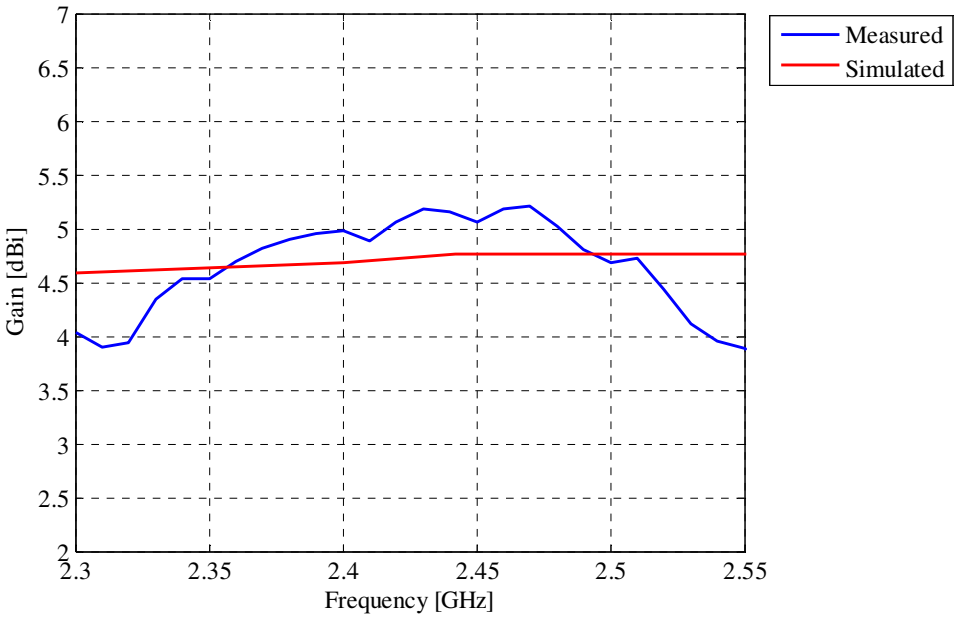

FIGURE 4.2: The measured and simulated gain over the 2.4 GHz band.

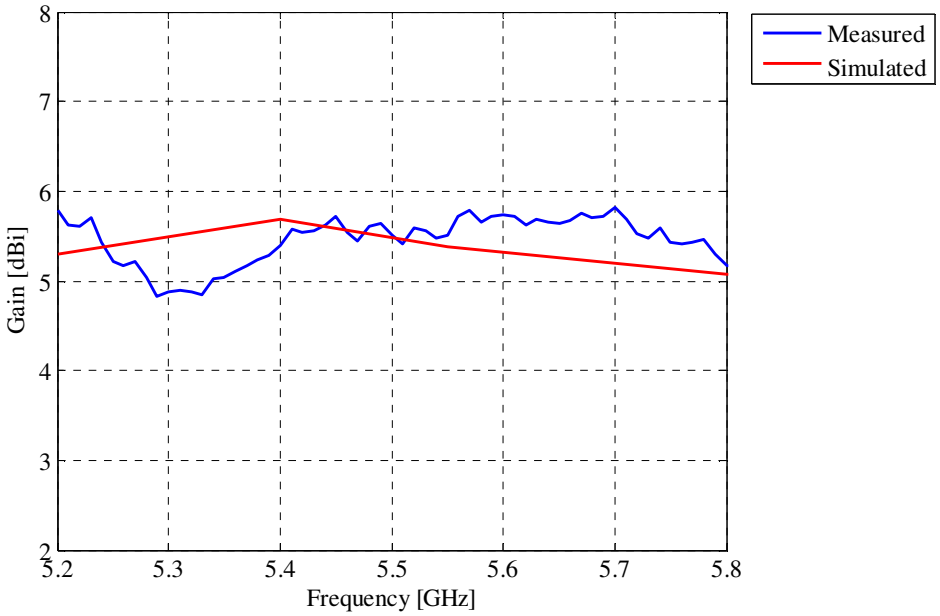

FIGURE 4.3: The measured and simulated gain over the 5.2 GHz band.

4.1.1.2 Radiation patterns

The radiation patterns were measured and simulated at selective frequencies that span across both operating bands, to provide a good representation of the general patterns exhibited by the antenna. Good correlation was also achieved between the simulated and measured radiation patterns in both the E- and H- plane, as shown in Figs. 4.4 – 4.8, at 2.44 GHz, 5.0 GHz, 5.55 GHz and 6.0 GHz. The simulated and measured co-polarized radiation patterns at 2.3 GHz, 2.44 GHz and 2.5 GHz proved to be very similar in form and magnitude and therefore only the radiation patterns for 2.44 GHz were included in this dissertation. The discrepancies between the simulated and measured cross-polarization levels can be attributed to the difference between the experimental setup of the single-element prototype at the Compact Antenna Range and the simulated version of the setup. Fabrication imperfections and the effect of the connector on the performance of the antenna can also contribute to the discrepancies. Similar trends were observed over the 5.2 GHz band and can be seen in Figs. 4.5 - 4.7. The maximum measured and simulated normalized cross-polarization levels can be seen in Table 4.1. The maximum levels were determined between the 3 dB beam width limits of the main lobe.

TABLE 4.1: Maximum normalized cross-polarization levels.

f (GHz)	Measured (dB)		Simulated (dB)	
	E-plane	H-plane	E-plane	H-plane
2.3	-20.5	-10	-31.3	-12
2.44	-21.9	-11.7	-30.5	-13.2
2.5	-25.2	-12.9	-30.3	-13.7
5.0	-17.7	-14.3	-23	-15.7
5.55	-23.9	-15.5	-24	-18.8
6.0	-20.7	-15.1	-24.4	-17.7

The average measured cross-polarization level in the E-plane over the first band proved to be -22.5 dB, which is somewhat higher than the simulated average level of -30.6 dB. The biggest deviation between the simulated and measured results was over the 2.4 GHz band. A smaller disparity was found between the simulated and measured levels over the second frequency band, with the average cross-polarization levels equal to -23.8 dB and -20.8 dB. Good agreement was shown between the various cross-polarization levels in the H-plane over the first- and second band. The simulated and measured levels over the 2.4 GHz band were equal to -13 dB and -11.5 dB respectively and equal to -17.4 dB and -15 dB over the 5.2 GHz band. The normalized cross-polarization levels in the boresight direction varied between -20 dB and -30 dB over the two frequency bands.

It can also be seen from Fig. 4.4 that the peak gain stayed around φ/θ equal to 90º, whereas the main beam shifted slightly to φ equal to 75º at the higher frequencies, as seen in Figs. 4.5 - 4.7. The 3dB beam width in the E-plane ranged from 80.3º to 57.2º over the first- and second band respectively, whereas the 3 dB beam widths associated with the H-plane ranged from 159.4º and 197.7º. The simulated E-plane side lobe levels, at 2.44 GHz and 5.55 GHz, were equal to -9.1 dB and -14.1 dB respectively. The radiation pattern was so broad that no real side lobes could be observed.

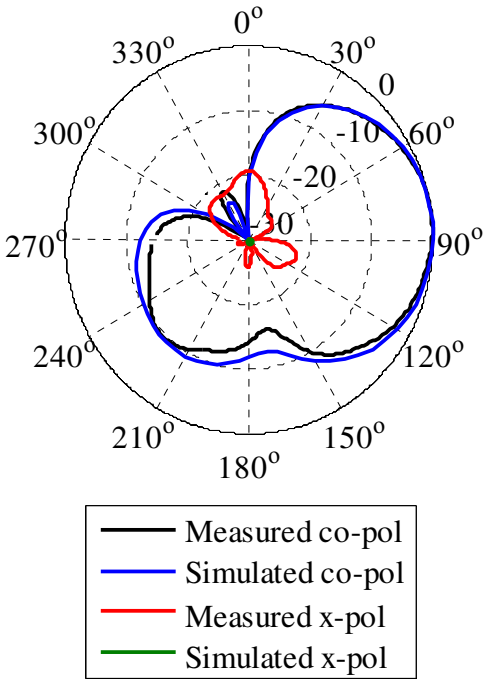

FIGURE 4.4: The measured and simulated normalized radiation pattern at 2.44 GHz in the E-plane.

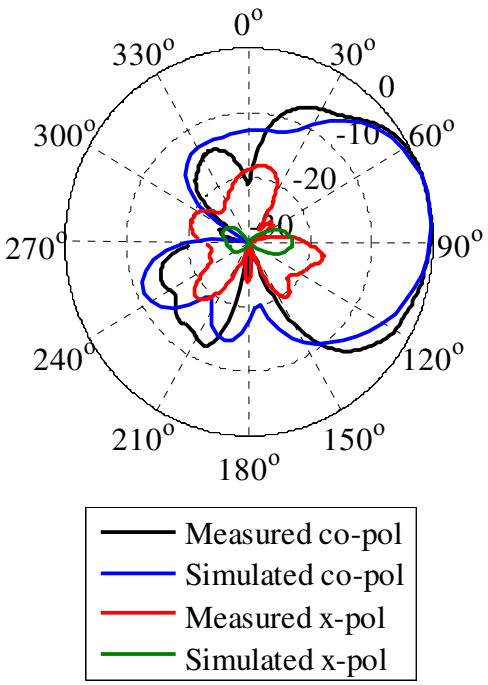

FIGURE 4.5: The measured and simulated normalized radiation pattern at 5.0 GHz in the E-plane.

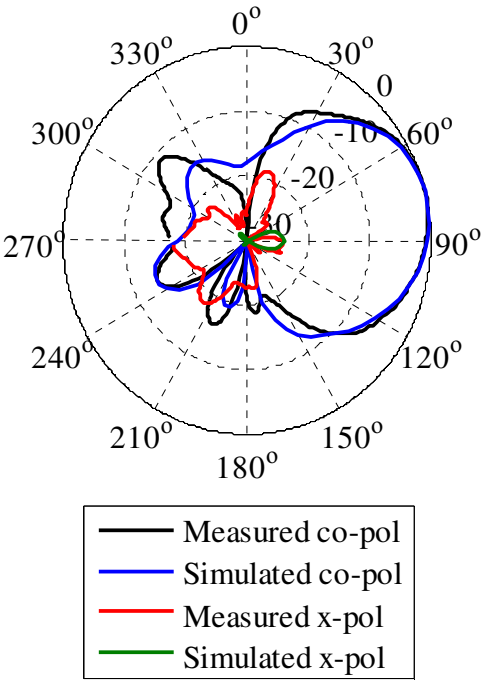

FIGURE 4.6: The measured and simulated normalized radiation pattern at 5.55 GHz in the E-plane.

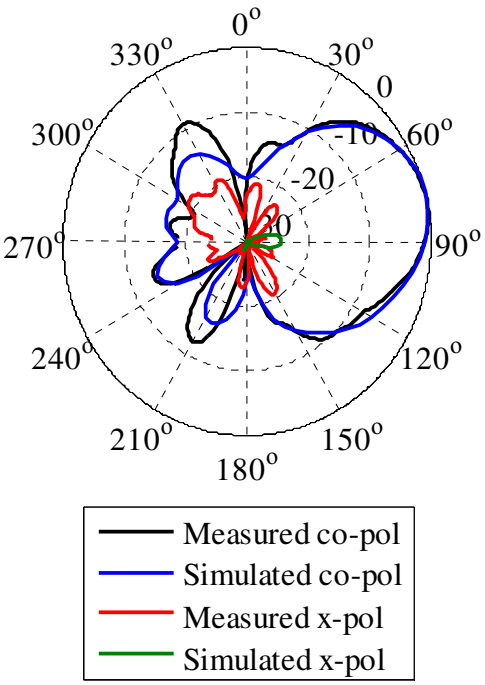

FIGURE 4.7: The measured and simulated normalized radiation pattern at 6.0 GHz in the E-plane.

As with the E-plane radiation patterns, good correlation was found between the measured and simulated co-polarized radiation patterns in the H-plane. Fig. 4.8 shows that the main beam is situated at φ/θ equal to 90º, as expected. The measured and simulated cross-polarization levels exhibited at the higher frequencies, as seen from Figs. 4.9 – 4.11, were slightly less comparable than seen at the lower frequencies. The discrepancies as mentioned in the beginning of this section can be attributed to small differences in the experimental setup and the simulation environment, such as misalignment of the element with the reference angles.

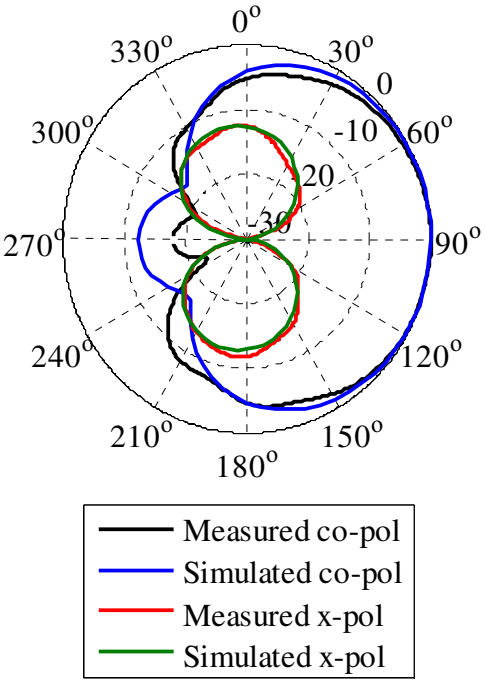

FIGURE 4.8: The measured and simulated normalized radiation pattern at 2.44 GHz in the H-plane.

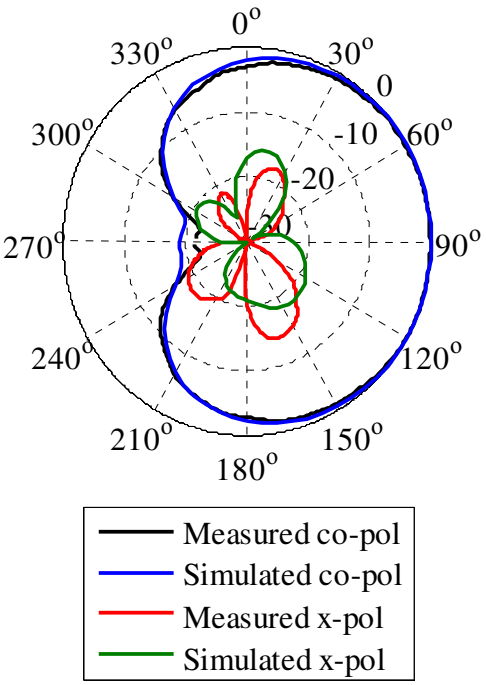

FIGURE 4.9: The measured and simulated normalized radiation pattern at 5.0 GHz in the H-plane.

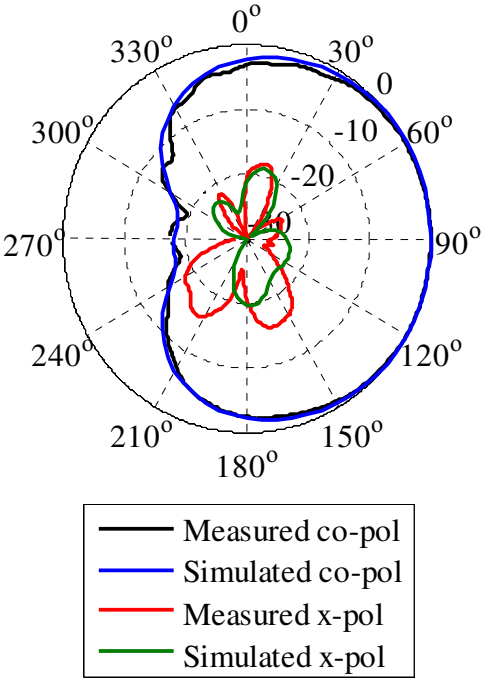

FIGURE 4.10: The measured and simulated normalized radiation pattern at 5.55 GHz in the H-plane.

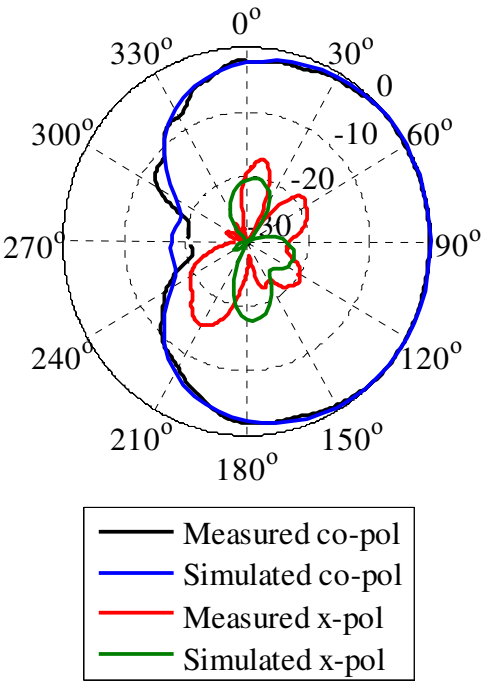

FIGURE 4.11: The measured and simulated normalized radiation pattern at 6.0 GHz in the H-plane.

The measured F-to-B (Front-to-Back) ratios of 13.7 dB, 13.9 dB and 12.4 dB at 2.3 GHz, 2.44 GHz and 2.5 GHz respectively, also compared well to the simulated F-to-B ratio of 12.3 dB at 2.44 GHz. The measured F-to-B ratios over the 5.2 GHz band were also close to the simulated value of 18 dB at 5.55 GHz. The recorded F-to-B ratios were 19.9 dB, 16.8 dB and 17.5 dB at 5.0 GHz, 5.55 GHz and 6.0 GHz respectively.

4.1.1.3 Interpretation of results

The minimum bandwidth requirements for the 2.4/5.2 GHz bands of 3.4% and 14.4% respectively, was met by the measured bandwidths of 5.8% and 17%, over the two bands respectively. Alternative designs such as the ring monopole presented in [10] did however exhibit wider bandwidths in the order of 12% and 39.3%, as with the designs presented in [12], [15], [16] and [18-20]. The bandwidths ranged from 8.8% to 37.1% over the first band and from 19.4% to 37% over the second band. These designs however did not meet the peak gains achieved with the initial design, as presented in this dissertation. It was thus

the aim to benefit from the high gains achieved with the initial design, but to incorporate alternative methods to increase the bandwidth, in order to achieve surplus bandwidth to ensure the success of the later designs. The design presented in this section also achieved high F-to-B ratios that ranged from 12.4 dB to 19.9 dB. The cross-polarization levels in the boresight direction were below the -20 dB level. Good correlations were seen in general between the various measured and simulated results.

4.1.2 Final optimized single-element design with passive director

4.1.2.1 Reflection coefficient and gain

The optimized single-element design with the passive director (see Fig. 3.15), compared to the design without the director, improved in terms of bandwidth, as well as the boresight gain, while adhering to the specified radiation pattern characteristics set forth in Chapter 1. The single-element design that followed the parameter study was first measured and simulated without the passive director as mentioned in Chapter 3. Due to the decrease in the boresight gain, the passive director was included to make use of the wide bandwidths of the new design, while ensuring that adequate gain was achieved. This modification firstly had a positive effect on the bandwidth, where the widths of the two frequency bands were substantially increased. The measured bandwidth increased from 15.6% (without director) to 17.8% (with director) and from 27.1% to 34.7% over the 2.4 GHz and the 5.2 GHz bands respectively. The simulated bandwidth of 17.9% (2.3 – 2.75 GHz) pertaining to the first band was corroborated by the measured bandwidth of 17.8% (2.32 – 2.77 GHz). A larger difference was recorded between the simulated and measured bandwidth of 26.4% (4.56 – 5.95 GHz) and 34.7% (4.25 – 6.03 GHz) respectively. The difference between the calculated (red graph) and measured (blue graph) results can be seen in Fig. 4.12.

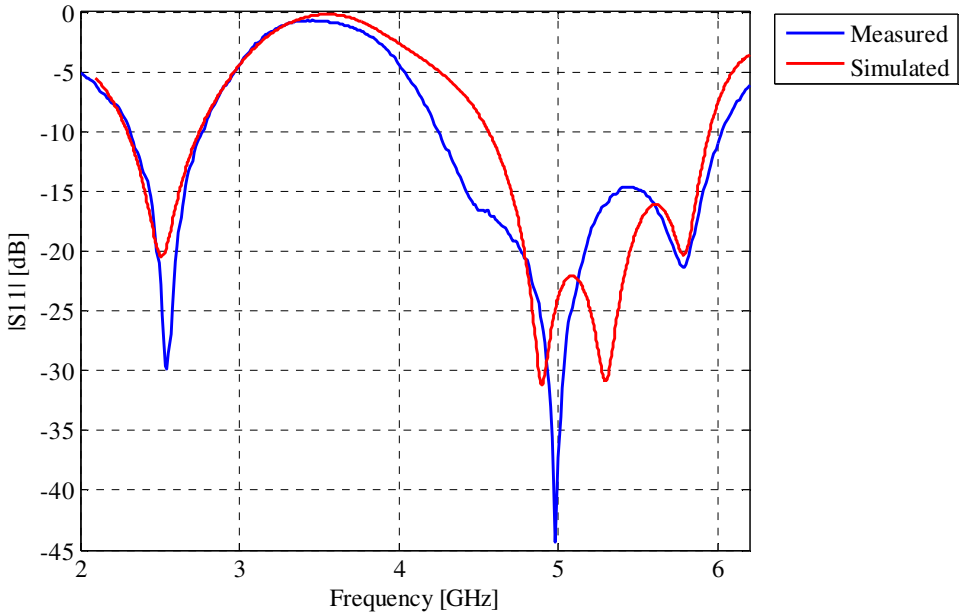

FIGURE 4.12: The measured and simulated reflection coefficient.

The main goal with the incorporation of the passive director was to increase the gain of the optimized design, which proliferated out of the parameter study. The improvement of the boresight gain can be seen in Figs. 4.13 and 4.14, which was also reverberated by the results seen in Figs. 4.15 – 4.22. The measured gain over the 2.4 GHz band surpassed the simulated results from 2.3 GHz to 2.45 GHz, whereas the simulated results proved to be higher from 5.2 GHz to 6.2 GHz, which constituted almost the whole 5.2 GHz band. Good agreement between the average measured and simulated gains over the first frequency band was achieved with values of 3.6 dBi and 4 dBi respectively. The average measured and simulated gain over the second frequency band was found to be very similar, where the gains were equal to 3.6 dBi and 4.1 dBi respectively. The maximum gain was achieved at 5.79 GHz and equal to 6 dBi.

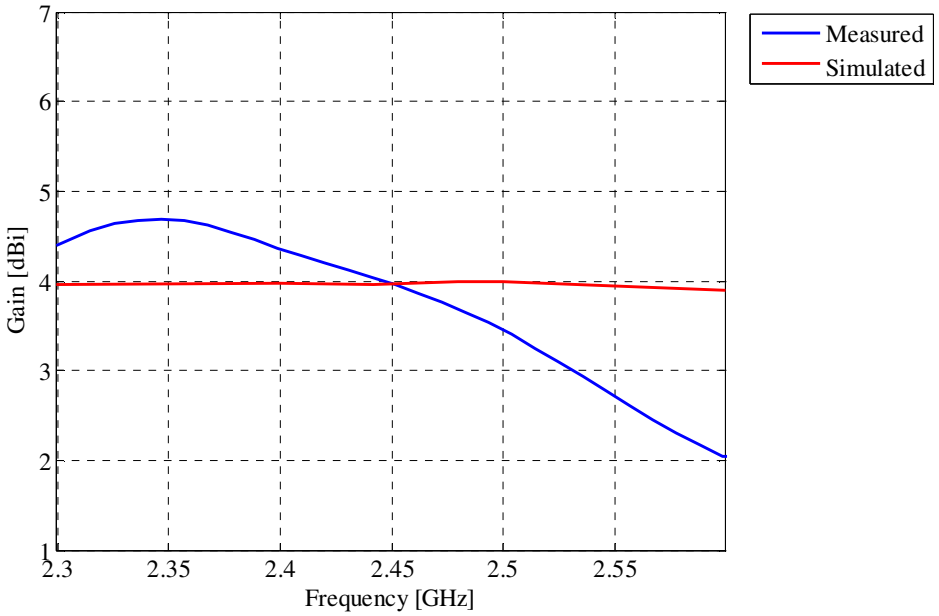

FIGURE 4.13: The measured and simulated gain over the 2.4 GHz band.

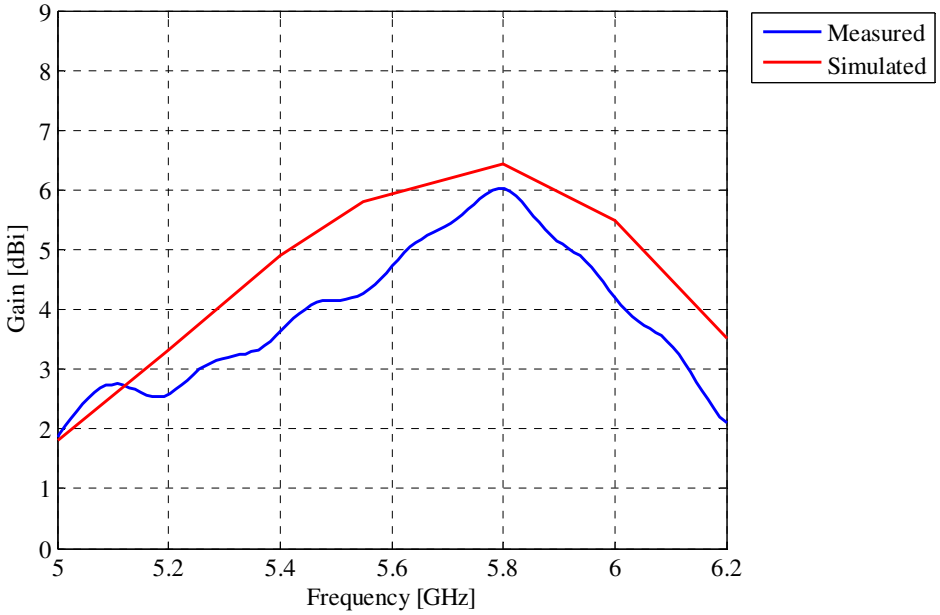

FIGURE 4.14: The measured and simulated gain over the 5.2 GHz band.

4.1.2.2 Radiation patterns

Only the radiation pattern at 2.44 GHz, the centre frequency of the first band, was used as a representation of the general performance of the design over the first band. This was done

due to the analogous appearance of the patterns in the first band. The second band was covered by calculating/measuring the radiation patterns at the frequencies 5.2 GHz, 5.55 GHz and 5.8 GHz, due to the larger span of the higher frequency band.

The measured cross-polarized levels in the E-plane were slightly higher than their simulated counterpart and this are shown in Fig. 4.15, where the simulated and measured results converged closer to each other over the higher frequency band. The discrepancies between the simulated and measured cross-polarization levels can be attributed to differences between the simulated model and the experimental setup. The maximum cross-polarized levels, within the main lobe, were summarized in Table 4.2. Good correlation was seen between the measured and simulated results of the H-plane. The most substantial outliers were at 2.44 GHz and 5.2 GHz in the E-plane and at 5.2 GHz in the H-plane. This was corroborated by the plotted radiation patterns seen in Figs. 4.15 – 4.18. These results also proved to be in the same category as the design presented in [9] where the highest cross-polarization levels were equal to -7 dB and -20 dB in the H-plane and the E-plane respectively. The normalized cross-polarization level at boresight proved to be close to -30 dB, over the majority of the frequency bands.

TABLE 4.2: Maximum normalized cross-polarization levels.

f (GHz)	Measured (dB)		Simulated (dB)	
	E-plane	H-plane	E-plane	H-plane
2.44	-22.7	-16.8	-30.4	-19.1
5.2	-16	-20.5	-25.9	-10
5.55	-27.9	-10	-28.9	-14
5.8	-27.5	-12.5	-30.1	-15.4

The main goal of this design was to increase the gain of the design by adding a passive director and to steer the direction of the main beam towards the boresight direction. This was achieved, where the majority of peak gains occurred at φ/θ equal to 90º. The direction of the main beam was in the vicinity of 75º to 85º in the E-plane. Improved boresight gain was achieved in the H-plane, where the biggest problem occurred with the optimized design without the director. The improvement can be seen in Figs. 4.19 – 4.22. The simulated side lobe levels also spanned from -8.9 dB at 2.44 GHz to as low as -13.3 dB at 5.55 GHz in the E-plane. The H-plane radiation patterns were so broad that no real side lobes could be observed.

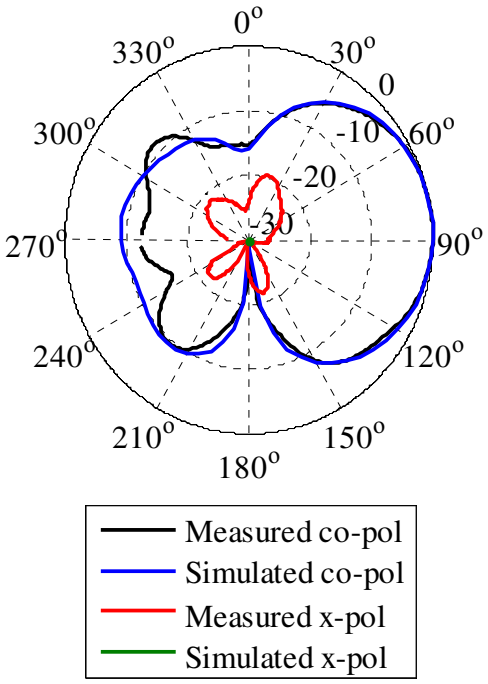

FIGURE 4.15: The measured and simulated normalized radiation pattern at 2.44 GHz in the E-plane.

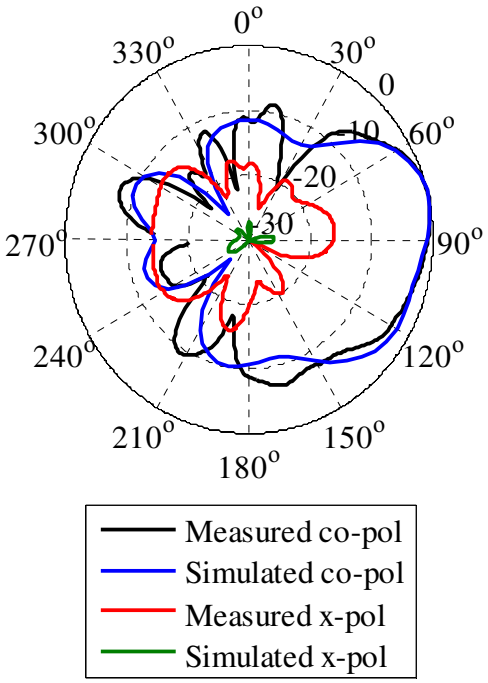

FIGURE 4.16: The measured and simulated normalized radiation pattern at 5.2 GHz in the E-plane.

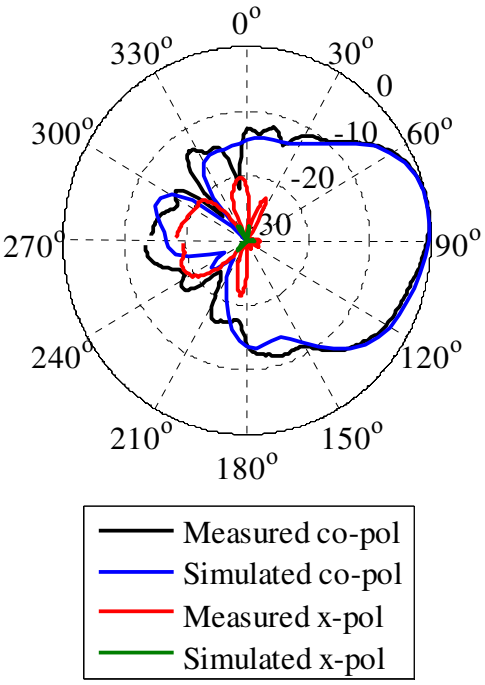

FIGURE 4.17: The measured and simulated normalized radiation pattern at 5.55 GHz in the E-plane.

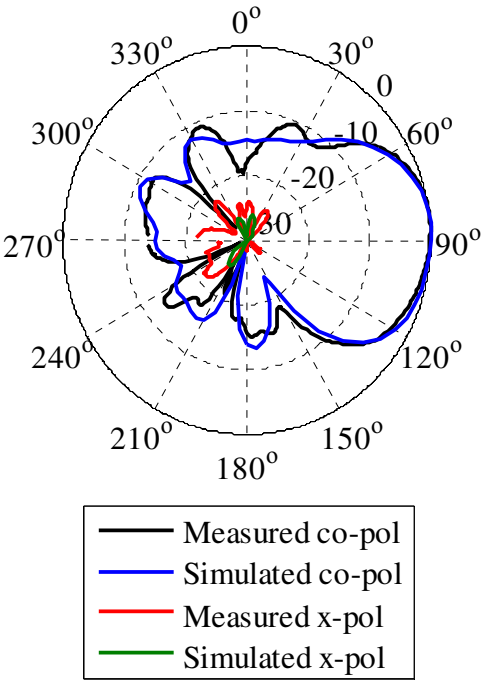

FIGURE 4.18: The measured and simulated normalized radiation pattern at 5.8 GHz in the E-plane.

The 3dB beam widths ranged from 58.3º to 84.7º in the E-plane, which correlated with the results achieved in [9], where the beam widths of the single double Rhombus design spanned from 60º to 110º. The results achieved with the current design showed an increase in the 3dB beam widths in the H-plane, compared to the 40º to 150º of the design presented in [9]. The 3dB beam widths of this design, in the H-plane, ranged from 178.8º to 194º.

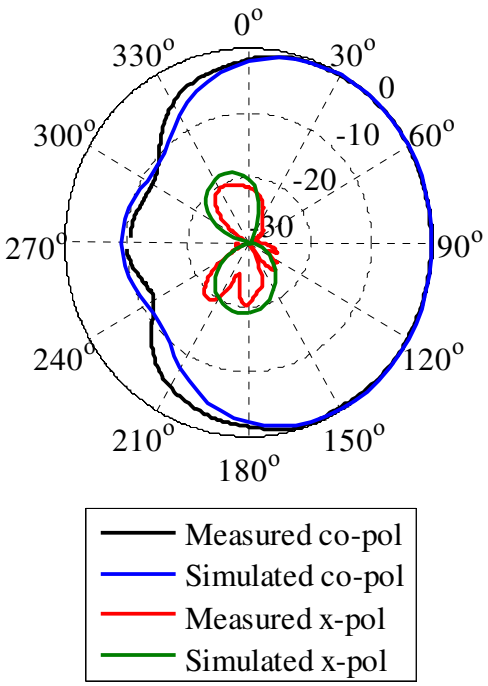

FIGURE 4.19: The measured and simulated normalized radiation pattern at 2.44 GHz in the H-plane.

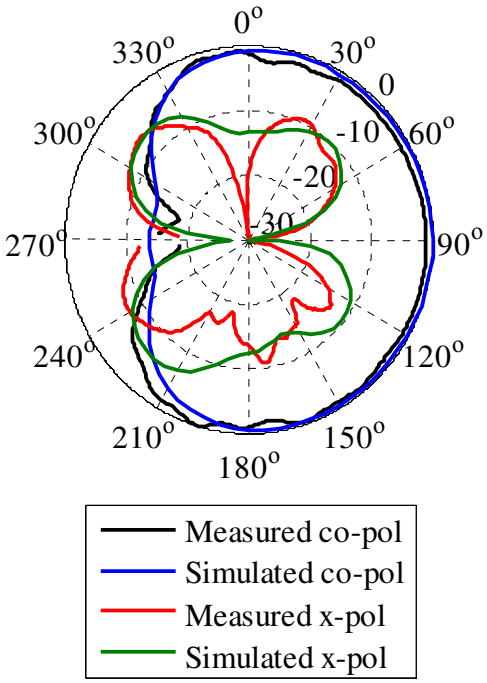

FIGURE 4.20: The measured and simulated normalized radiation pattern at 5.2 GHz in the H-plane.

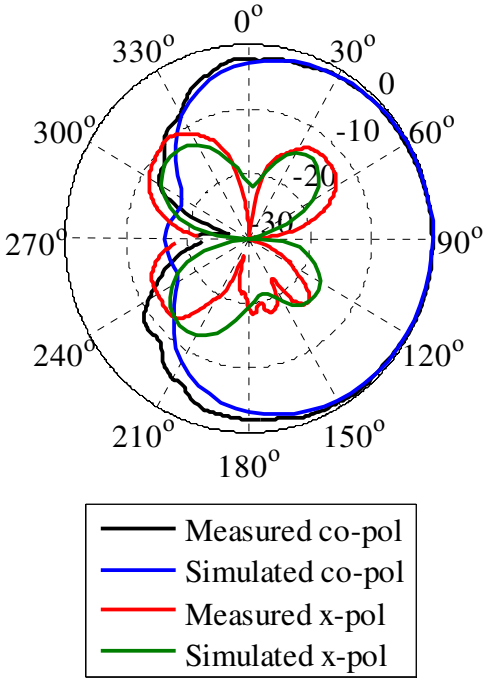

FIGURE 4.21: The measured and simulated normalized radiation pattern at 5.55 GHz in the H-plane.

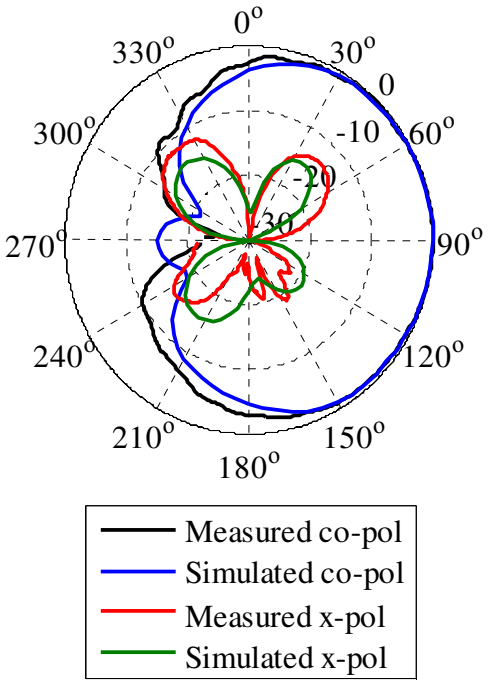

FIGURE 4.22: The measured and simulated normalized radiation pattern at 5.8 GHz in the H-plane.

The measured F-to-B ratio of 12.2 dB was also somewhat higher than the simulated ratio of 9.1 dB at 2.44 GHz. The highest measured F-to-B ratio of 19.1 dB was achieved at 5.2 GHz, which compared well to the highest F-to-B ratio of 20 dB exhibited by the double Rhombus design presented in [9]. The simulated F-to-B ratio of 15.1 dB proved to be higher than the measured value of 12.9 dB at 5.55 GHz, with the latter results ranging from 12.9 dB to 19.1 dB.

4.1.2.3 Interpretation of results

As mentioned in Section 4.1.2.1, the use of a passive director led to an increase in bandwidth and gain. The optimized design, with the passive director, exhibited bandwidths of 17.8% and 34.7% over the two bands respectively and average boresight gains in the range of 3.6 dBi. The inclusion of the director thus resulted in a single-element design with the peak gains equal to 4.6 dBi and 6 dBi, over the two respective frequency bands. These peak gains compared well with other existing designs, such as presented in [10], [12], [15], [16], [19] and [20] and surpassed the results presented in [17] and [18]. The desired wider bandwidths of the optimized design, with the director, created room for possible reductions

that might occur with the assembly of more than one element. The F-to-B ratios of 12.2 dB and 19.1 dB exhibited by the final optimized design with the director, also concurred with the 12.4 dB and 19.9 dB of the initial "trial and error" design. These ratios are also in line with other existing designs such as the double Rhombus antenna presented in [9]. The final optimized single-element design, with the director, exhibited normalized cross-polarization levels close to -30 dB, at boresight. The simulated and measured co-polarized radiation patterns showed a very good correlation in both planes, as well as the cross-polarized radiation patterns in the H-plane. As mentioned in Section 4.1.2.2, the discrepancies between the simulated and measured cross-polarization levels in the E-plane can be attributed to the difference between the simulated and experimental setup of the single-element, as well as fabrication imperfections and the possible negative effect of the connector.

4.2 TWO-ELEMENT ARRAY

Two two-element configurations with different feeding networks were designed, simulated and built separately as discussed in Chapter 3, Section 3.2. The measured and simulated results of both configurations are shown in the following section.

4.2.1 Reflection coefficient and gain

The aim with the design of the two configurations was to make the necessary modifications beforehand to enable the two different two-element arrays to be incorporated into one design, capable of supporting dual-polarization operations. It was thus essential and sagacious to develop arrays that exhibit approximately the same results in terms of bandwidth, gain and far field radiation characteristics. The two configurations were built according to the dimensions given in Tables 3.3 and 3.5. The results presented in Chapter 3 were corroborated by the measured results as seen from Fig. 4.23. Adequate correlation between the measured and simulated results of both configurations was achieved. The simulated bandwidth (blue graph) of the 1st configuration (straight off-centre microstrip feedfine) over the 2.4/5.2 GHz bands were 23.8% and 29.9% respectively. The measured bandwidths (black graph) of 33.3% (2 – 2.8 GHz) and 37% (4.21 – 6.12 GHz) proved to be wider compared to the simulated results. The discrepancies can be attributed to the limitation of the mesh density, used with the simulations, due to the size of the array. The

bandwidths of the 2nd configuration (modified off-centre microstrip feedline) also delivered very similar results as seen with the 1st configuration, with the simulated bandwidths (green graph) equal to 12.7% and 26.7% over the first and second bands respectively. The same tendency was seen with the measured bandwidths of the 2nd configuration, where the results proved to be substantially wider, with the respective bandwidths equal to 25.2% (2.12 – 2.72 GHz) and 31.8% (4.5 – 6.2 GHz) over the 2.4/5.2 GHz bands. The disparity seen between the simulated 12.7% over the first band compared to the measured 25.2% can be attributed to the slight overreach of the -10 dB mark between 2.2 – 2.3 GHz. Good correlation was seen between the measured results of both configurations.

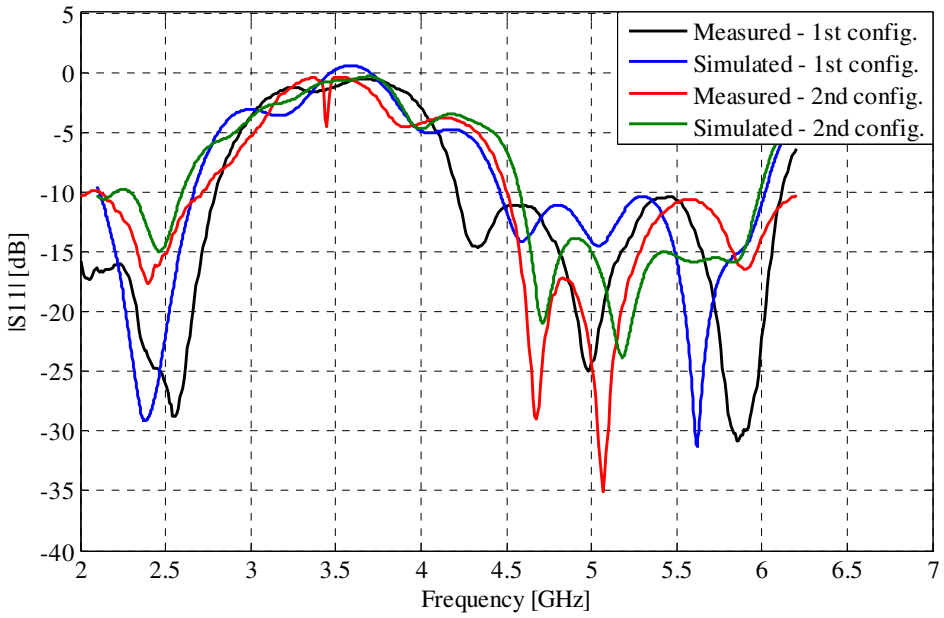

FIGURE 4.23: The reflection coefficients of the 1st configuration and the 2nd configuration.

The average simulated gains shown in Chapter 3, which were equal to 5.6 dBi and 7.5 dBi over the 2.4/5.2 GHz bands, as seen in Figs. 4.24 and 4.25 respectively, proved to be higher than the measured averages of 4.8 dBi and 6.3 dBi. The measured gain was lower than the predicted gain (blue graph), with the highest discrepancy seen at 2.25 GHz, where the disparity was equal to 1.22 dBi. The measured gain (red graph) of the 2nd configuration alternated around the more constant simulated gain and surpassed the simulated results (green graph) from 2.15 GHz to 2.35 GHz as seen in Fig. 4.24. The simulated averages of the 2nd configuration was found to be slightly higher, with the respective averages equal to 5.2 dBi and 7.6 dBi over the 2.4/5.2 GHz bands, compared to the measured averages of 5

dBi and 6.4 dBi. Good correlation was overall achieved between the measured data of the two configurations, with the 2nd configuration exhibiting slightly higher gains.

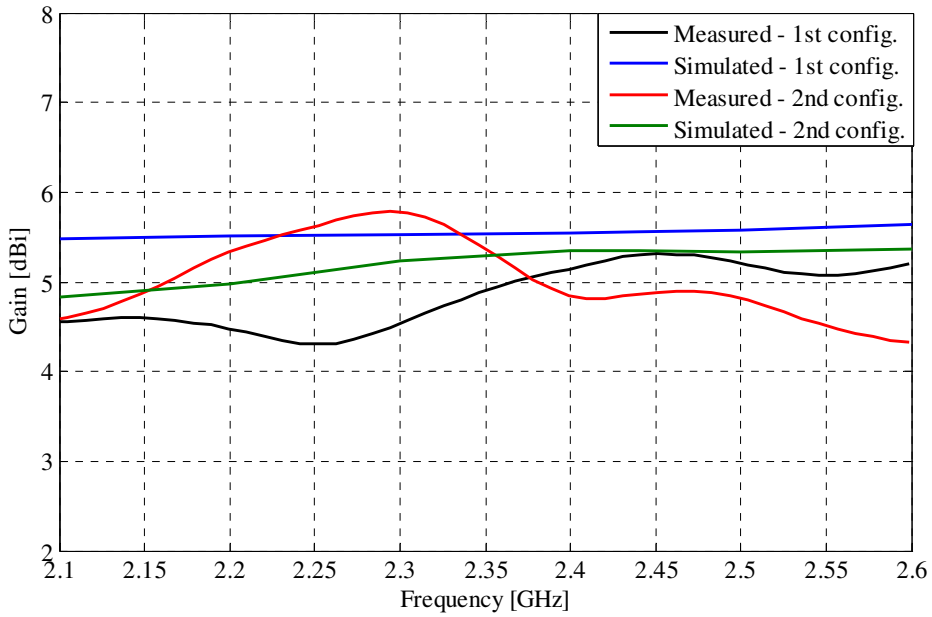

FIGURE 4.24: The measured and simulated gain of the 1st configuration and the 2nd configuration over the 2.4 GHz band.

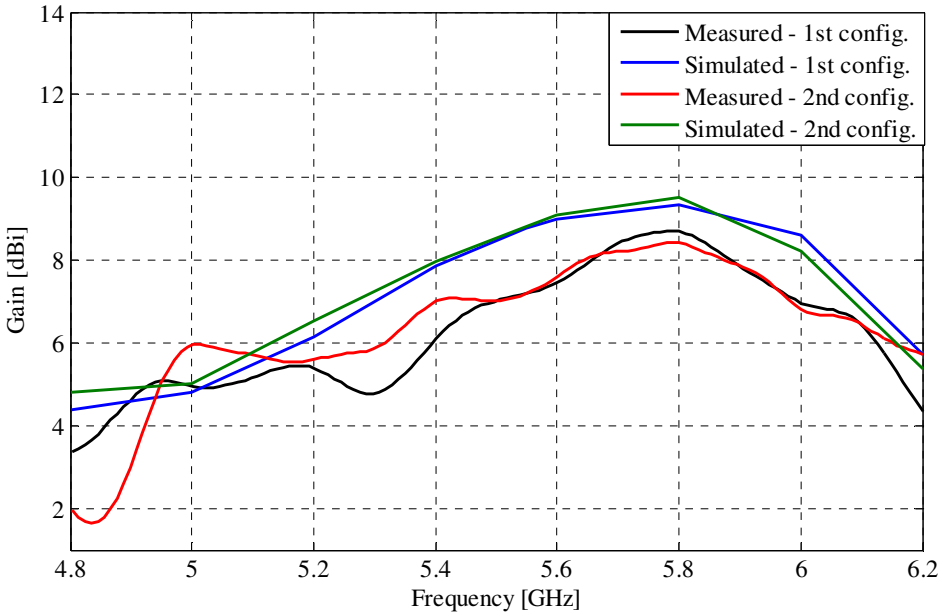

FIGURE 4.25: The measured and simulated gain of the 1st configuration and the 2nd configuration over the 5.2 GHz band.

4.2.2 Radiation patterns

The high gain seen from the previous section was reverberated by the good far field radiation patterns of both configurations, as seen from Figs. 4.26 - 4.29 in the E-plane and from Figs. 4.30 - 4.33 in the H-plane. As with the results of the final optimized single-element design with the director, only the radiation pattern at 2.44 GHz, the centre frequency of the first band, was used due to the analogous appearance of the patterns in the first band. The second band was covered by calculating the radiation patterns at the frequencies 5.2 GHz, 5.55 GHz and 5.8 GHz, due to the larger span of the higher frequency band.

Very good correlation between the measured and simulated co-polarized radiation patterns of both configurations can be observed from Figs. 4.26 – 4.33, in both planes. The direction of the main beam was found to be around φ/θ equal to 90º, as desired for the final design, due to the directional requirements stipulated in the beginning of this study. The cross-polarization levels however also exhibited the same tendency as the results of the final single-element configuration, where the levels correlated well in the H-plane, but diverged slightly from each other in the E-plane. The biggest outlier pertaining to the 2nd configuration was observed at 2.44 GHz in the E-plane, with the difference being equal to 12.1 dB. The 1st configuration exhibited slightly lower measured cross-polarization levels in the E-plane compared to the 2nd configuration, whereas the results of the 1st configuration were closely imitated by the 2nd configuration in the H-plane. The maximum cross-polarization levels of both configurations, within the main lobe, were summarized in Table 4.3. The normalized cross-polarization levels ranged between -20 dB to -30 dB in the boresight direction.

TABLE 4.3: Maximum normalized cross-polarization levels.

Array	f (GHz)	Measured (dB)		Simulated (dB)	
		E-plane	H-plane	E-plane	H-plane
1	2.44	-21.4	-15.9	-29.3	-16
	5.2	-19.2	-15.2	-26	-10
	5.55	-25.1	-11.7	-36	-16
	5.8	-23	-13	-30	-18.4
2	2.44	-17.2	-12	-29.3	-14.8
	5.2	-17.5	-13.3	-24.9	-11.1
	5.55	-20.4	-12.4	-27	-15.9
	5.8	-24.5	-14.7	-26.3	-17.6

The highest and lowest simulated side lobe levels exhibited by the 1st configuration were equal to -4.8 dB and -8.8 dB and occurred at 5.2 GHz and 2.44 GHz in the E-plane respectively. No real side lobes could be observed in the H-plane, due to the broad radiation patterns associated with this plane. The simulated side lobe levels of the 2nd configuration were slightly lower with maximum and minimum levels obtained equal to -7.3 dB and -9.9 dB in the E-plane respectively.

The simulated and measured 3 dB beam widths again proved to be very close with very wide beam widths seen in the H-plane and narrower beam widths in the E-plane. The 1st configuration showed 3 dB beam widths of between 163.5º and 234º, which were closely imitated by the 2nd configuration that exhibited beam widths of between 158.9º and 233.2º. Similar results were seen in the E-plane, with the 1st configuration and 2nd configuration exhibiting 3 dB beam widths that ranged from 22.8º to 50.6º and from 22.9º to 50º.

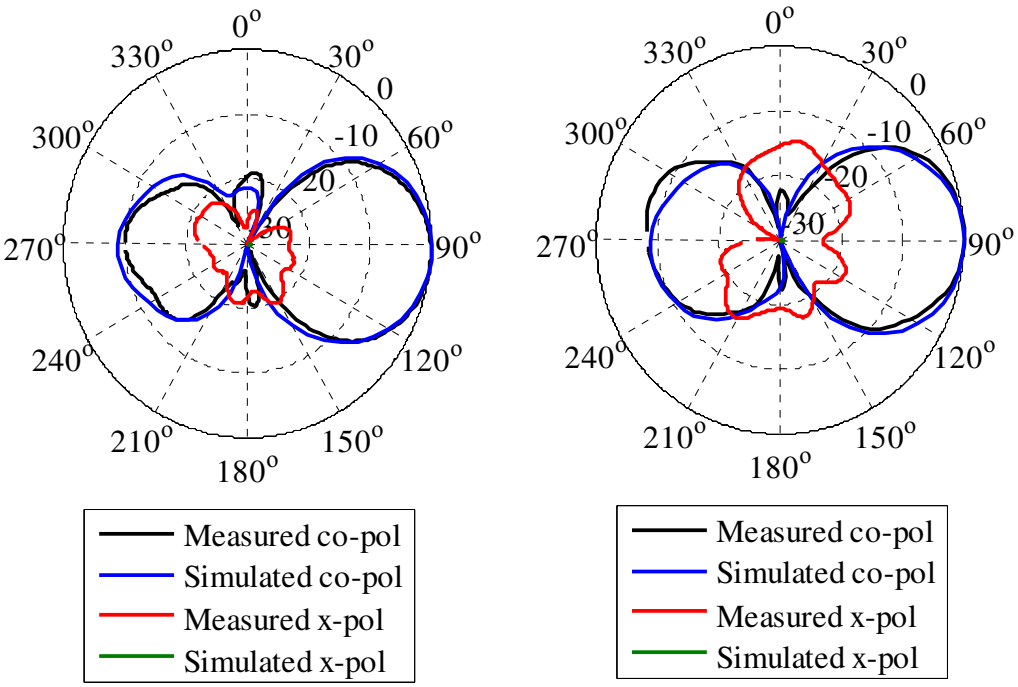

FIGURE 4.26: The measured and simulated normalized radiation pattern at 2.44 GHz in the E-plane. (a) 1st configuration. (b) 2nd configuration.

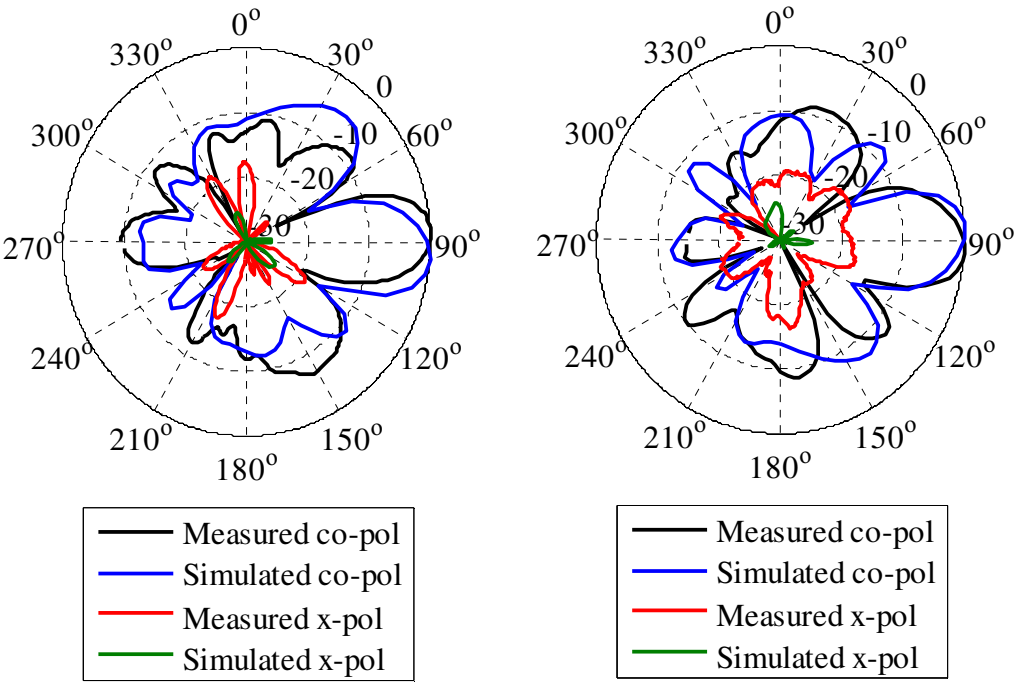

FIGURE 4.27: The measured and simulated normalized radiation pattern at 5.2 GHz in the E-plane. (a) 1st configuration. (b) 2nd configuration.

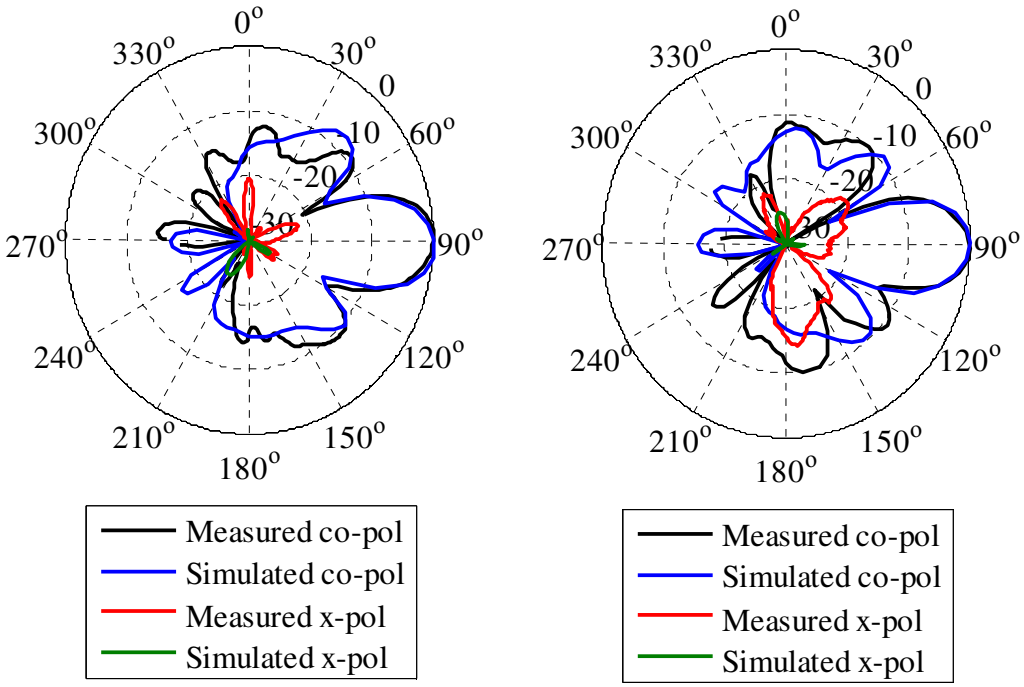

FIGURE 4.28: The measured and simulated normalized radiation pattern at 5.55 GHz in the E-plane. (a) 1st configuration. (b) 2nd configuration.

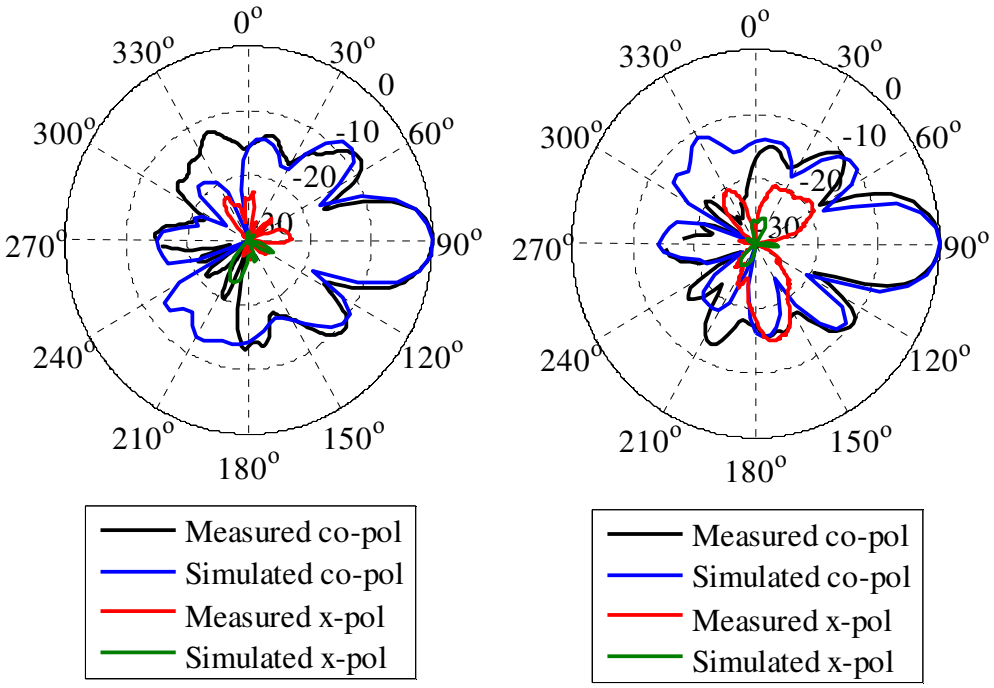

FIGURE 4.29: The measured and simulated normalized radiation pattern at 5.8 GHz in the E-plane. (a) 1st configuration. (b) 2nd configuration.

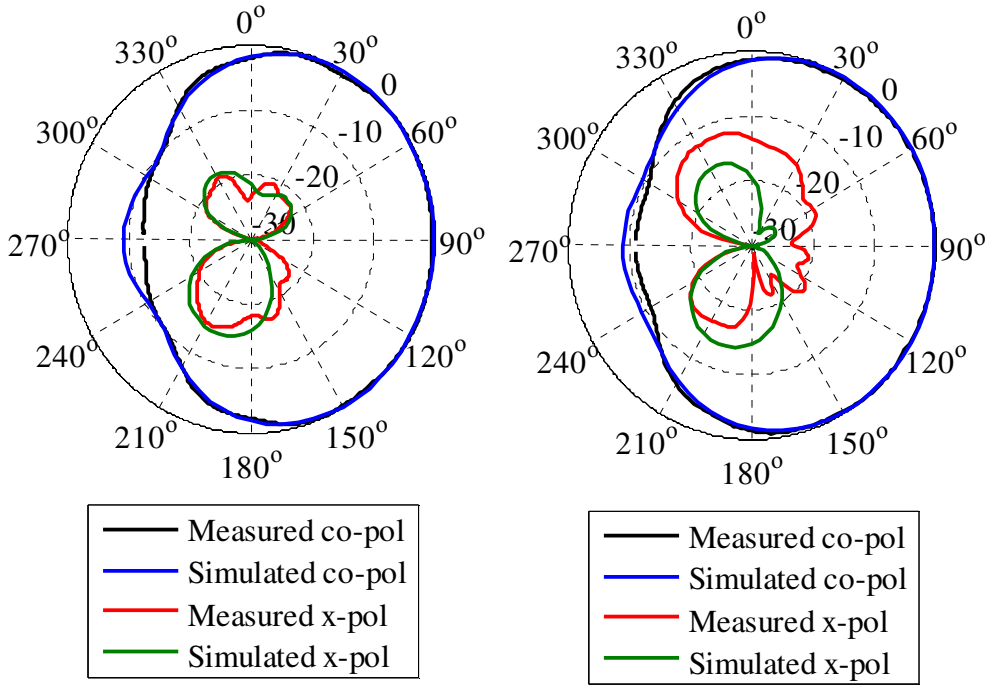

FIGURE 4.30: The measured and simulated normalized radiation pattern at 2.44 GHz in the H-plane. (a) 1st configuration. (b) 2nd configuration.

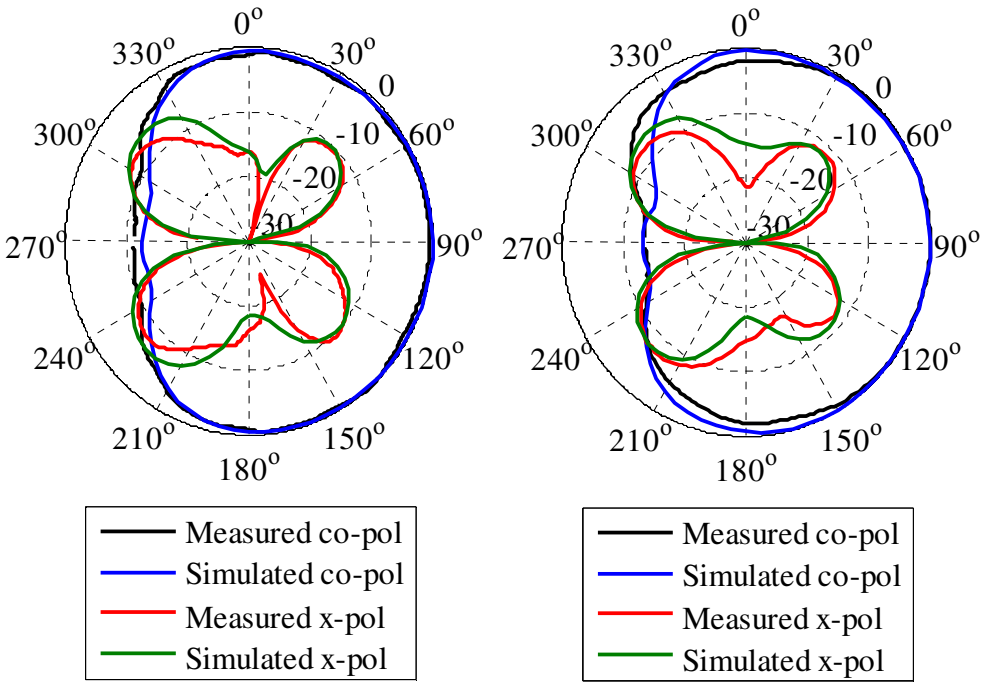

FIGURE 4.31: The measured and simulated normalized radiation pattern at 5.2 GHz in the H-plane. (a) 1st configuration. (b) 2nd configuration.

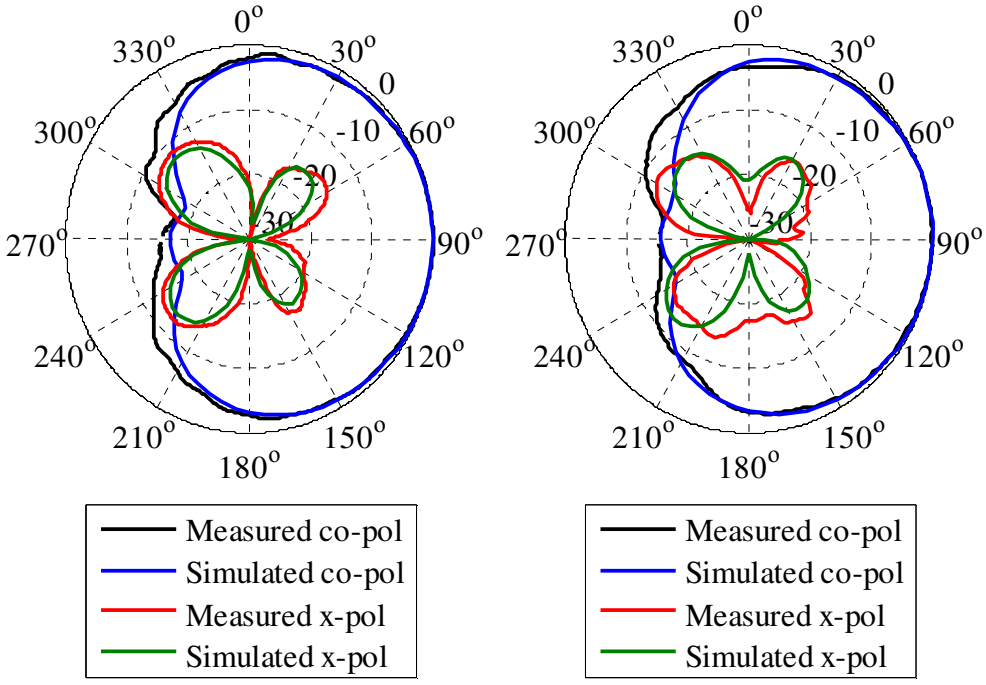

FIGURE 4.32: The measured and simulated normalized radiation pattern at 5.55 GHz in the H-plane. (a) 1st configuration. (b) 2nd configuration.

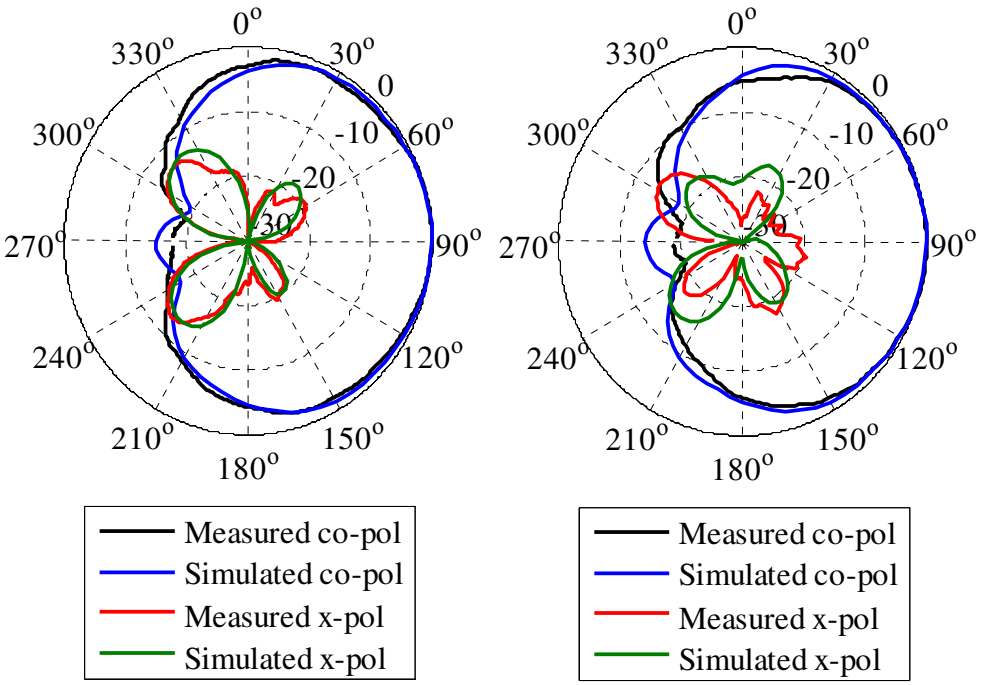

FIGURE 4.33: The measured and simulated normalized radiation pattern at 5.8 GHz in the H-plane. (a) 1st configuration. (b) 2nd configuration.

The measured F-to-B ratios of the 1st configuration surpassed the simulated results of 8.9 dB at 2.44 GHz by 1.1 dB and 17 dB at 5.55 GHz by 1.6 dB, the two centre of each band. The measured F-to-B ratios of the 2nd configuration also proved to be slightly higher than the results predicted by the simulated results. The measured F-to-B ratios ranged from 8.6 dB at 2.44 GHz to as high as 17.8 dB at 5.55 GHz, compared to the simulated F-to-B ratio of 15.7 dB at 5.55 GHz. The results are summarized in Table 4.4.

TABLE 4.4: Front-to-Back (F-to-B) ratios.

f (GHz)	Measured (dB)		Simulated (dB)	
	1st config.	2nd config.	1st config.	2nd config.
2.44	10	8.6	8.9	8.8
5.2	9.7	14.6	12.6	13
5.55	18.6	17.8	17	15.7
5.8	16	15.3	15.1	14.1

4.2.3 Interpretation of results

The measured bandwidths of the two configurations ranged from 25.2% to 33.3% over the first band and from 31.8% to 37% over the second band. Similar dipole configurations such as the folded half-wave dipole and the modified quasi-Yagi antenna presented in [19] and [20] respectively delivered very comparable bandwidths. The bandwidths achieved with the two configurations presented in the above section were thus in line and even surpassed many of the current monopole and slot designs. Surplus bandwidth was thus also achieved to ensure that the specifications of the two standard WLAN bands were still met in the event of a reduction in width, due to possible changes associated with the assembly of more elements.

The peak gains of 5.4 dBi and 5.8 dBi associated with the 1st- and 2nd configuration respectively, over the first band, in conjunction with the 8.8 dBi and 8.5 dBi over the second band, concurred with the aim to increase the gain by adding an additional element. The peak gains of the final optimized single-element design with the director were 4.6 dBi and 6 dBi over the 2.4/5.2 GHz bands respectively, with the increase equal to 1.2 dBi and 2.5 dBi. The average gain of 6.4 dBi over the second band was slightly less than the two-element configuration presented in [9], where the average gain was 8.4 dBi.

Very good correlation was seen between the measured and simulated radiation patterns, especially in the H-plane. The simulated and measured co-polarized radiation patterns exhibited a strong correlation in the E- as well as the H-plane. The normalized cross-polarization levels ranged between -20 dB and -30 dB in the boresight direction, which confirmed that the levels did not degrade with the assembly of the two elements compared to the final single-element design. The highest measured cross-polarization levels in the E-plane were -19.6 dB and -14.1 dB pertaining to the 1st- and 2nd configuration respectively. These levels compare well with the highest level of -20 dB exhibited by the two-element array presented in [9]. The F-to-B ratios pertaining to the two configurations also ranged between 10 dB and 29 dB, similar to the two-element design in [9].

4.3 DUAL-POLARIZED FOUR-ELEMENT ARRAY

The two configurations as presented in Section 4.2, consisting of two identical single-element optimized designs with a director (as seen in Chapter 3), was combined into a four-element array with the aim of developing a dual-polarized array capable of sending and/or receiving arbitrary orthogonal polarizations. The results obtained from each polarization were compared, as done previously with the two configurations in Section 4.2. The H-Array, as referred to in Chapter 3, represents the two-element array excited by Port 1, whereas the V-Array represents the array excited by Port 2 and was arbitrary associated with the horizontal- and vertical polarizations respectively.

4.3.1 Reflection coefficient, coupling and gain

The horizontally polarized array (H-Array) produced a simulated bandwidth of 24.3% (2.08 – 2.65 GHz) and 29.8% (4.43 – 5.98 GHz), with the band only slightly separated by the section ranging from 4.72 GHz to 4.96 GHz. The vertically polarized array (V-Array) imbued the frequency range from 2 GHz to 2.52 GHz and from 4.59 GHz to 5.91 GHz, which resulted in bandwidths equal to 22.9% and 25.2% respectively. These simulated results are compared to the measured result in Fig. 4.34. The measured bandwidths of the H-Array were 32.5% (2 – 2.78 GHz) and 37.1% (4.22 – 6.14 GHz), which more than adequately covered the 2.4/5.2 GHz bands respectively. Discernible wider bandwidths were achieved compared to the simulated bandwidths of both frequency bands. The discrepancies can be attributed to the lower mesh density used with the simulation runs, due to the size of the array. The V-Array also surpassed the expected results with only small sections of the frequency bands above the -10 dB level. The 2.4 GHz band was covered from 2 GHz to 2.64 GHz, with the section ranging from 2.07 GHz to 2.22 GHz above -10 dB, with the highest level recorded as -9.12 dB. The overall bandwidth was thus equal to 27.6%, which were 4.9% less than the bandwidth of the H-Array. The 5.2 GHz band was also unevenly divided by a small section from 5.43 GHz to 5.68 GHz, with the overall bandwidth ranging from 4.6 GHz to 6.2 GHz, which surmounted to a wide bandwidth of 29.7%.

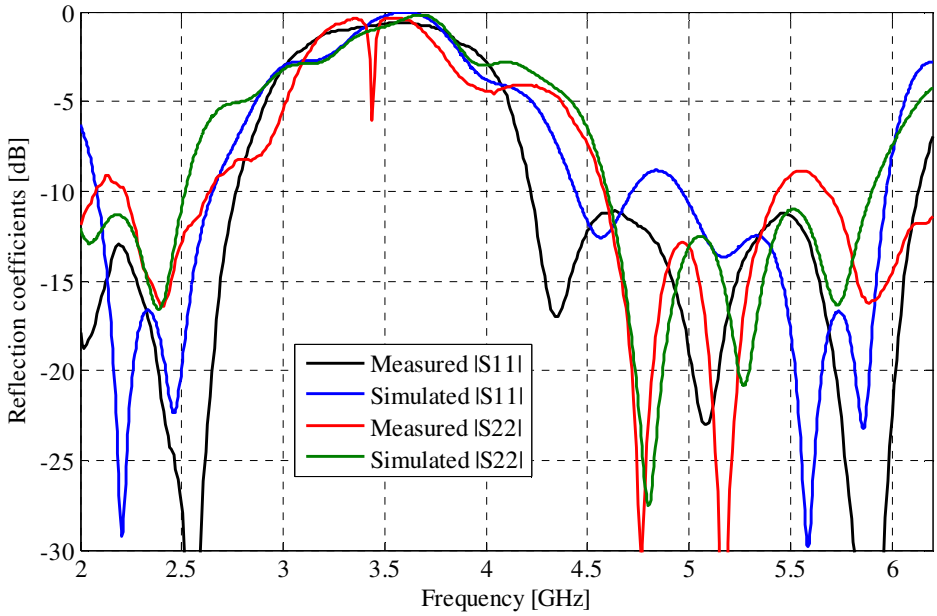

FIGURE 4.34: The reflection coefficient levels pertaining to the horizontal (Port 1) and the vertical (Port 2) polarization.

Good correlation was seen between the simulated and measured coupling levels between the arrays, as shown in Fig. 4.35. The highest coupling was seen across the second frequency band and barely went above the -20 dB level. The highest measured coupling was seen at 4.89 GHz and was equal to -17.3 dB.

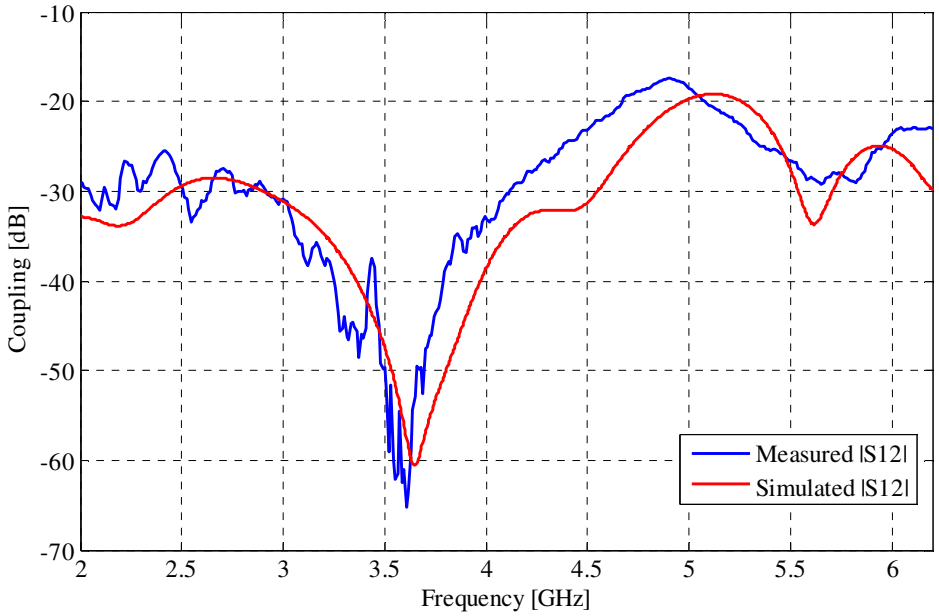

FIGURE 4.35: The coupling between the horizontal (Port 1) and the vertical (Port 2) arrays.

The simulated gain as shown in Figs. 4.36 and 4.37 was also very close to the gain achieved with the separate two-element arrays. The average simulated gain of the H-Array proved to be equal to 5.5 dBi over the 2.4 GHz band and equal to 7 dBi over the 5.2 GHz band. The average simulated gain of 5.1 dBi of the V-Array was slightly lower over the first frequency band compared to the H-Array, whereas the opposite was true for the gain of 7.4 dBi over the second frequency band. The highest simulated gain achieved by the H- and V-Array was equal to 9.4 dBi at 5.8 GHz and at 5.6 GHz. The measured gain of both polarizations was lower than their simulated counterparts, where the average gain over the first band was 5.1 dBi and 4.4 dBi pertaining to the H- and V-Array respectively. The same tendency was seen over the second band with the average gain of the H- and V-Array equal to 6.2 dBi and 6 dBi respectively. The measured gain over the first band was closer to the expected values, as determined with the aid of the simulation software, whereas a bigger difference was noted between the measured and simulated results obtained over the second frequency band. The highest measured gain was achieved with the H-Array and was equal to 8.8 dBi at 5.72 GHz.

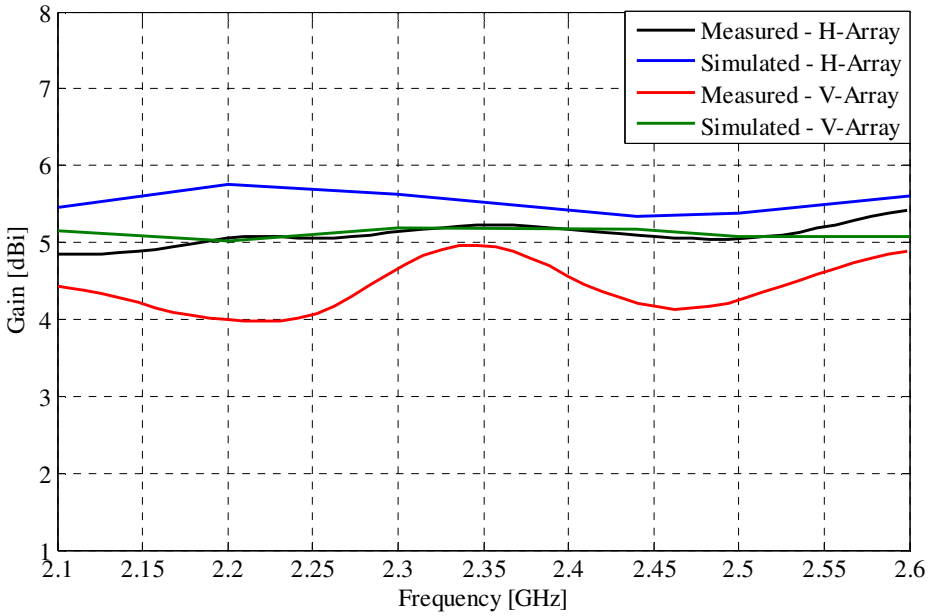

FIGURE 4.36: The measured and simulated gain of the horizontal (Port 1) and the vertical (Port 2) polarization, over the 2.4 GHz band.

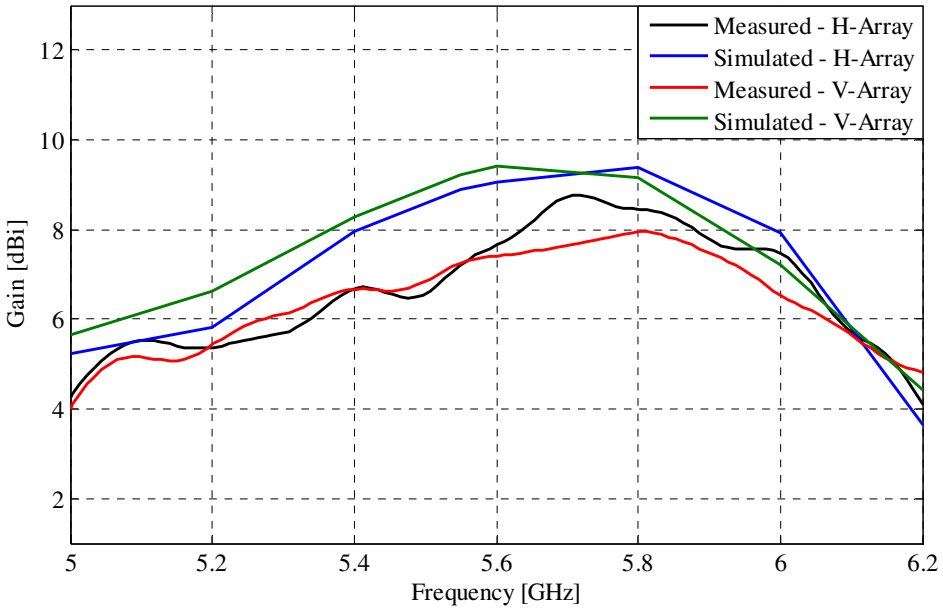

FIGURE 4.37: The measured and simulated gain of the horizontal (Port 1) and the vertical (Port 2) polarization, over the 5.2 GHz band.

4.3.2 Radiation patterns

The high gain achieved with this four-element array was confirmed by the good far field radiation patterns in the E-plane, as well as in the H-plane. The radiation patterns of each polarization were placed next to each other for the sole purpose of easy comparison, as shown from Figs. 4.38 – 4.45. Both arrays delivered directive radiation patterns in the E- and H-plane, with good correlations between the measured and simulated co-polarized patterns. Good agreement was found between the measured co- and cross- polarization levels of both polarizations in the H-, as well as the E-plane, specifically at φ/θ equal to 90º. The biggest deviation between the simulated and measured cross-polarization levels was at 2.44 GHz in the E-plane, exhibited by the vertical polarization. Again, this can be attributed to the difference between the simulated setup of the model and the physical setup of the array. The simulated and measured cross-polarization levels showed better agreement than achieved with the two separate two-element arrays. The maximum cross-polarization levels within the main lobe, for both polarizations, are summarized in Table 4.5.

TABLE 4.5: Maximum normalized cross-polarization levels.

Array	f (GHz)	Measured (dB)		Simulated (dB)	
		E-plane	H-plane	E-plane	H-plane
H	2.44	-19.4	-17.7	-23.1	-15.1
	5.2	-18.5	-14.2	-18.5	-10.9
	5.55	-22.4	-12.5	-26.3	-20.2
	5.8	-24.6	-22	-25.7	-17.1
V	2.44	-19.4	-17.7	-30.9	-15.1
	5.2	-16.7	-14.4	-18	-10
	5.55	-22.1	-12.5	-23	-18.6
	5.8	-23.4	-22	-25.9	-15.1

The cross-polarization levels at φ/θ equal to 90º again ranged between -20 dB and -30 dB, as seen with the single-element, as well as the two separate two-element configurations. The performance in terms of the cross-polarization levels in the boresight direction was thus not degraded with the integration of more elements.

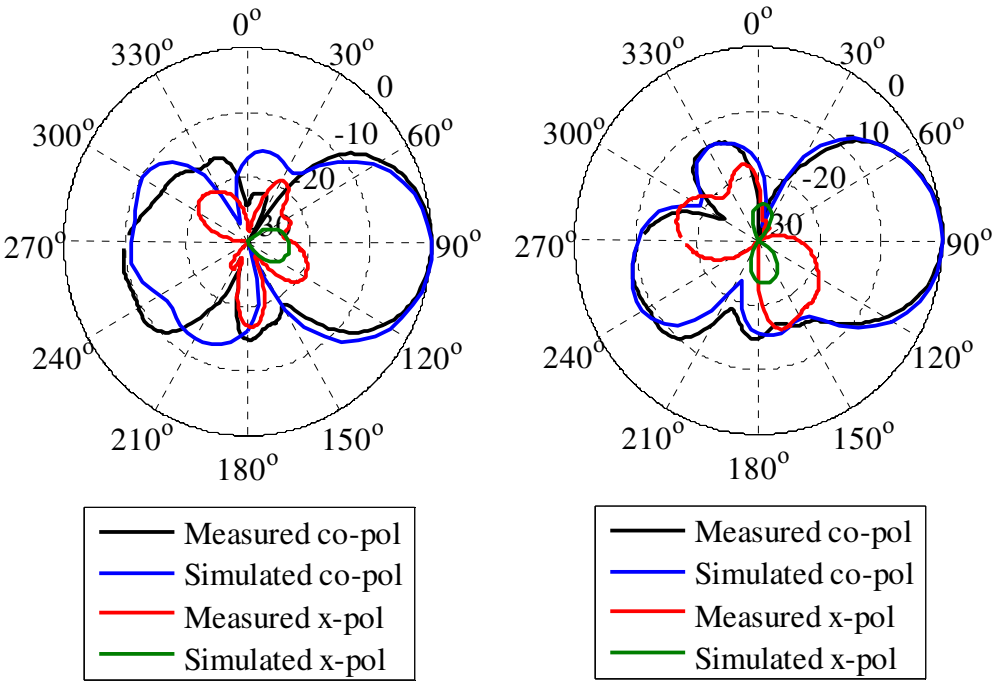

FIGURE 4.38: The measured and simulated normalized radiation pattern at 2.44 GHz in the E-plane. (a) Horizontal polarization. (b) Vertical polarization.

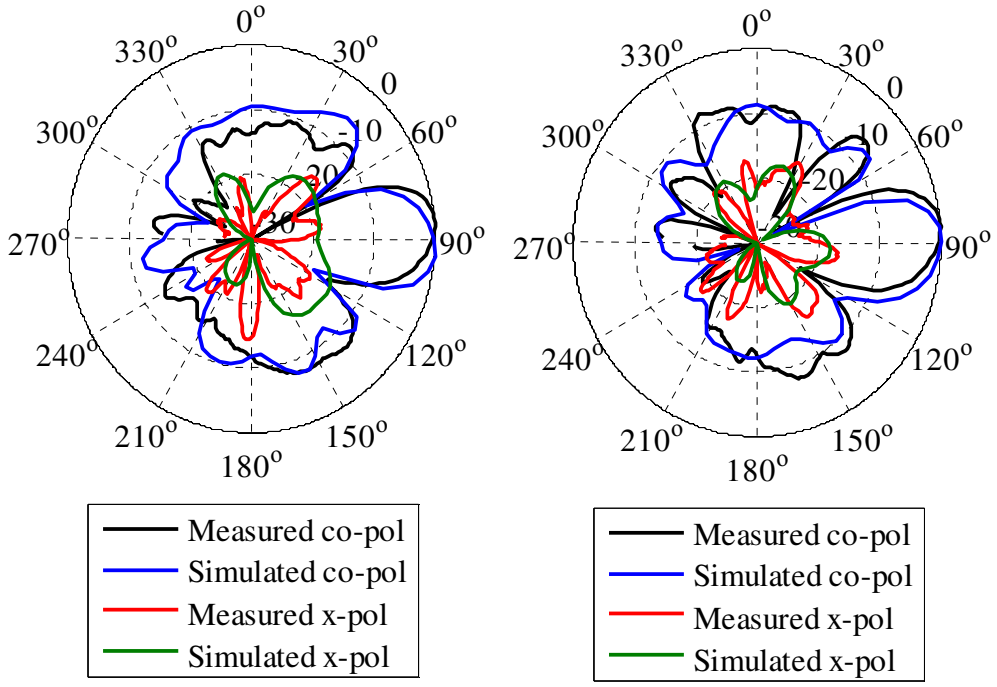

FIGURE 4.39: The measured and simulated normalized radiation pattern at 5.2 GHz in the E-plane. (a) Horizontal polarization. (b) Vertical polarization.

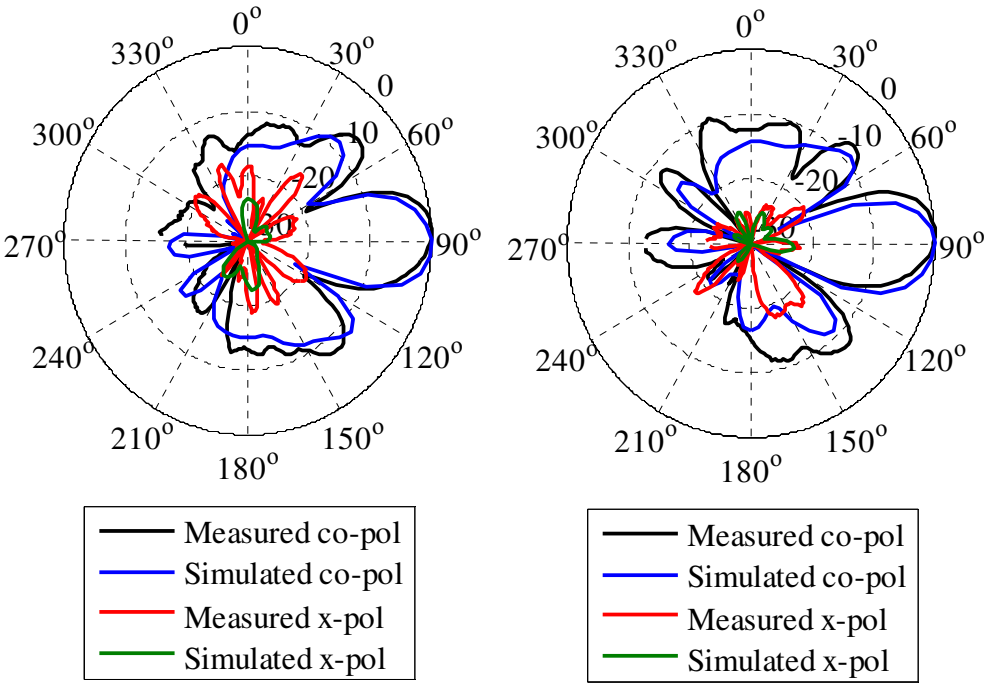

FIGURE 4.40: The measured and simulated normalized radiation pattern at 5.55 GHz in the E-plane. (a) Horizontal polarization. (b) Vertical polarization.

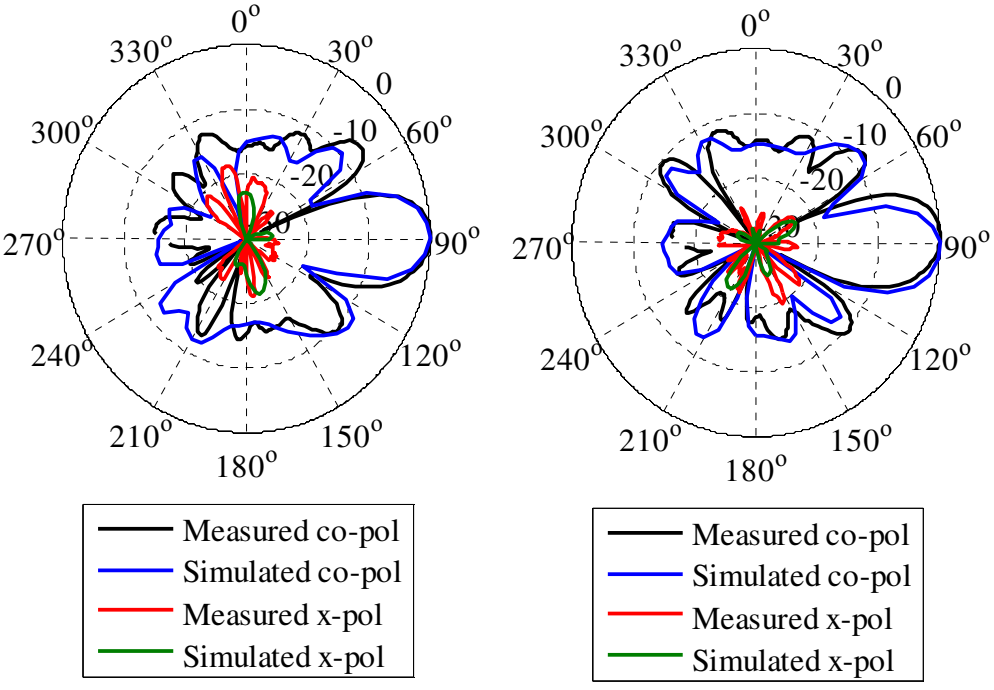

FIGURE 4.41: The measured and simulated normalized radiation pattern at 5.8 GHz in the E-plane. (a) Horizontal polarization. (b) Vertical polarization.

The side lobe levels associated with each polarization imitated the results achieved with the separate two-element configurations. The radiation patterns in the H-plane were so broad that no real side lobes could be observed. Both frequency bands in the E-plane exhibited side lobes and ranged from -5.6 dB to -10.1 dB and from -7.5 dB to -9.2 dB pertaining to the H- and V-Array respectively. These results were corroborated by the measured results as seen in the figures below. The measured side lobe levels were generally lower than the simulated levels as seen in Figs. 4.38 - 4.41.

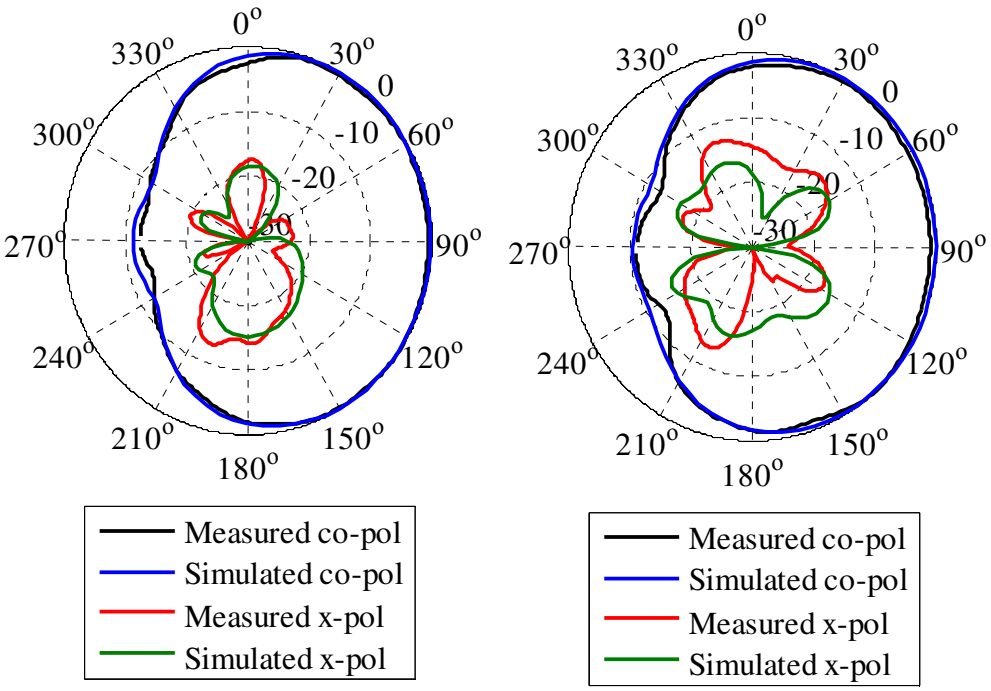

FIGURE 4.42: The measured and simulated normalized radiation pattern at 2.44 GHz in the H-plane. (a) Horizontal polarization. (b) Vertical polarization.

The measured 3 dB beam widths exhibited in the E-plane were slightly wider than the simulated beam widths, whereas approximately the same results were achieved in the H-plane. Again as with the two-element arrays, the 3 dB beam widths were close to 50º at 2.44 GHz and close to 25º over the second frequency band in the E-plane. The characteristic wide 3 dB beam widths in the H-plane associated with this design ranged from 160º to 205º.

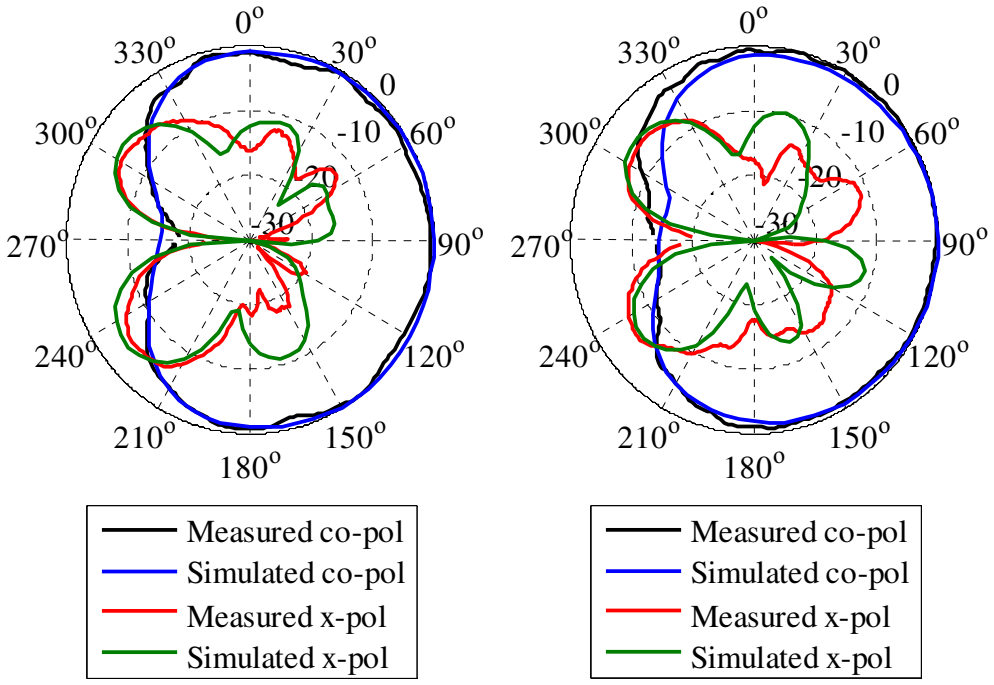

FIGURE 4.43: The measured and simulated normalized radiation pattern at 5.2 GHz in the H-plane. (a) Horizontal polarization. (b) Vertical polarization.

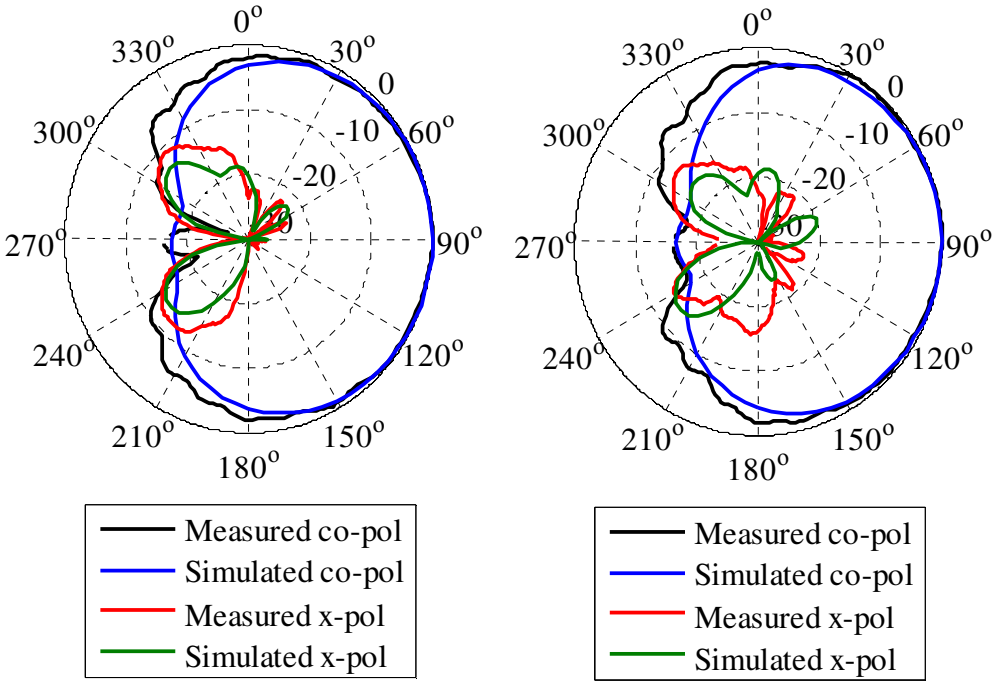

FIGURE 4.44: The measured and simulated normalized radiation pattern at 5.55 GHz in the H-plane. (a) Horizontal polarization. (b) Vertical polarization.

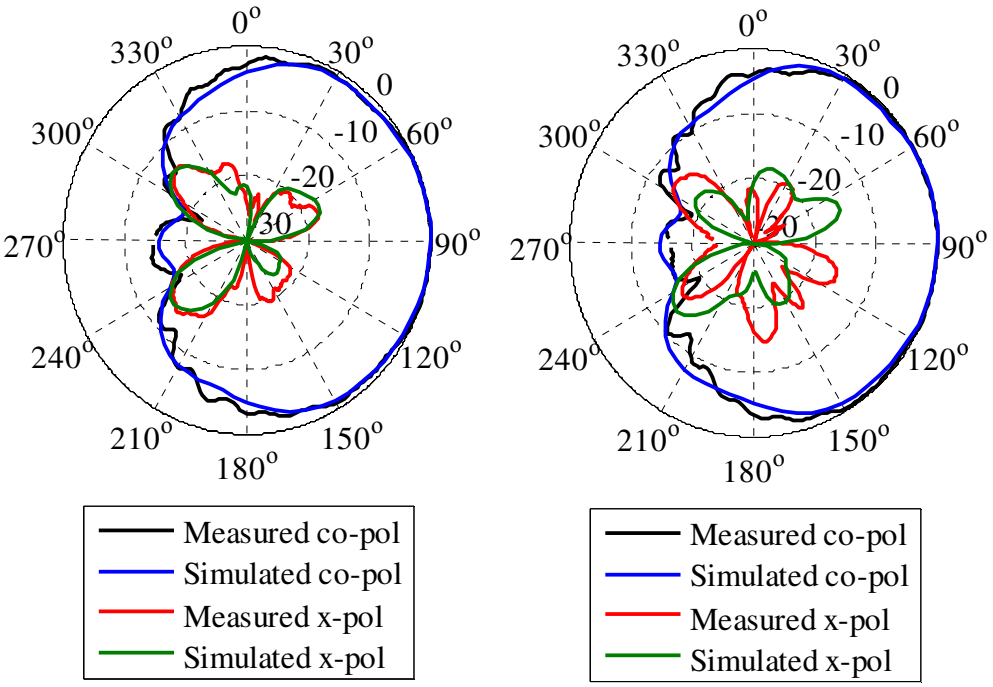

FIGURE 4.45: The measured and simulated normalized radiation pattern at 5.8 GHz in the H-plane. (a) Horizontal polarization. (b) Vertical polarization.

The simulated F-to-B ratios of each polarization were approximately the same as the results obtained from the measurements taken at the Compact Antenna Range of the University of Pretoria. The H-Array exhibited a minimum simulated F-to-B ratio of 11 dB as predicted in Chapter 3 over the lower frequency band, which was close to the measured ratio of 9.7 dB. The lowest simulated F-to-B ratio of the V-Array was also exhibited at 2.44 GHz and was equal to 10.4 dB, which was also close to the measured ratio of 10 dB. The highest F-to-B ratio was exhibited by the H-Array and was equal to 24 dB, which was more than the simulated ratio of 15.3 dB at 5.2 GHz. Both arrays also delivered simulated F-to-B ratios that ranged between 14.2 dB to 16.6 dB, which also showed a good correlation with the measured results that ranged from 12.6 dB to 19 dB, with the F-to-B ratio of 24 dB being the outlier. The results are tabulated in Table 4.6.

TABLE 4.6: Front-to-Back (F-to-B) ratios.

f (GHz)	Measured (dB)		Simulated (dB)	
	H-Array	V-Array	H-Array	V-Array
2.44	9.7	10	11	10.4
5.2	24	19	15.3	14.2
5.55	19.2	12.6	17.4	16.6
5.8	17.4	18.3	15.6	14.8

4.3.3 Conclusion and interpretation of results

The widest measured bandwidths were achieved with the H-Array. The bandwidths ranged from 32.5% to 37.1% over the 2.4/5.2 GHz bands respectively, assuming a VSWR of 2:1. The measured bandwidths of the V-Array were marginally narrower than exhibited by the H-Array, if the small sections of the band that slightly overreached the -10 dB level were taken into account in the overall calculation of the bandwidths. The orthogonal interleaving of the two-element arrays did thus not have a major effect on the respective bandwidths of the horizontal- and vertical polarizations. Most of the current DBDP designs such as presented in [4], [21], [23] and [25-27] exhibited narrower bandwidths, where the design in [23] did not adhere to the minimum requirement associated with the 5.2 GHz band. The main goal was thus achieved with the DBDP design presented in this dissertation, where the standard WLAN frequency bands were more than adequately covered by the nouveau design.

The second specification for the DBDP design was to achieve adequate gain. By taking into account that most DBDP designs exhibited peak gains in the order of 4 dBi, the goal was thus to develop a design with directive radiation patterns in conjunction with peak gains equal and higher than 4 dBi, to provide a sufficient advantage compared to other configurations. The average gains achieved with the various polarizations ranged from 4.4 dBi to 5.1 dBi over the 2.4 GHz band and from 6 dBi to 6.2 dBi over the 5.2 GHz band. The highest gain of 8.8 dBi was achieved over the second frequency band, whereas the peak gain achieved over the 2.4 GHz band was 5.4 dBi. These values surpassed the peak gains achieved over both bands in [24] and [27] and surpassed the gains achieved in [23] and [26] over the second band. The F-to-B ratios also compared well with current designs. Very good correlation was also seen between the simulated and measured radiation patterns achieved in the H-plane, as well as the E-plane, for both polarizations.

Most of the normalized cross-polarization levels of the DBDP designs were around -20 dB at boresight. The -20 dB to -30 dB levels achieved with the presented DBDP configuration thus concur with the characteristics the other designs.

The good correlations exhibited between the measured and simulated results in conjunction with the more than adequate bandwidths, relatively high gains, stable radiation patterns, compact structure and low cross-polarization levels corroborated the potential of the presented DBDP configuration.

CHAPTER 5

CONCLUSION AND FUTURE WORK

"Although nature commences with reason and ends in experience it is necessary to do the opposite that is to commence with experience and from this to proceed to investigate the reason."
- Leonardo da Vinci

"Wireless is all very well but I'd rather send a message by a boy on a pony!"
- Lord Kelvin [Quoted in *My Father, Marconi* by Degna Marconi]

5.1 BACKGROUND

The recent growth in the ambit of modern wireless communication has increased the demand for multi-band multi-polarized antenna configurations as discussed in Chapter 1. A large body of research was done on dual-band antennas, where all the attributes of each design was discussed in Chapter 2. The first section of the chapter was dedicated to the advantages and disadvantages of each dual-band design, where the monopole and dipole designs received centre stage. The viability of patch antennas were also ascertained in Chapters 1 and 2. The nouveau challenge was to incorporate the dual-band and dual-polarized capabilities desired in modern systems, into one design. This was done for SAR (Synthetic Aperture Radar) applications, where layered structures that employ patch elements [23] were used and exhibited very narrow bandwidths of between 1% and 7%, at different frequency bands. DBDP (Dual-Band Dual-Polarized) arrays were also developed for spaceborne SAR to cover the 1.25 GHz and 5.3 GHz bands, but also exhibited very narrow bandwidths in the order of 5% [25].

Another challenge was to make use of only two ports, each assigned to the various polarizations, in order to reduce installation and equipment costs [21], while obtaining adequate bandwidths. The size of the dipole designs, as well as the wide bandwidths directed the design process towards the modified bow-tie and double Rhombus antennas also conversed in Chapter 2. The two- and four- element Rhombus designs presented in [9]

was chosen as inspiration for the rest of the design development conveyed in this dissertation. In Chapter 3 the single antenna used in the later configurations were first optimized in terms of bandwidth and later in terms of gain. Section 3.1 was dedicated to the development of a suitable dual-band antenna that made use of only one port for both WLAN frequency bands. Section 3.2 focussed on the two-element designs that were later incorporated into the four-element design, the main aim of this dissertation. The simulated and measured results were compared in Chapter 4 to validate the practicality and reproducibility of the design. This last chapter, on retrospect, conveys the contributions made to this specific area of applied electromagnetism and the knowledge obtained, in order to highlight certain areas where future improvement might be possible.

5.2 CONTRIBUTIONS

In this dissertation a four-element prototype was developed with both dual-band and dual-polarized capabilities in conjunction with a compact structure on a relatively inexpensive substrate, with only two ports. This concurred with the objectives, as stipulated in Chapter 1, to develop an alternative DBDP configuration with adequate bandwidth and gain. The development of the design was presented in Chapter 3, as well as the simulated results which evidently supported the notion that the latter could be a viable option. This was confirmed by the good correlations achieved between the measured and simulated results, as seen in Chapter 4.

The final optimized single-element with the director, achieved 17.8% and 34.7% bandwidths over the 2.4/5.2 GHz bands respectively, with the frequency bands ranging from 2.32 to 2.77 GHz and from 4.25 to 6.03 GHz. The specified standard WLAN bands range from 2.4 to 2.484 GHz and from 5.15 to 5.85 GHz, which translates to 3.4% and 14.4%, respectively. The wide bandwidths of the new single-element design, in conjunction with an average gain of 3.6 dBi over both bands, compared well with existing monopole, patch and other dipole designs, discussed in Chapter 2. The maximum boresight gain achieved over the first- and second band was equal to 4.6 dBi and 6 dBi. The design surpassed both the lower frequency bands of the ring and G-shaped monopoles with the respective bandwidths equal to 12% and 15.2%. The 5.2 GHz band was also adequately covered by the new design in comparison with bandwidths of the ring and G-shaped monopoles, which were reported to be equal to 39.3% and 19.4%. The ring and G-shaped

monopole designs also exhibited omni-directional patterns and thus lower gains were achieved. The CPW-fed monopole antenna designs claimed to have bandwidths ranging from 20% to 23.3% over the 2.4 GHz band and from 29.5% to 37% over the 5.2 GHz. The final single-element design presented in Chapters 3 and 4 compared well with these bandwidths and delivered even higher gain than achieved with the CPW and meander line technology. The patch antennas delivered very narrow bandwidths over the 2.4 GHz band, with low gain. The same propensity was seen with the folded-dipole and modified quasi-Yagi designs also examined in Chapter 2. The final design exhibited high measured F-to-B ratios of between 12.2 dB and 19.1 dB.

The two-element design also provided wide bandwidths that ranged from 12.7% to 23.8% over the first band and from 26.7% to 29.9% over the second frequency band, with the various arrays. The gain proved to be high and ranged from 5 dBi to 9.5 dBi, which correlated with the expectation of increased gain by means of the amalgamation of the two single-elements. The highest coupling was found to be equal to -12.8 dB and the average coupling around -29.2 dB. The two different arrays also exhibited very similar characteristics, such as very wide 3 dB beam widths in the H-plane which ranged from 158.9º to 234º and narrower beam widths in the E-plane, which remained close to 25º. As with the single-elements the measured cross-polarization was also still within reasonable limits. The highest levels achieved by both configurations were equal to -10 dB and -17.2 dB in the H- and E-plane respectively. The cross-polarization levels delivered by the two-element designs ranged between 20 dB to 30 dB down on boresight.

The four-element array performed in accordance with the results obtained from the two two-element arrays, since additional care was taken to ensure that the feedlines did not touch each other or the ground plane of each array. Different feeding networks were also used to minimize the effect of each slit through the ground planes. In this undertaking a four-element with dual-band dual-polarization capabilities were realized with only two ports, in conjunction with wide bandwidths and high gain. The measured bandwidths were very close to the results obtained from the separate two-element arrays, with the widths ranging from 27.6% to 32.5% over the first band and from 29.7% to 37.1% over the second band. The coupling improved with the orthogonal interleaving of the two two-element arrays, where the highest recorded coupling was equal to -17.3 dB. The gain was somewhat lower compared to the various two-element arrays, with the average gain

ranging from 4.4 dBi to 5.1 dBi over the first band and from 6 dBi to 6.2 dBi over the second band. The highest gain of 8.8 dBi was achieved over the second frequency band, whereas the peak gain achieved over the 2.4 GHz band was 5.4 dBi. These values surpassed the peak gains achieved over both bands in [24] and [27] and surpassed the gains achieved in [23] and [26] over the second band. Good correlation was seen between the simulated and measured radiation patterns, with the low cross-polarization levels at boresight and very high F-to-B ratios, in the order of 19 dB. The characteristic wide 3 dB beam widths in the H-plane and narrower beam widths in the E-plane was also exhibited by this configuration.

5.3 CHALLENGES AND ISSUES FOR FUTURE WORK

The design was developed with the main objectives being the bandwidth, gain, number of ports and dual-band dual-polarization capabilities, where the cross-polarization and side lobe levels received second chair. The design can however be modified for a variety of other applications, such as phased arrays or focal plane arrays, where the cross-polarization levels or the side lobes might play more prominent roles.

The main focus in recent development and growth in the area of radio astronomy was the development of instrumentation fit for the 21st century. The scientific community therefore conceived the idea of a telescope that far surpasses the capabilities of current radio telescopes in terms of sensitivity, FOV (Field Of View), frequency range and multi-beam forming capacity, in order to facilitate the observation of phenomena such as pulsars over sources spaced far apart [44]. The SKA (Square Kilometre Array) project was proposed to fulfil the above specifications, in order to facilitate studies that delve into the evolution of cosmic bodies and galaxies, the mysteries surrounding black holes and the question whether there exits planets like ours with the capability to sustain life [45]. In order to realize the SKA, appropriate feeds for the reflector antennas need to be developed where FPAs (Focal Plane Arrays) are set forth as a possible candidate. The desired characteristics of the FPA (Focal Plane Arrays) array elements are ultra-wide bands, end-fire radiation patterns, small antenna dimensions and low cross-polarization levels. The design presented in this dissertation can thus be modified to operate over the specific frequency range, where mitigation methods need to be further investigated to lower the cross-polarization levels in the H-plane below the -20 dB level along the whole plane,

while ensuring the coupling levels also stay below this mark. Different methods can be ascertained to increase or decrease the 3 dB beam width, depending on the purpose of the design.

REFERENCES

[1] A.A. Eldek, A.Z. Elsherbeni, and C.E. Smith, "Wide-band modified printed bow-tie antenna with single and dual polarization for c- and x-band applications." *IEEE Trans. Antennas Propag.,* vol. 53, no. 9, pp. 3067 – 3072, Sept. 2005.

[2] R. Piechocki, P. Fletcher, A. Nix, N. Canagarajah, and J. McGeehan, "A measurement based feasibility study of space-frequency MIMO detection and decoding techniques for next generation wireless LANS." *IEEE Trans. Consumer Electr.,* vol. 48, no. 3, pp. 732 – 737, Aug. 2002.

[3] N.K. Das, M. Shinozawa, N. Miyadai, T. Taniguchi, and Y. Karasawa, "Experiments on a MIMO system having dual polarization diversity branches." *IEICE Trans. Commun.*, vol. e89-b, pp. 2522 – 2529, Sept. 2006.

[4] S.D. Targonski, and D.M. Pozar, "Dual-band and dual polarized printed antenna element." *Elect. Lett.,* vol. 34, no. 23, pp. 2193 – 2194, Nov. 1998.

[5] M. Yamazaki, E.T. Rahardjo, and M. Haneishi, "Construction of a slot-coupled planar antenna for dual polarization." *Elect. Lett.,* vol. 30, no. 22, pp. 1814 – 1815, Oct. 1994.

[6] R. Pokuls, J. Uher, and D.M. Pozar, "Dual-frequency and dual-polarization microstrip antennas for SAR applications." *IEEE Trans. Antennas Propag.,* vol. 46, no. 9, pp. 1289 – 1296, Sept. 1998.

[7] T.-W. Chiou, and K.-L. Wong, "A compact dual-band dual-polarized patch antenna for 900/1800-MHz cellular systems." *IEEE Trans. Antennas Propag.,* vol. 51, no. 8, pp. 1936 – 1940, Aug. 2003.

[8] A.A. Eldek, A.Z. Elsherbeni, and C.E. Smith, "Dual-polarized dual-band square slot antenna with a u-shaped printed tuning stub for wireless communications." *IEEE Antennas Propag. Society Int. Symp.,* vol. 1b, pp. 451 – 454, 2005.

[9] A.A. Eldek, "Ultrawideband double rhombus antenna with stable radiation patterns for phased array applications." *IEEE Trans. Antennas Propag.,* vol. 55, no. 1, pp. 84 – 91, Jan. 2007.

[10] G. Zhao, F.-S. Zhang, Y. Song, Z.-B. Weng, and Y.-C. Jiao, "Compact ring monopole antenna with double meander lines for 2.4/5 GHz dual-band operation." *Progress Electromag. Research,* vol. 72, pp. 187 – 194, 2007.

[11] Y.-F. Lin, H.-D. Chen, and H.-M. Chen, "A dual-band printed L-shaped monopole for WLAN applications." *Microw. Opt. Tech. Lett.,* vol. 37, no. 3, pp. 214 – 216, May 2003.

[12] C.-Y. Pan, C.-H. Huang, and T.-S. Horng, "A new printed G-shaped monopole antenna for dual-band WLAN applications." *Microw. Opt. Tech. Lett.,* vol. 45, no. 4, pp. 295 – 297, May 2005.

[13] Y.-L. Kuo, T.-W. Chiou, and K.-L. Wong, "A novel dual-band printed inverted-F antenna." *Microw. Opt. Tech. Lett.,* vol. 31, no. 5, pp. 353 – 355, Dec. 2001.

[14] J.H. Yoon, "Fabrication and measurement of rectangular ring with open-ended CPW-fed monopole antenna for 2.4/5.2-GHz WLAN operation." *Microw. Opt. Tech. Lett.,* vol. 48, no. 8, pp. 1480 – 1483, Aug. 2006.

[15] W.-C. Liu, "Broadband dual-frequency meandered CPW-fed monopole antenna." *Elect. Lett.,* vol. 40, no. 21, pp. 1319 – 1320, Oct. 2004.

[16] W.-C. Liu, "Broadband dual-frequency cross-shaped slot CPW-fed monopole antenna for WLAN operation." *Microw. Opt. Tech. Lett.,* vol. 46, no. 4, pp. 353 – 355, Aug. 2005.

[17] T.-H. Kim, and D.-C. Park, "Compact dual-band antenna with double L-slits for WLAN operations." *IEEE Antennas Wireless Propag. Lett.,* vol. 4, pp. 249 – 252, 2005.

[18] L. Lu, and J.C. Coetzee, "A modified dual-band microstrip monopole antenna." *Microw. Opt. Tech. Lett.,* vol. 48, no. 7, pp. 1401 – 1403, Jul. 2006.

[19] C.-C. Lin, C.-M. Su, F.-R. Hsiao, and K.-L. Wong, "Printed folded dipole array antenna with directional radiation for 2.4/5 GHz WLAN operation." *Elect. Lett.,* vol. 39, no. 24, pp. 1698 - 1699, Nov. 2003.

[20] D. Chang, C.-B. Chang, and J.-C. Liu, "Modified planar quasi-Yagi antenna for WLAN dual-band operations." *Microw. Opt. Tech. Lett.,* vol. 46, no. 5, pp. 443 – 446, Sept. 2005.

[21] B. Lindmark, "A dual polarized dual band microstrip antenna for wireless communications." *IEEE Proc. Aerospace Conf.,* vol. 3, pp. 333 – 338, Mar. 1998.

[22] H. Loui, J.P. Weem, and Z. Popović, "A dual-band dual-polarized nested Vivaldi slot array with multilevel ground plane." *IEEE Trans. Antennas Propag.,* vol. 51, no. 9, pp. 2168 – 2175, Sept. 2003.

[23] L. Shafai, W. Chamma, G. Seguin, and N. Sultan, "Dual-band dual-polarized microstrip antennas for SAR applications." *IEEE Antennas Propag. Society Int. Symp.,* vol. 3, pp. 1866 – 1869, Jul. 1997.

[24] D.H. Choi, Y.J. Cho, and S.O. Park, "Dual-band dual-polarized microstrip antenna." *IEEE Electr. Lett.,* vol. 42, no. 2, pp. 68 - 69, Jan. 2006.

[25] D.M. Pozar, D.H. Schaubert, S.D. Targonski, and M. Zawadski, "A dual-band dual-polarized array for spaceborne SAR." *IEEE Antennas Propag. Society Int. Symp.,* vol. 4, pp. 2112 – 2115, Jun. 1998.

[26] J.-S. Row, "A dual-frequency dual-polarized microstrip antenna fed by an inclined slot." *Microw. Opt. Tech. Lett.,* vol. 41, no. 6, pp. 512 – 514, Jun. 2004.

[27] R.K. Raj, M. Joseph, C.K. Aanandan, K. Vasudevan, and P. Mohanan, "A new compact microstrip-fed dual-band coplanar antenna for WLAN applications." *IEEE Trans. Antennas Propag.,* vol. 54, no. 12, pp. 3755 – 3762, Dec. 2006.

[28] A.A. Eldek, "Design of double dipole with enhanced usable bandwidth for wideband phased arrays." *Progress Electromag. Research,* vol. 59, pp. 1 – 15, 2006.

[29] A.A. Serra, P. Nepa, G. Manara, G. Tribellini, and S. Cioci, "A wide-band dual-polarized stacked patch antenna." *IEEE Antennas Wireless Propag. Lett.,* vol. 6, pp. 141 – 143, Jan. 2007.

[30] X. Yao, and W. Hong, "A -45º/+45º dual polarized microstrip antenna for wireless communication." *IEEE Antennas Propag. Int. Symp.,* vol. 4, pp. 458 – 461, Jul. 2001.

[31] D.T. Notis, P.C. Liakou, and D.P. Chrissoulidis, "Dual polarized microstrip patch antenna, reduced in size by use of peripheral slits." *European Conf. Wireless Techn.,* pp. 273 – 276, 2004.

[32] S.-Y. Suh, W.L. Stutzman, and W.A. Davis, "Low-profile, dual-polarized broadband antennas." *IEEE Antennas Propag. Int. Symp.,* vol. 2, pp. 256 – 259, Jun. 2003.

[33] E.A. Soliman, M.S. Ibrahim, and A.K. Abdelmageed, "Dual-polarized omnidirectional planar slot antenna for WLAN applications." *IEEE Trans. Antennas Propag.,* vol. 53, no. 9, pp. 3093 – 3097, Sept. 2005.

[34] V.P. Sarin, N. Nisha, G. Augustine, P. Mohanan, C.K. Anandan, and K. Vasudevan, "A dual band dual polarized microstrip antenna for WLAN applications." *IEEE Antennas Propag. Int. Symp.,* pp. 1 – 4, Jul. 2008.

[35] G. Deng, and B. Vassilakis, "A broadband dual polarized antenna element for wireless communications." *IEEE Antennas Propag. Int. Symp.,* pp. 4717 – 4720, Jun. 2007.

[36] E. Levine, and S. Shtrikman, "Broadband dual-polarized printed arrays." *European Microw. Conf.,* pp. 337 – 342, Oct. 1989.

[37] A.A. Eldek, A.Z. Elsherbeni, and C.E. Smith, "Characteristics of microstrip fed printed bow-tie antenna." *Microw. Opt. Tech. Lett.,* vol. 43, no. 2, pp. 123 – 126, Oct. 2004.

[38] A.A. Eldek, A.Z. Elsherbeni, and C.E. Smith, "Microstrip-fed printed Lotus antenna for wideband wireless communication systems." *IEEE Antennas Propag. Magaz.*, vol. 46, no. 6, pp. 164 – 173, Dec. 2004.

[39] W-H. Tu, and K. Chang, "Wide-band microstrip-to-coplanar stripline/slotline transitions." *IEEE Trans. Microw. Theory Techn.,* vol. 54, no. 3, pp. 1084 – 1089, Mar. 2006.

[40] J.J. Carr, *Practical Antenna Handbook,* 2nd ed. New York: McGraw-Hill, Inc., 1994.

[41] H. Yagi, "Beam transmission of the ultra short waves." *Proc. IRE,* vol. 16, pp. 715 – 741, Jun. 1928.

[42] N. Kaneda, Y. Qian, and T. Itoh, "A broad-band microstrip-to-waveguide transition using quasi-Yagi antenna." *IEEE Trans. Microw. Theory Techn.,* vol. 47, no. 12, pp. 2562 – 2567, Dec. 1999.

[43] C.R. Paul, *Electromagnetics for Engineers with applications,* 1st ed. New York: John Wiley & Sons, Inc., 2004.

[44] A.J. Parfitt, J.S. Kot, and G.L. James, "The Luneburg lens as a radio telescope element." *Proc. IEEE Antennas Propag. Society Int. Symp.,* vol. 1, pp. 170 – 173, Jul. 2000.

[45] R. Olsson, P.-S. Kildal, and S. Weinreb, "The eleven antenna: a compact low-profile decade bandwidth dual polarized feed for reflector antennas." *IEEE Trans. Antennas Propag.,* vol. 54, no. 2, pp. 368 – 375, Feb. 2006.